# AN EXPERIMENTAL AND COMPUTATIONAL STUDY OF THE EFFECT OF BIOCERAMIC POROSITY ON DRUG RELEASE KINETICS

by

Rahul R Upadhyay

A thesis submitted to the faculty of
The University of North Carolina at Charlotte
in partial fulfillment of the requirements
for the degree of Master of Science in
Mechanical Engineering

Charlotte

2016

Approved by:

Dr. Harish P. Cherukuri

Dr. Ahmed El-Ghannam

Dr. Didier Dréau

# ABSTRACT

RAHUL R UPADHYAY. An experimental and computational study of the effect of Bioceramic Porosity on Drug Release Kinetics. (Under the direction of DR. HARISH P. CHERUKURI and DR. AHMED EL-GHANNAM)

Porous bioceramics have been explored for drug delivery applications. The goal is to design a material that can provide controlled release of therapeutic doses of the drug for a duration long enough to cause complete healing. For drug carriers, the parameters of importance are the drug release rate, cumulative drug release (CDR) and duration of release. These parameters are largely dependent on the porosity characteristics. In the present study, porous -Cristobalite disks with different porosities are studied as carriers of the drug Vancomycin. The studies comprise of both experiments and simulations. The experimental work focused on preparation of -Cristobalite disks followed by a study of the drug binding and release kinetics. -Cristobalite particles in the size range of 38-90 m were mixed with 15%, 30% and 45% by mass of Poly-Ethylene Glycol (PEG). The Cris-PEG mixtures were pressed at 283 MPa, heat treated at 100 °C/1 hr and 350 °C/24 hr and sintered at 1150 °C for 24 hours to obtain porous disks with different porosity characteristics. The disks were immersed in Vancomycin solution (8 mg/ml) for 16 hours at room temperature. The amount of drug absorbed by the disks was measured using Gravimetric analysis. The amount of drug adsorbed on the disk surface was calculated using HPLC analysis. For the analysis of drug release kinetics, the disks were immersed separately in 3 ml of PBS in polystyrene jars and incubated at 37 °C on an orbital shaker. After 1 hr, 4 hrs, 8 hrs, 16 hrs, 24 hrs and every 48 hrs thereafter, 1 ml of the solution was withdrawn

and stored and replenished by the same volume of fresh PBS. The concentrations of Vancomycin in the collected samples were measured to calculate the CDR over time. Also, SEM analysis of Cris-PEG disk sections was performed to quantitatively and qualitatively study the surface morphology and pore size distribution of the disks. The purpose of the computational work was to study the significance of various mechanisms that drive the diffusion of drug from the ceramic disks and provide insights into the use of computational tools in developing ideal drug delivery vehicles. Drug release process from the disks involves two main phases: Burst Release phase, in which there is a dissolution of the adsorbed layer of drug on the disk surface into the physiological solution and the Sustained Release phase, in which there is diffusion of drug through the internal pores of the disks into the physiological solution. These two mechanisms are modeled using the Fickian Theory of Diffusion and the Finite Element Method. Axisymmetric finite element models of the disk and the PBS region were developed and solved using the FEM package ABAQUS and the results were post-processed by MATLAB to compute the CDR. Two quantities, Diffusion Coefficient and Mass-Transfer Coefficient, are essential for these models. These were obtained by matching the computational and experimental values of CDR. Relation between the drug release kinetics and the Pore Size distribution was also studied to identify the pore size categories which control the release kinetics.

# ACKNOWLEDGMENTS

I would like to thank my advisors, Dr. Harish P. Cherukuri and Dr. Ahmed El-Ghannam for their excellent mentorship, guidance and motivation. Dr. Cherukuri's wisdom and commitment towards research motivated and propelled me to complete this thesis to the best of my abilities. I profoundly thank him for the encouragement and support he gave me throughout my research. Dr. El-Ghannam's passion for scientific research and inquiry motivated me to become an independent researcher. I deeply acknowledge his support and guidance. I would also like to thank Dr. Didier Dréau for being a part of my thesis committee and for his valuable suggestions and inputs.

I would like to thank Christopher Trujillo for training and helping me in getting acquainted with the lab equipment and various experimental procedures. I thank and acknowledge his patience and support. I would like to thank Mr. James Haig for helping me with the SEM analysis of my samples and for his valuable suggestions for my research. I thank Dr. Hassan, Ms. Siang Yee Chang, Mr. Franklin Green and Mr. John Hudak for their help and valuable inputs at different stages of my research. I would like to thank Ms. Sanjana Chintalacheruvu for her support, encouragement and unique inputs throughout my research. Finally, I would like to thank all the faculty and staff of the department of Mechanical Engineering and Engineering Sciences at UNC-Charlotte that helped and contributed in the completion of this thesis.

TABLE OF CONTENTS

# LIST OF FIGURES

# LIST OF TABLES

# CHAPTER 1: INTRODUCTION TO CONTROLLED DRUG DELIVERY SYSTEMS

## 1.1 Targeted and Controlled Drug Delivery

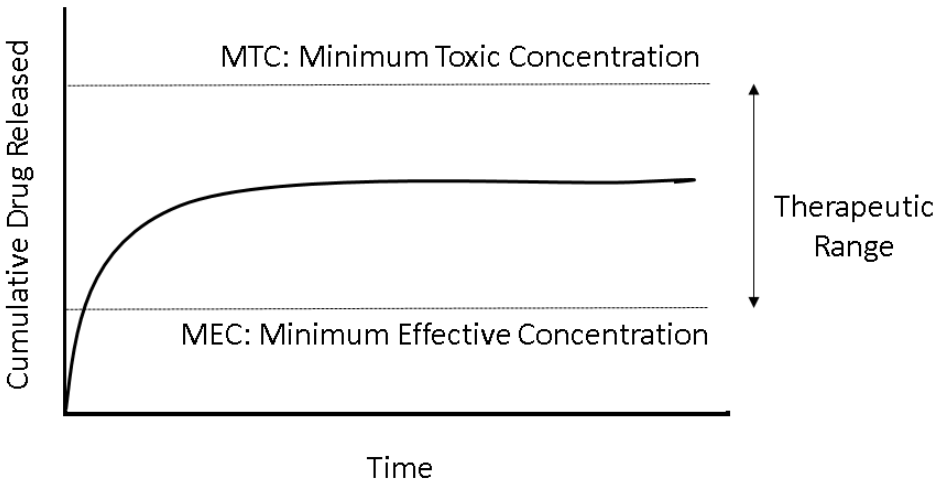


Figure 1: Illustration of the Release Profile a typical Controlled Drug Delivery System.

*Drug Delivery* is the process of transporting a therapeutic material or drug in a body. When a drug is administered using conventional delivery systems such as oral tablets and intravenous injections, the concentration of drug rises and reaches a peak value after which it begins to decline [25]. *Controlled Drug Delivery* is the process of effectively transporting drug in the body in a rate-controlled manner so as to deliver sustained dosage within the therapeutic range, as shown in figure 1. In Controlled Drug Delivery, the goal is to maintain the drug levels in the body above the *MEC* or *Minimum Effective Concentration* and below the *MTC* or *Minimum Toxic Concentration* [14].

Several kinds of pharmaceutical materials such as anti-cancer drugs, when administered using conventional drug delivery methods such as intravenous injections can spread over the entire body and can harm healthy cells [28]. *Targeted Drug Delivery* involves transporting drug internally (invasive) or externally (non-invasive) around a region where a comparatively higher dosage of drug needs to be administered. *Targeted Drug Delivery* is also referred to as *Smart Drug Delivery* which involves localized administration of drug [16].

Novel drug delivery systems, many of which are currently commercially available, offer *Spatial* as well as *Temporal* control of drug release [25]. These devices can be designed to achieve the required drug release rate by controlling their physical or chemical characteristics. *Porous Matrix Scaffolds*, *Hydrogels*, *Semi-Permeable Polymer Membranes* etc. are examples of some of the *localized* and *controlled* drug delivery systems.

## 1.2 Diffusion Controlled Drug Delivery

Controlling molecular diffusion is an effective method for achieving the required release rate and release profile from drug delivery systems [19]. Drug release from porous matrix based drug delivery systems is a predominantly diffusion controlled phenomena ([21], [24]).

Diffusion controlled drug delivery systems can be primarily categorized as *Reservoir* systems and *Monolithic* systems. In *Reservoir* devices, drug is contained within a rate controlling *barrier* whereas in *Monolithic* devices, there is a homogeneous distribution of drug in the matrix. In the former, only the *barrier* affects the release profile whereas in the latter, the release rate and profile are functions of the physical and chemical

characteristics of the entire matrix, such as pore size distribution, porosity, surface chemistry etc.

The release of drug from diffusion controlled drug delivery systems can be quantified using *Fickian Diffusion Laws* [11]. The first and second *Fick's laws* of diffusion are given by equations 1 and 3.

$$F = -D\nabla c \tag{1}$$

$$\frac{\partial c}{\partial t} = -D\nabla F \tag{2}$$

$$\frac{\partial c}{\partial t} = D\nabla^2 c \tag{3}$$

In equation 1, $F$ is the rate of mass transfer per unit area of a section, i.e. *flux*; $D$ is the Diffusion Co-efficient and $c$ is the concentration of the species that is diffusing. In equation 3, $t$ denotes the time. According to *Fickian Diffusion laws*, the rate of change of concentration wrt. time is proportional to the concentration gradient, with Diffusion Co-efficient being the constant of proportionality.

The solution of *Fickian* governing differential equations to quantify the release of a pharmaceutical material is dependent on the initial concentration of drug as well as the boundary conditions to which the drug delivery system is subjected to [11].

In drug delivery systems, with multiple diffusion steps, the slowest step is considered as the *Rate Determining Step*. For example, in porous ceramic matrix based drug delivery systems, there is an initial diffusion of solution in the matrix followed by molecular diffusion of drug out of the matrix. As the diffusion of drug molecules from the matrix is much slower compared to the penetration of the solution into the

matrix, it is considered as the *rate determining step* [21]. In mathematical analysis only the *rate determining step* is taken into consideration.

## 1.3 Literature Review

The aim of this review is to outline and summarize the objectives and findings of some of the published literature in the field of experimental and computational Controlled and Targeted Drug Delivery with an emphasis on matrix based drug delivery systems.

Drug delivery systems such as *emulsions, liposomes, miscelles* have been widely studied and have shown good potential as Controlled and Targeted drug delivery systems (DDS) ([6], [23], [4]). Recently, inorganic porous matrix based frameworks have emerged as potential Controlled and Targeted drug delivery systems [26]. Among the various inorganic materials that have been used to develop and study porous scaffolds as DDS, *Bioceramics* have been one of the most promising and attractive materials due to the feasibility in controlling their porosity characteristics which in-turn can be utilized to control the release kinetics. Several bioceramics have been explored by different researchers as potential DDS including Synthetic Zeolite by Fischer et al. [9], Silica Nano-Particles by Li et al. [15], Hydroxyapatite by Kim et al. [13] and the novel Silica Calcium Phosphate Composite (SCPC) by El-Ghannam et al. [7].

Previous Studies ([8], [17]) have shown that the release of drug from the ceramic matrix based DDS commences with an initial bulk release of drug at a high rate, called Burst Release Phase, followed by a slower rate of release called the Sustained Release Phase. By identifying the parameters that affect the diffusion of drug molecules

from the bioceramic matrix, drug release rate can be effectively controlled in both the Burst as well as the Sustained release stages of the release profile. For SCPC scaffolds, El-Ghannam et al. [8] showed that the porosity, pore distribution and other physical characteristics of the DDS can be tailored to control the drug release kinetics of the scaffolds.

One of the first and most pioneering works done in the field of mathematical modeling of drug release kinetics from matrix based drug delivery systems was by Takeru Higuchi. He derived the famous *Higuchi Equation* in 1961 to quantify drug release from planar systems. In 1963 he extended his work to other geometries including sphere [12]. He obtained mathematical equations for quantifying cumulative release for various model systems including *monolithic* systems, i.e the ones in which drug particles are homogeneously distributed within the matrix framework. After Higuchi, much work has been done to develop close approximate mathematical models to analyze drug release kinetics. Within the past two decades, Juergen Siepmann and his group have published a number of studies involving the computational modeling of drug delivery systems.

J.Siepmann and N.A.Peppas [18] developed mathematical models to quantitatively predict controlled drug delivery from hydroxypropyl methylcellulose (HPMC)-matrix based drug delivery systems of cylindrical geometries. Their model was based on Fick's second law of diffusion and solved for axial and radial mass transport whilst also taking matrix swelling into consideration. The work was extended in 1999 by Siepmann et al. [20] in which they improved the earlier model which allowed for the calculation of the dimensions of HPMC tablets to obtain the required drug release

profile.

Siepmann et al [22] studied the physiochemical phenomena related to drug release from matrix based drug delivery systems by using the "Sequential Layer" model to predict the release profile based on the geometry of the DDS.

J.Siepmann and F.Siepmann [21] studied how *in silico* simulations can be used to quantitatively predict the drug release kinetics. For matrix based drug delivery systems of different geometries (slab, sphere, cylinders) and types (*reservoir sytems, monolithic systems etc.*), they studied the mathematical relation between the Cumulative Drug Release ($M_t$) with the Diffusion Co-Efficient (D) of the drug within the matrix. They also provided a straightforward "roadmap" for the identification of the appropriate mathematical equations that need to be applied corresponding to the drug delivery system based on factors such as *initial drug concentration*, *drug solubility* and *device geometry*.

Y.Zhou and X.Y Wu [27] used Finite Element Method to study the diffusion controlled drug release from complex matrix based drug delivery systems. They investigated the release kinetics from matrix systems of different geometries such as inward-release hemispheres, convex tablets, rings and hollow cylinders. The effect of composite structure on the release kinetics was also investigated by them.

Chen Yin and Xicheng Li [29] presented mathematical models of drug release from non-degradable and degradable slab matrices. The mathematical models presented by them were explicitly for the cases in which the initial drug loading of the drug delivery systems were higher than the solubility. In their analysis, they also took *Anomalous Diffusions* in the drug release process into account and introduced *Frac-*

*tional Calculus* to model the phenomena. In the classical models of drug release, they replaced the diffusion equations by corresponding fractional ones and investigated anomalous diffusions.

G. Frenning and M.Stromme [10] presented a novel drug delivery model for drug delivery tablets that combined dissolution, diffusion along with taking into account the *immobilization* of drug molecules caused by adsorption to the tablets. The model proposed by them was formulated as a pair of coupled non-linear partial differential equations which were solved using Finite Difference method.

## 1.4 Vancomycin and $\alpha$-Cristobalite

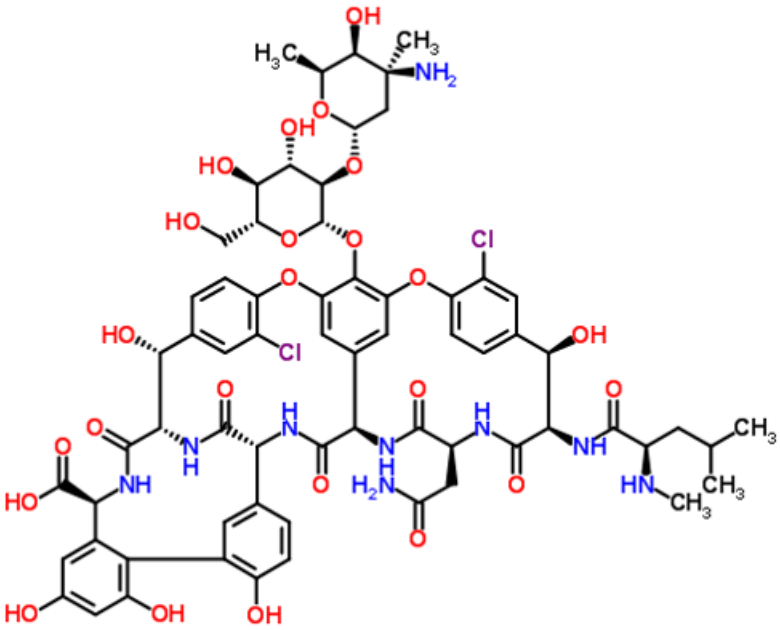


Figure 2: Molecular structure of Vancomycin (Image taken from [3].)

Figure 2 shows the molecular structure of the Vancomycin molecule. Vancomycin is a *tri-cyclic glycopeptide* antibiotic drug used commonly for treating bacterial infections.

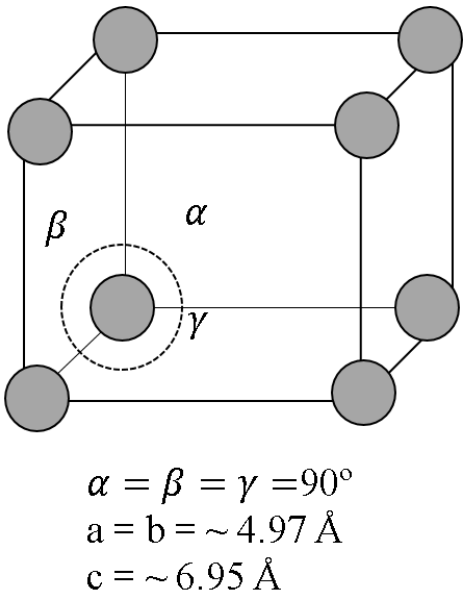


Figure 3: Unit cell of $\alpha$-Cristobalite.

$\alpha$-Cristobalite has a Tetragonal unit cell and is a highly stable polymorph of silicon dioxide $SiO_2$. It can be synthesized from $\alpha$-Quartz at temperatures higher than 1470 °C. In this study, $\alpha$-Cristobalite based porous scaffolds are developed and their efficacy as a potential drug delivery system for Vancomycin is studied. $\alpha$-Cristobalite has been chosen because it has a simple structure and does not show any significant chemical activity with Vancomycin. Thus the effect of bioceramic porosity on Vancomycin release kinetics can be independently studied.

## 1.5 Objectives of the Research

The objectives of the current study can be summarized as follows:

1. To develop porous disks of $\alpha$-Cristobalite powder with three different porosity characteristics. Also, use dense *Quartz* disks to create a reference case for 0 % porosity.

2. To perform a quantitative study to calculate the amount of *Vancomycin* loaded on disks by virtue of *adsorption* and *absorption* during drug impregnation period.

3. To perform an *in vitro* quantitative study of the release of drug in PBS, a physiological solution similar to blood in pH value and ion-concentration, and calculate the cumulative drug released (CDR) from different types of disks over time.

4. To qualitatively and quantitatively study the surface morphology and pore-size distribution of the disks using image processing technique.

5. To develop a *Finite Element Method* based computational model to study the drug release kinetics from the disks.

6. To obtain the values *Mass Transfer Co-efficient* of disk-PBS interface and *Diffusion Co-efficient* of the disks to quantify the diffusional mass transport of *Vancomycin* from the disks into the PBS.

7. To relate the results of drug release kinetics with pore size distributions.

# CHAPTER 2: EXPERIMENTAL METHODS AND ANALYSES

## 2.1 High Pressure Liquid Chromatography Analysis

### 2.1.1 Introduction and Working of HPLC System

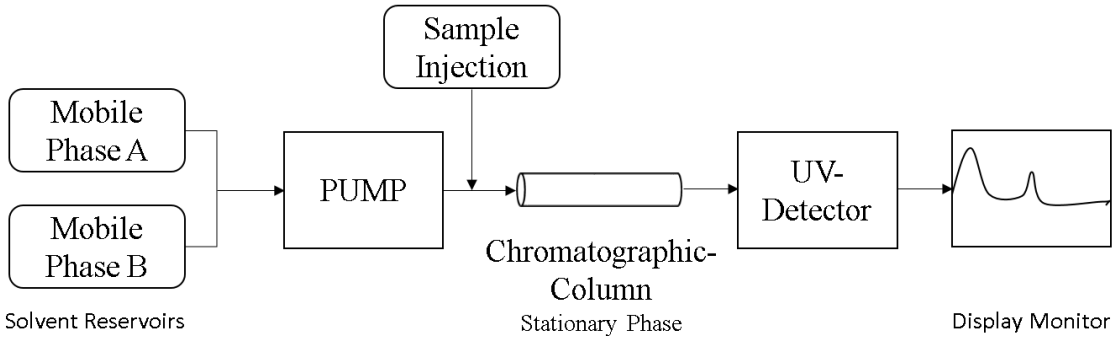


Figure 4: Schematic of the HPLC system.

*HPLC* stands for *High Pressure Liquid Chromatography*. Figure 4 shows the general schematic of an HPLC system. A high pressure pump extracts the *Mobile Phase(s)* from the solvent reservoir and passes it through a *column chromatograph* at a specified flowrate. The solution to be tested is injected into the solvent flow before it passes into the *column*. The *column*, also called *stationary phase* is packed with functional groups. When a solution passes through a column, the individual compounds of the solution acquire different velocities depending on their individual interaction with the *stationary phase*. Thus, the different compounds in the solution separate in the column due to *chromatographic* action and elude as individual bundles. Each compound *eludes* at a specific time called the *elution time*. For a given set of operating

conditions, the *elution time* remains constant irrespective of the concentration of the compound in the solution.

The flow carrying the separated compounds then travels through a UV detector which produces an analog signal whose intensity is proportional to the concentrations of the compounds in the solution. The intensity of signals corresponding to samples with known concentration of compounds, i.e *Standards*, is first obtained and a calibration curve is developed. The concentration of compounds of test samples are then obtained using the *Calibration Equation* which is the equation that mathematically represents the *Calibration Curve*.

### 2.1.2 Method for Analyzing Vancomycin Concentrations

In this study, the efficacy of $\alpha$-Cristobalite disks as a potential drug delivery vehicle for *Vancomycin* was studied. The following method parameters and operating conditions were used in the concentration analysis of *Vancomycin* solutions.

1. *Mobile Phases:* Mobile Phase A was 5 % mM $KH_2PO_4$ aqueous solution and Mobile Phase B was 100 % acetonitrile.

2. *Test Sample Preparation:* Drug solution samples that were obtained during *drug loading* and *drug release* experiments were stored in *Eppendorf Centrifuge* tubes. Before HPLC analysis, the tubes were centrifuged at 5000 rpm for 5 minutes to force particulate matter such as ceramic particles, dust etc. towards the bottom end of the tube. Then, 150 $\mu$l aliquot from the top end of the tubes were extracted and mixed in 1:1 ratio with Mobile Phase A in HPLC vials. The vials were then placed on orbital shaker for 5 minutes to mix the solutions.

3. *Injection Volume:* This is the volume of the sample that is injected into the flow stream before it enters the *chromatographic column*. The injection volume was set to be 50 $\mu$l.

4. *Column and Detector:* Eclipse XDB-C18 column (4.6 x 150 mm; 5 $\mu$m) was used to separate *Vancomycin* from solution. *Vancomycin* drug molecules were detected at a wavelength of 282 nm in UV detector.

5. *Pump Flow Setup:* Table 1 tabulates the pump setup for the HPLC analysis of *Vancomycin* solution.

Table 1: Flow scheme of Mobile Phase solvents into the chromatographic column.

| **Time (min)** | **Flow Rate (ml/min)** | **Mobile Phase A (5% mM $KH_2PO_4$** | **Mobile Phase B (100 % Acetonitrile)** |
|---|---|---|---|
| 0 | 1.5 | 80 | 20 |
| 4.0 | 1.5 | 80 | 20 |
| 4.5 | 1.5 | 0 | 100 |
| 7.0 | 1.5 | 0 | 100 |
| 7.5 | 1.5 | 80 | 20 |
| 9.0 | 1.5 | 80 | 20 |

For the given method, *Vancomycin* drug molecules eluded at around 6.2 minutes on an average in all the samples. A calibration curve for *Vancomycin* was developed using the following standards: 8 mg/ml, 4 mg/ml, 2 mg/ml, 1 mg/ml, 0.5 mg/ml, 0.25 mg/ml, 0.125 mg/ml, 0.0625 mg/ml and 0.03125 mg/ml. Using the given method, the *Coefficient of Determination*, i.e *R2* factor of the calibration curves for were around 0.997 on an average.

## 2.2 Fabrication of Porous $\alpha$-Cristobalite Scaffolds

### 2.2.1 Overview of Disk Making Procedure

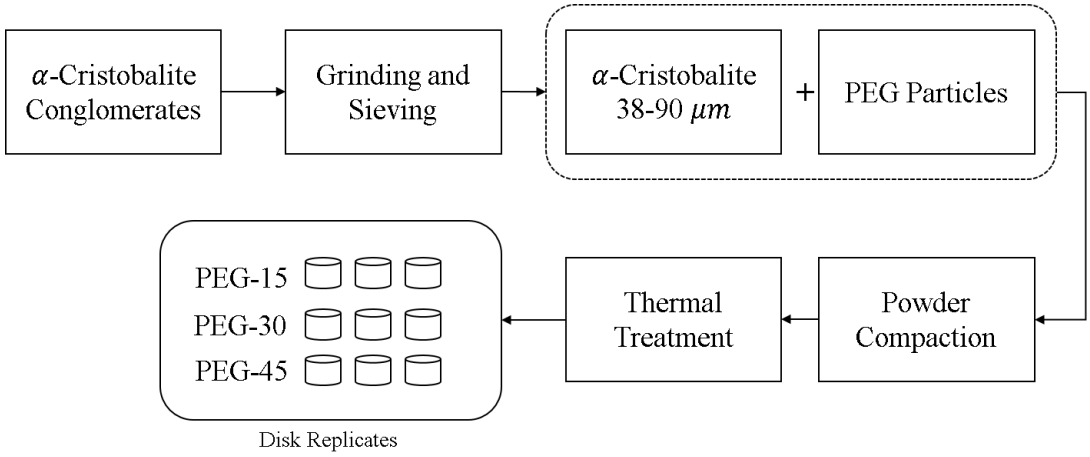


Figure 5: Flowchart of Preparation of Porous $\alpha$-Cristobalite Scaffolds.

Porous $\alpha$-Cristobalite disks of different pore size distribution were developed and their efficacy as drug delivery systems for *Vancomycin* was studied. The relation between the pore size distributions and release kinetics of $\alpha$-Cristobalite disks was also established. For creating a reference for 0 % porosity, dense $\alpha$-*Quartz* disks of the same geometric dimensions as other $\alpha$-Cristobalite disks were procured from *Quartz Scientific Inc*; see figure 9. The difference in the release kinetics between porous $\alpha$-Cristobalite disks and the dense $\alpha$-*Quartz* disks was studied.

Figure 5 shows the outline of the preparation of $\alpha$-Cristobalite disk scaffolds. $\alpha$-Cristobalite conglomerates were ground and sieved to obtain particles in the size range of 38-90 $\mu$m. The particles were then mixed with temporary space holding particles (SHP), and were compacted at high pressure to form cylindrical scaffolds. The scaffolds were then thermally treated to vaporize and exit the SHP particles

(creating a porous framework) from the disks followed by *sintering* the $\alpha$-Cristobalite particles.

### 2.2.2 Preparation of Ceramic Powder

As earlier stated, $\alpha$-Cristobalite particles in the range of 38-90 $\mu$m were used to make cylindrical disk scaffolds. The coarse conglomerates of $\alpha$-Cristobalite particles were first manually ground and then strained through a column of stack of sieves. The stack of sieves were arranged in the order of decreasing mesh size such that the lowest and the second lowest sieves had opening mesh sizes of 38$\mu$m and 90$\mu$m respectively. Vigorous horizontal shaking was used as a mean to sift the particles through the sieves. The powder accumulated over the bottom most sieve, having particles in the range of 38-90 $\mu$m, were stored and the particles from over the other sieves were extracted and ground again. This process was continued until enough $\alpha$-Cristobalite was obtained to make the required amount of disk replicates.

### 2.2.3 Pore Insemination Using Space Holding Method

A method called *Space Holding Technique* (SHT) was used for developing ceramic scaffolds with porous structure. SHT method involves mixing $\alpha$-Cristobalite particles with *Space Holding Particles*, also called *temporary particles*, homogeneously to form *ceramic-SHP* mixture. Cylindrical disks were prepared using the mixture followed by thermal treatment to vaporize and exit the temporary particles from the scaffolds. Thus, creating a porous structure.The porosity of the ceramic scaffolds is related to the % composition of the SHP in the ceramic-SHP mixture used to make the scaffolds and is higher for scaffolds made with higher composition of SHP [5].

In this study, *Polyethylene Glycol* (PEG) powder was used as a *Space Holding Material*. PEG is a biodegradable polyether compound and is a high temperature polymorph of Silica. PEG vaporizes and completely exits the ceramic scaffold during thermal treatment at much lower temperatures compared to the sintering temperature of $\alpha$-Cristobalite particles. The fumes of the PEG creates new channels and pores to facilitate its exit from the scaffold.

$\alpha$-Cristobalite particles were mixed with PEG to prepare Cris-PEG mixtures with three different compositions by mass: PEG-15 (15% PEG), PEG-30 (15% PEG) and PEG-45(15% PEG). The mixtures were thoroughly mixed using Roller Mixing method for 24 hours. It is important to note that besides porosity, which is dependent on the concentration of SHM, the pore distribution is dependent on the efficiency of the mixing procedure. Porosity levels will deviate from designed values if the efficiency of the mixing procedure is low. [5]. A number of disk scaffolds of 500 mg mass were prepared using the different Cris-PEG mixtures and then thermally treated to produce porous scaffolds; see table 2.

Table 2: Material needed for making one Cris-PEG disk scaffold.

| Type | % PEG | Material for 1 Disk (500 mg) | |
|---|---|---|---|
| | | PEG | $\alpha-$Cristobalite |
| PEG-15 | 15 % | 75 mg | 425 mg |
| PEG-30 | 30% | 150 mg | 350 mg |
| PEG-45 | 45% | 225 mg | 275 mg |

### 2.2.4 Compaction of Ceramic Powder

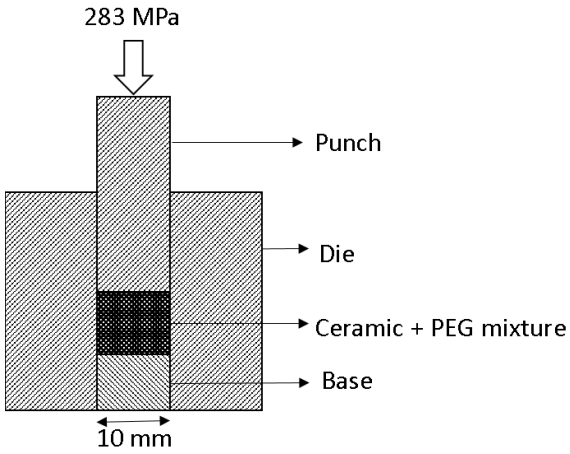


Figure 6: Illustration of compaction of Cris-PEG powder mixture in a die-Punch assembly.

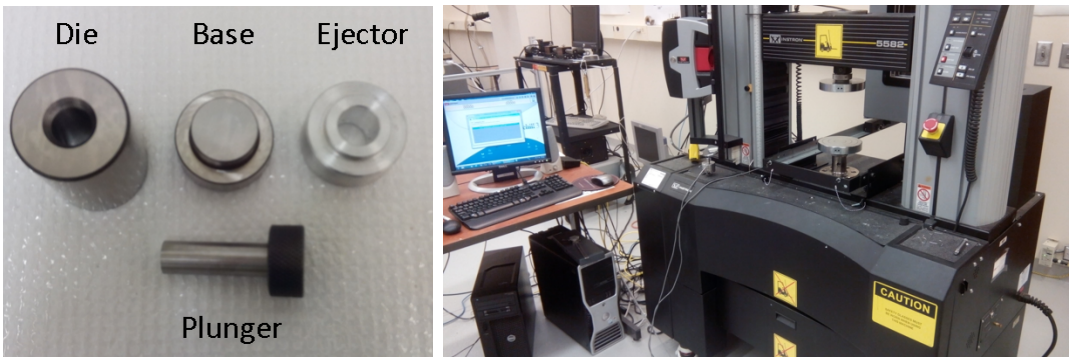


Figure 7: Photograph of the die-Punch assembly (Left) and Instron Universal Testing System (Right)

A number of cylindrical disk replicates of each type of Cris-PEG mixture (PEG-15, PEG-30 and PEG-45) were developed. For making one disk, 500 mg of Cris-PEG mixture was put in a cylindrical die of 10 mm diameter and pressed using an *Instron* hydraulic press; see figure 6 and 7. The mixtures were pressed at 283 MPa and held at this pressure for 5 minutes. At this load and holding time, the powder compacted into 5 mm disks of 10mm diameter. To increase the adhesion force between the pow-

der particles, 50-60$\mu$m of iso-propanol was added to PEG-15 mixture and 20-30 $\mu$m of water was added to PEG-30 and PEG-45 mixtures respectively before the load was applied.

### 2.2.5 Thermal Treatment of Ceramic Disks

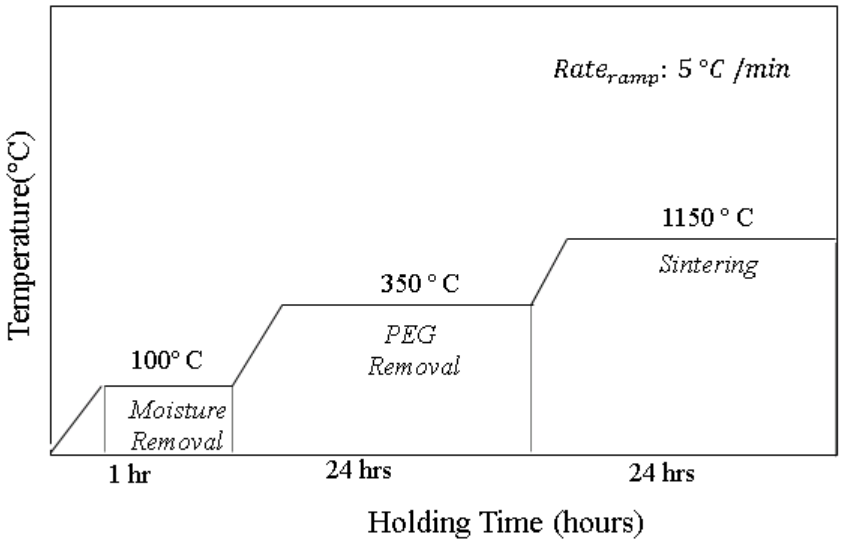


Figure 8: Thermal treatment scheme (Temperature vs Holding Time) of the Cris-PEG disks.

Table 3: Attributes of the various segments of the thermal treatment scheme.

| **Segment No** | **Segment Type** | **Attributes** |
|---|---|---|
| Segment 1 | Ramp | Target: 100 ° C<br>Rate : 5 °C/min |
| Segment 2 | Dwell | Duration: 1 hour |
| Segment 3 | Ramp | Target: 350 ° C<br>Rate : 5 ° C/min |
| Segment 4 | Dwell | Duration: 24 hours |
| Segment 5 | Ramp | Target: 1150 ° C<br>Rate : 5 ° C/min |
| Segment 6 | Dwell | Duration: 24 hours |
| Segment 7 | END | - |

Figure 8 shows the Thermal treatment scheme (Temperature vs Holding Time) of the Cris-PEG disks and table 3 tabulates and describes the attributes associated with the various segments of the thermal scheme. There are two types of segments: *ramp* and *dwell*; the former is associated with the rate of the change in temperature whereas the latter is related to the duration for which a given temperature is held. All the *ramp* segments have a 5°/min rate of ascend. The holding time or *dwell duration* is based on the time required to achieve a given specific goal like removal of space holder or to achieve *sintering*. The heat treatment was performed in a *Thermolyne Benchtop Furnace*; see figure 9.

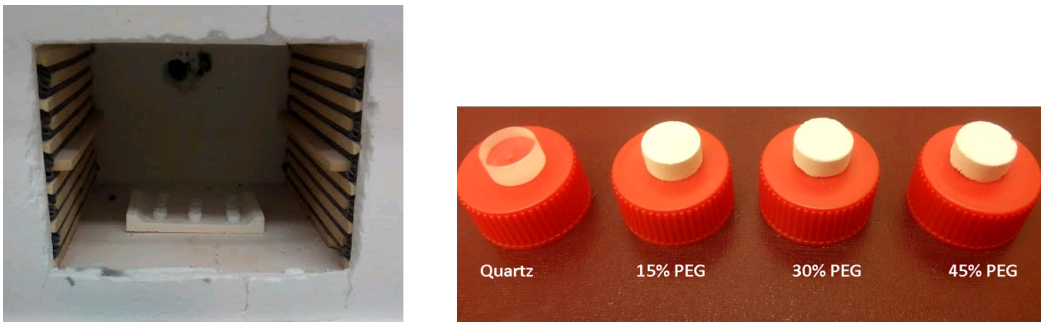


Figure 9: Picture of ceramic disks placed in the furnace before heating (left). Picture of Quartz,PEG-15,PEG-30 and PEG-45 disks (right).

The temperature of the furnace was increased from the room temperature at a rate of 5°/min to a temperature of 100°C and held at it for 1 hour. During this time all the iso-propanol/water that was used to bind the disks during powder compaction is vaporized.

The disks are then heated to a temperature of 350°C; at this temperature the PEG particles vaporize and exit the ceramic scaffold in gaseous form. The disks are held

at this temperature for 24 hours to ensure complete extraction of PEG particles from the disks. The disks are then heated to a temperature of 1150°C and held at this temperature for 24 hours to *sinter* the disks. During *sintering*, the atoms of the ceramic particles are thermally activated which leads to mass diffusion, forming a continuous framework of bonded ceramics particles [5].

## 2.3 Study of Surface Morphology of the Disks

To characterize the surface morphology and pore size distribution of the sintered disks, image analysis of sections of the disks was performed. Following subsections enumerate and explain in detail about the various steps involved in the analysis of surface characteristics of the disks.

### 2.3.1 Sample Preparation

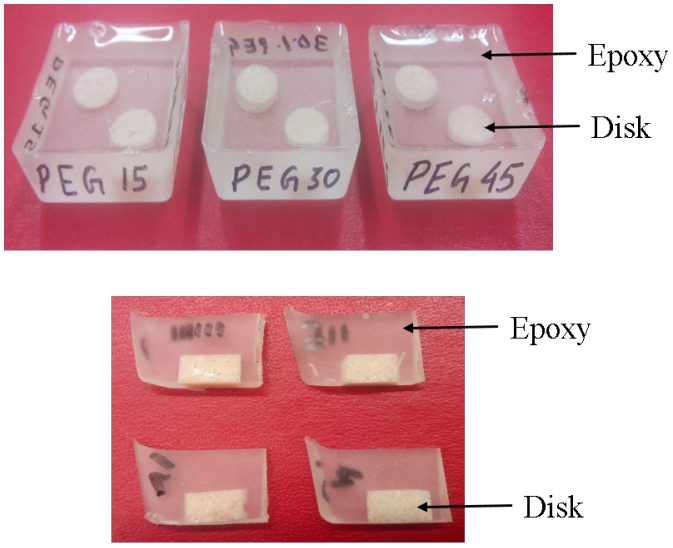


Figure 10: Image of cured Disk-Epoxy amalgamate(top). Image of thin cut sections of Disk-Epoxy amalgamate using Diamond Cutter(bottom).

The $\alpha$-Cristobalite disks were placed in an epoxy-hardener solution (*Easy-Cast Clear Casting Epoxy; Manufactured by/Fabricado por*) and cured for 48 hours in a convection oven at 60 °C. During curing process, the epoxy-hardener solution penetrates the porous framework of the disks and occupy the pore voids. After curing process, the hardened epoxy was cut using a diamond cutting tool at 400 rpm to obtain thin sections of disk-epoxy amalgamate. Figure 10 shows the image of the

hardened disk-epoxy amalgamate and the thin sections obtained from them.

### 2.3.2 SEM Imaging of Disk Sections

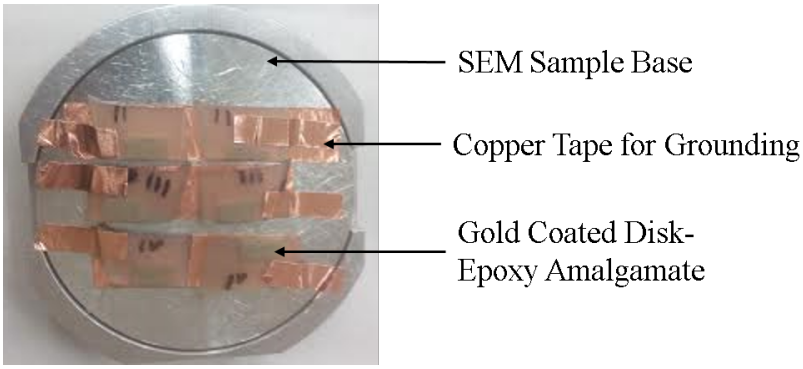


Figure 11: Image of Gold coated Disk-Epoxy amalgamate sections.

In SEM imaging, electron beams are incident on a sample and the reflected beams are scanned by a detector in a raster pattern. The intensity of the reflected beam is converted into equivalent brightness and displayed on the monitor screen. In case of non-conducting samples, a thin layer of a conducting material needs to be applied over the sample before it can be analyzed using the SEM method. As $\alpha$-Cristoabalite is a non-conducting material, the sliced sections of Disk-Epoxy amalgamate were coated with a layer of gold particles of 10 nm thickness using *Denton Desk IV-TCS Sputter Coater*. The gold coated Disk-Epoxy amalgamate sections were placed on a metallic SEM sample base and were constrained using two-sided adhesive copper tapes. These copper tapes also served as *ground* mechanism to stop the accumulation of electronic charge on the gold coated samples. Figure 11 shows the image of the gold coated sections of Disk-Epoxy amalgamate on a SEM sample base.

After coating the disks, images of the section of the disks were taken using *JEOL JSM 6480 Scanning Electron Microscope* at 5 kV. Images of different spots in the section

were taken at several magnification values ranging from *X20* to *X9000* to capture the surface morphology and pore size distribution of the samples.

### 2.3.3 Surface Characterization using Image Analysis

To analyze the surface morphology, image analysis of SEM images of the disks was performed using *ImageJ 1.50i* (modified by Wayne Rasband, National Institute of Health, USA), an image analysis package. In the analysis, the difference in the brightness intensity of pixels was utilized as a differentiating factor to filter the pores from the regular sintered surface.

The pores were found to be darker compared to the regular surface. The pore size distribution analysis involved studying the pore density (i.e. no of pores/mm$^2$) of pores in a number of pore size categories. SEM images of disks at 20x magnification was used to analyze the pore density of pores larger than 5 $\mu$m whereas SEM images of disks at 1000x+ $\mu$m were used to analyze the pore density of pores in the range of 0.1-5 $\mu$m.

It was found that several pores were occupied by epoxy-hardener solution whose brightness intensities were significantly larger compared to the empty pores. For images of disks at around 20x magnification, the pores filled with epoxy were manually *Masked* and artificially *filled* with a color of brightness intensity similar to the average empty pores. Figure 12 shows the outline of the process of identifying pores filled with epoxy followed by manually *masking* them and finally fetching the boundaries of the pores from the *masked* image.

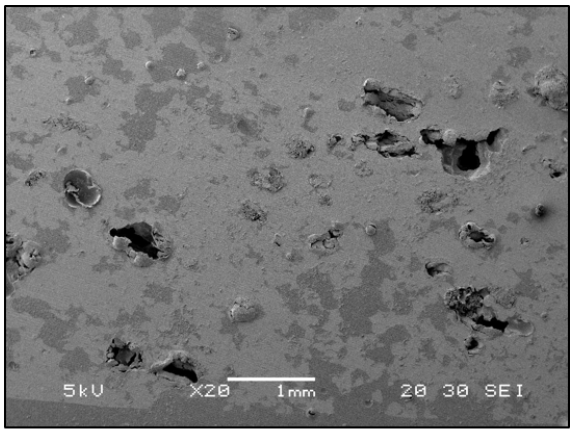


Pores Filled With Epoxy

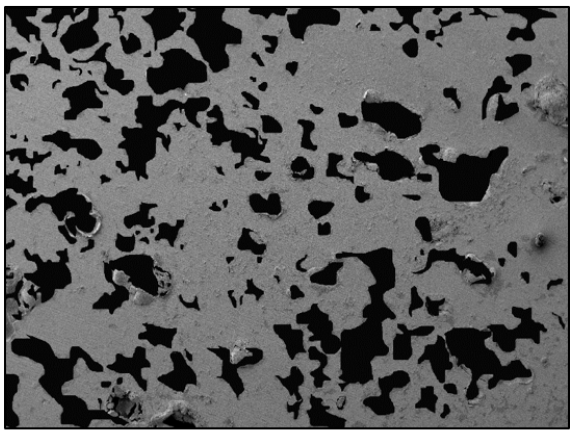

Pores identified and *Masked*.

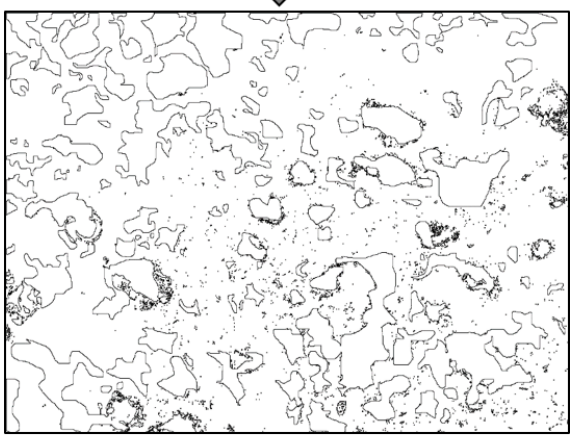

Pore Boundaries Fetched from Image

Figure 12: SEM Image of a PEG-45 disk section at 20x magnification (top). Pores filled with Epoxy identified and *masked* (middle). Image of Pore Boundaries of pores fetched from the *masked image* (bottom).

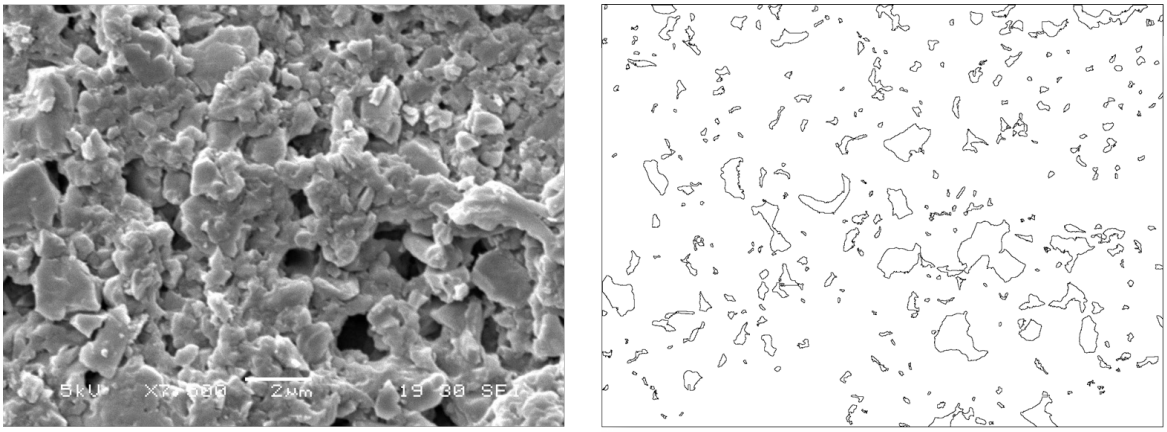


Figure 13: SEM Image of a PEG-30 disk section at 7500x magnification(left). Image of Pore Boundaries of pores larger than $0.005\mu m^2$ on PEG-30 disk section(right).

Figure 13 shows a SEM image of a PEG-30 disk section along with the pore boundaries filtered out from the image. The results obtained from the *ImageJ* were post processed using MATLAB to calculate the pore size distribution. The MATLAB code is provided in the Appendix section of this thesis.

## 2.4 Drug Loading Experiment and Analysis

### 2.4.1 Procedure of Drug Loading

*Polyphosphate Buffered Saline*(PBS), is a water based buffer solution. It is commonly used in biological research due to the similarity of PBS' ion-concentration and *osmolarity* with human blood. Also, the pH value of PBS is 7.4 which is the same as human blood [2].

*Vancomycin* drug in powdered form was added to PBS and mixed thoroughly using a magnetic stirrer for 4 hours to obtain a drug solution of 8 mg/ml concentration. The disks were placed in 22.1 mm *polystyrene* cylindrical containers and 3 ml of the drug solution was added to the containers. The axis of the disks were roughly aligned with the axis of the containers to get symmetric boundary conditions. The containers were closed using the lid and sealed by parafilm paper to minimize evaporation and left for 16 hours. The procedure was carried out at room temperature.

After 16 hours, the disks were removed and dried under ventilation hood for 24 hours to vaporize the PBS, thus leaving behind the drug molecules adhered to the exterior and the interior of the disks.

### 2.4.2 Analysis of amount of drug loaded

During the drug loading period, drug molecules in the solution adhere to the exterior surface of the disks. Also, drug solution penetrates the disks taking along drug molecules in the interior of the disks. The former process is called *adsorption* and the latter is called *absorption*. Thus, the total amount of drug loaded on the disks is due to *adsorption* as well as *absorption*. *Gravimetric* analysis was performed to calculate

the amount of drug loaded due to *absorption* and *HPLC* analysis of drug solution post drug loading was performed to calculate the amount of drug loaded due to *adsorption*.

1. *HPLC analysis of drug solution:*

   After 16 hours of drug loading, the disks were removed and 1 ml of drug solution sample was stored and labeled corresponding to the disk which was immersed in it. This sample of drug solution was analyzed by HPLC for concentration. As earlier stated, the initial concentration of the drug solution was 8 mg/ml; the change in concentration of the drug solution post drug loading is indicative of the amount of the drug loaded on the disks by virtue of the adsorption of drug molecules on the surface of the disks.

2. *Gravimetric analysis of drug absorbed:*

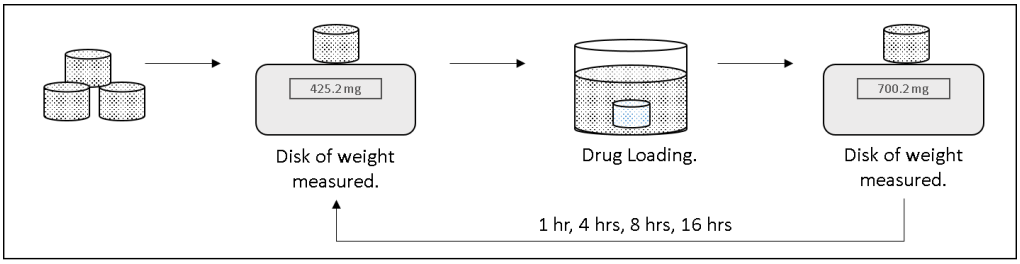


Figure 14: Illustration of the process of Gravimetric analysis to measure the volume of drug solution absorbed into the porous framework of the disks.

   (a) The disks were weighed and placed in 3 ml PBS in 22.1 mm diameter *polystyrene* cylindrical containers.

   (b) The disks were extracted from the solution using tweezers and air was blown over them using a rubber pippette bulb to blow the excess solution

adhered to the exterior of the disks back into the container. This is done so as to ensure that only the amount of drug *absorbed* into the disks is measured. The disks were weighed again and then placed back in the solution.

(c) The above steps were performed after 1 hour, 4 hours, 8 hour and 16 hours.

The value of the change in the mass of the disks was used to calculate the volume of drug solution *absorbed* by the disk using the following equation. Here, $V_{abs}$ is the volume of solution *absorbed*, $\Delta M$ is the change in the mass of the disk and $\rho_{PBS}$ is the density of the PBS solution.

$$V_{abs} = \frac{\Delta M}{\rho_{PBS}} \tag{4}$$

## 2.5 Drug Release Experiment and Analysis

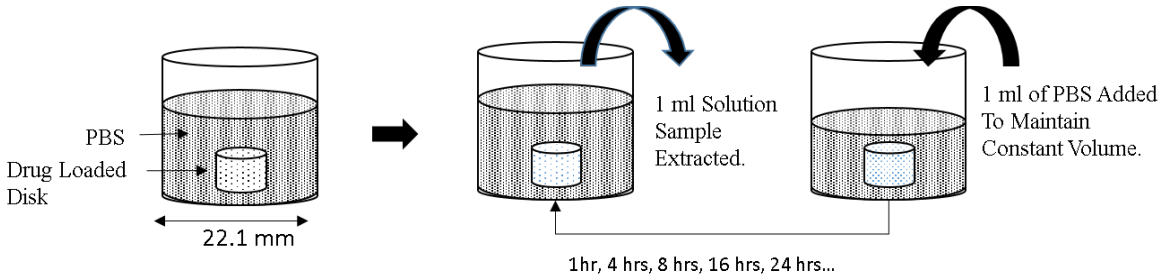


Figure 15: Illustration of the Drug Release Experiment to measure the amount of Cumulative Drug Release (CDR) wrt. time.

The purpose of this experiment was to perform an in-vitro drug release analysis from disks under physical and chemical conditions which are similar to the human body. The drug loaded disks were placed at the center of polystyrene cylindrical containers filled with 3 ml of PBS on an orbital shaker. The analysis was carried out in

Fisher Scientific's $CO_2$ incubator at 37°C, which is same as the normal human body temperature.

When the disks are placed in the PBS, drug molecules loaded on the disks start releasing into the solution. To calculate the cumulative drug release over a period of time, 1ml of solution was removed at a number of time intervals and replenished with the same volume of fresh PBS to maintain the constant volume. The samples obtained were analyzed by HPLC for concentration.

From earlier studies on ceramic based drug delivery systems, we know that the rate of drug release is highest during the first few hours followed by which a more sustained release of drug is obtained [8]. Thus, for an accurate study of the drug release phenomenon, more samples need to be taken during the first few hours after the disks are placed in the physiological solution. The time points chosen to study the drug release phenomenon were 1 hour, 4 hours, 8 hours, 16 hours, 24 hours and after which the sampling was done after every 48 hour interval. The concentration values of the samples at different time points were used to calculate the cumulative drug released into the PBS using equation 5.

$$CDR^n = C_n V_T + \sum_{i=1}^{n-1} C_i V_S \tag{5}$$

The nomenclature associated with equation 5 are as follows:

$CDR^n$: Cumulative Drug Released by the nth sampling. $C_n$: Concentration of nth sample of solution. $V_T$: Total volume of the solution in the container(3ml). $V_S$: Volume of Sample Extracted(1ml).

# CHAPTER 3: COMPUTATIONAL MODELING AND ANALYSIS

## 3.1 Overview of the Drug Release Process

An overview of the results from the Drug Release experiment that are relevant to the development of the computational model of the drug delivery system have been summarized as follows:

1. From the study of Cumulative Drug Release (CDR) over time, it was found that in all the disk types, there was a bulk release of drug during the first 1 hour. This phase of the drug release profile is called the *Burst Release* phase. Maximum amount of drug was released during this period. Burst Release phase involves the sudden dissolution of the drug molecules that are deposited on the outer surface of the disk into the PBS. The drug release as a percentage of the total drug loaded was highest in the first 1 hour.

2. After the burst release phase, the rate of drug release decreased and a more sustained release profile was obtained. This phase of the drug release regime is called the *Sustained Release* phase. The sustained release phase involves the gradual release of drug molecules from the inner portions of the disk matrix into the PBS.

## 3.2 Assumptions Made for Developing the Model

Drug release from matrix based drug delivery systems is a complex phenomenon which is affected by several factors and physical processes. The primary or significant factors need to be taken into account for developing the computational model while the secondary factors can be ignored so as to simplify the problem without compromising much on the accuracy of the solution. Following assumptions were made in developing the FEM model:

1. $\alpha$-Cristobalite disks are Monolithic drug delivery systems, i.e the distribution of drug molecules within the disks is homogeneous.

2. The problem is assumed to be axisymmetric.

3. The penetration of PBS solution within the disks is a rapid process and the diffusion of drug molecules from the disks into the PBS solution is the rate limiting step.

4. There is no significant swelling, contraction or erosion of disk scaffold in the solution during analysis, i.e the domain and the boundaries of the disks are *static* and do not vary with time. Also, the volume of drug solution is assumed to be constant through out the analysis and the amount of vaporization of the drug solution is considered insignificant.

5. Their is no chemical activity between Vancomycin and $\alpha-$Cristobalite. Also, there is no degradation of Vancomycin molecules during the analysis.

6. Dissolution of drug from the outer surface of disk into the physiological solution is followed by the diffusion of the drug from within the ceramic matrix into the solution, i.e drug release is a *sequential process* with Burst Release phase of the drug molecules occurring first followed by a Sustained Release phase.

### 3.3 Modeling Burst Release as a Mass Convection Problem

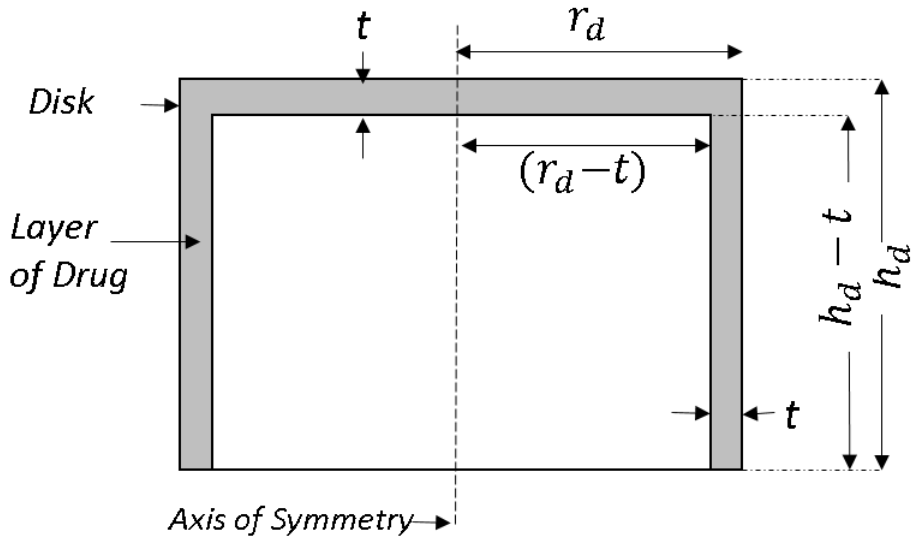


Figure 16: Nominal dimensions of the adhered layer of drug on the disks based on the assumption that the drug was uniformly adsorbed on all the exposed surfaces of the disks during drug loading.

$$V_{ads} = \frac{M_{Burst}}{\rho_{vanc}} \tag{6}$$

$$h_d \pi r_d^2 - (h_d - t)\pi(r_d - t)^2 = \frac{M_{Burst}}{\rho_{vanc}} \tag{7}$$

$$r_d = h_d \tag{8}$$

$$t = r_d - \sqrt[3]{\frac{1}{\pi}\left(\pi r_d^3 - \frac{M_{Burst}}{\rho_{vanc}}\right)} \tag{9}$$

During the burst release phase, layers of drug molecules that are adhered to the outer surface of the disks diffuse into the physiological solution. Based on the assumption that the layer of adhered drug molecules has a uniform thickness, the value of the thickness($t$) was calculated using equations 6-9. In equation 6, $\rho_{vanc}$ is the density of Vancomycin drug, $V_{ads}$ is the volume of adsorbed drug layer and $M_{burst}$ is the average mass of drug released from disks by the end of burst release phase, which was found by experimental analysis. The dimensions of the adsorbed drug layers are illustrated in figure 16. Here, $r_d$ is the radius of the drug and $h_d$ is the height of the disk.
Using equation 9, the average thickness of the adsorbed drug layers were calculated for Quarts, PEG-15, PEG-30 and PEG-45 disks. The nominal value of the thickness of the adsorbed layer of drug on the disks are reported in table 4.

Table 4: Nominal value of the thickness of the adsorbed layer of drug on the disks based on the assumption that the drug was uniformly adsorbed on all the exposed surfaces of the disks during drug loading.

| Type | $M_{Burst}$ (mg) | t ($\mu$m) |
|---|---|---|
| Quartz | 0.2177 | 0.54 |
| PEG-15 | 1.6620 | 4.15 |
| PEG-30 | 1.9226 | 4.8 |
| PEG-45 | 2.5074 | 6.26 |

As reported in table 4, the thickness of adhered drug molecules range from 0.5 $\mu$m to 6.26 $\mu$m. The value of thickness is negligible compared to the dimensions of the

disks. Based on this result, the Burst Release phase, i.e the dissolution of adhered drug molecules into the PBS was treated as a mass convection boundary problem. The interaction layer between the PBS and the disk was set a mass convection boundary with $\rho_{PBS}$ as the sink concentration.

## 3.4 Overview of Modeling Technique

The drug release process was modeled as a sequential two step process. The first step was the Burst Release process which was followed by the Sustained Release process. For the former step, only the PBS region was modeled whereas for the latter step, both the PBS and the disk were modeled.

The computational analysis of the burst release phase was done to study the bulk release of drug molecules adhered to the outer surface of the disk into the PBS. The study involved the calculation of $K_c$, Mass Transfer Co-efficient. $K_c$ is an interaction characteristic of the Disk-PBS interface. Higher the $K_c$, higher would be the bulk release during the Burst-Release phase.

The computational analysis of the sustained phase was done to study the rate of drug release from the inner regions of the disk into the PBS. The study involved the calculation of $D$, Diffusion Co-Efficient of the disks. $D$ characterizes the rate of drug transport within the disk. Higher the $D$, higher would be the rate of drug release during the sustained phase.

Due to the axisymmetric nature of the problem 1D-Axisymmetric and 2D-Axisymmetric Finite Element Models for the two processes were developed and solved for concentration. The nodal concentration values of the elements of the PBS region were used to

compute the cumulative drug release (CDR) from 1D and 2D models. The equations for calculating the CDR from the nodal concentration values of the PBS regions from 1D and 2D models are stated and derived in section 3.5. ABAQUS/Standard v6.11-3, a commercial FEM package, was used to develop the computational model. *Python* was used to run the analysis and fetch *Field Output* and *History Output* data from *ABAQUS*. *MATLAB 2013b* was used to post process the results and calculate the CDR using the nodal concentration values of the PBS domain.

### 3.4.1 Modeling Burst Release Phase

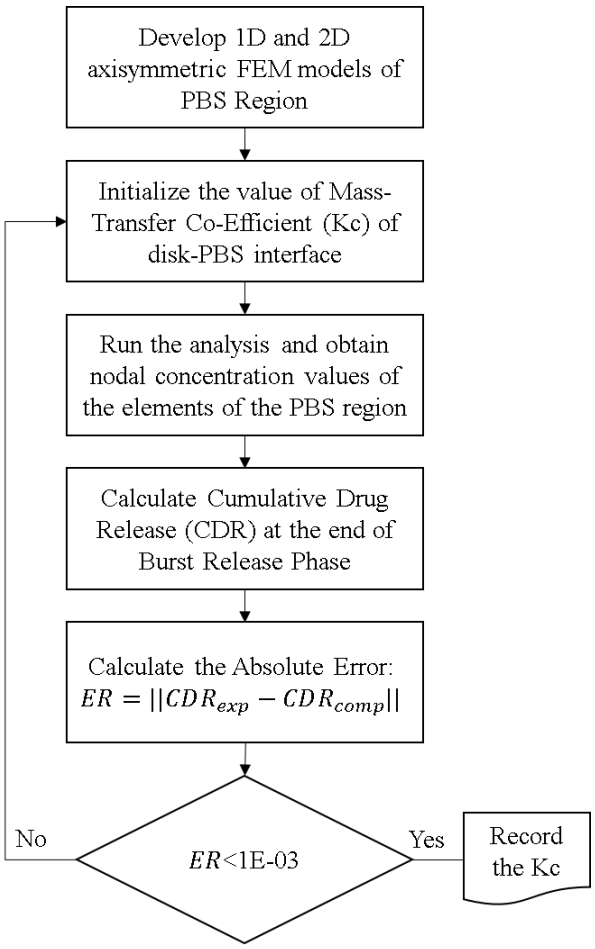


Figure 17: Flowchart of the Burst Release analysis and calculation of the Mass Transfer Co-Efficient(Kc) of the disk-PBS interface.

The disk-PBS interface region was set as a convective mass transfer boundary. The Mass Transfer Co-efficient of the disk-PBS interface region was initialized and the corresponding CDR was calculated using the nodal concentrations of the elements in the PBS region. The process was iteratively repeated until the *Absolute Error* between the experimental and computationally computed CDR was below the threshold value of 1E-03.

### 3.4.2 Modeling Sustained Release Phase

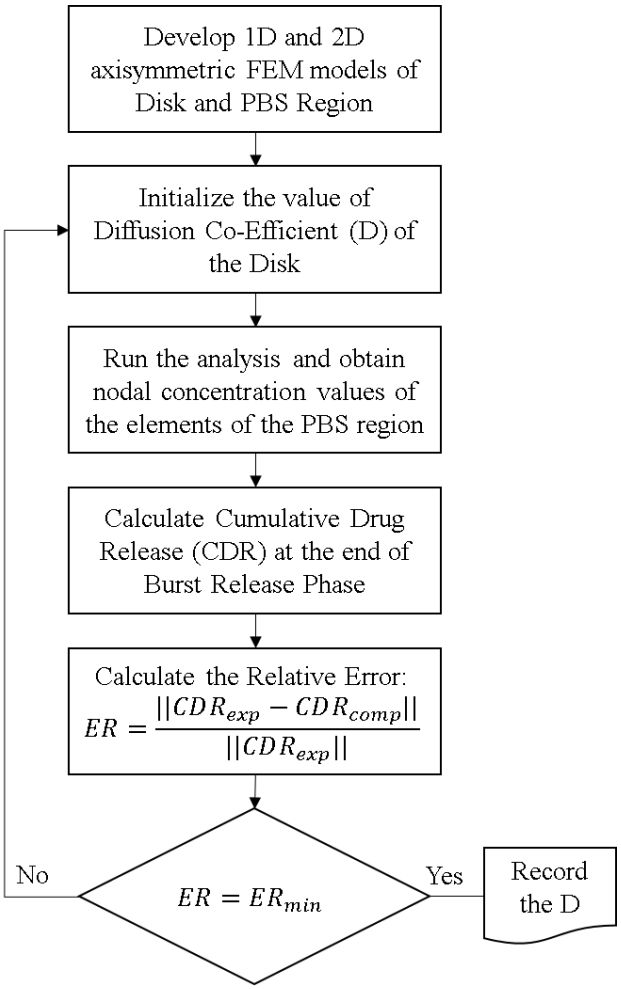


Figure 18: Flowchart of the Sustained Release analysis and calculation of the Diffusion Co-Efficient(D) of the disk.

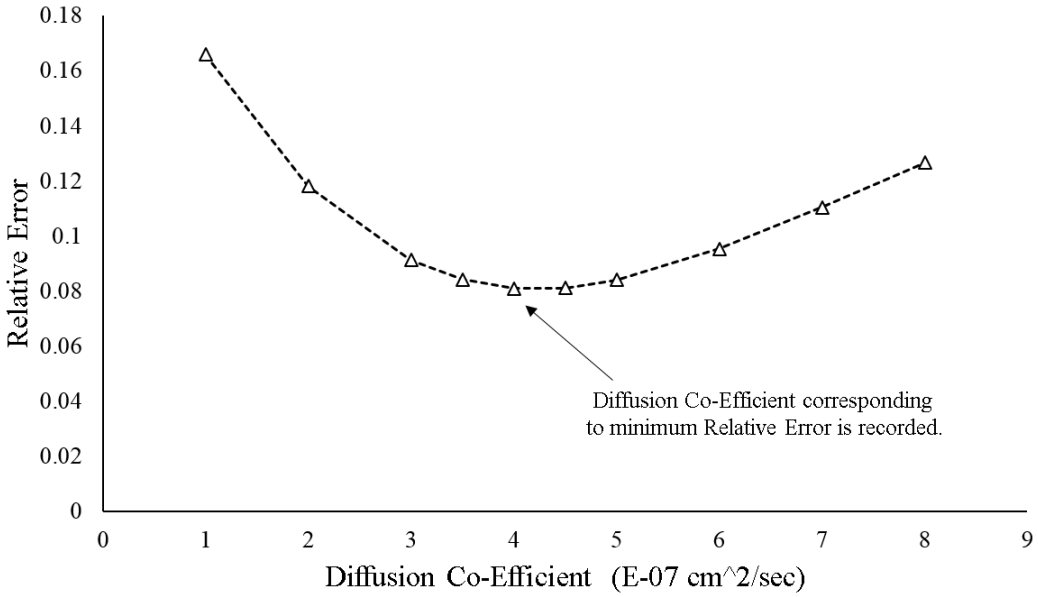


Figure 19: Illustration of the change in Relative Error (between experimental and computational CDR) wrt. Diffusion Co-Efficient for one of the disk replicates.

The concentration field of the PBS region at the last increment of the Burst Release phase was set as the initial condition of the PBS region in the Sustained Release phase. The Diffusion Co-efficient of the disk region was initialized and the corresponding CDR was calculated using the nodal concentration values of the elements in the PBS region as outlined in the flowchart in figure 18. The value of Relative Error between the experimental and computationally computed CDR in the PBS region is a function of the value of the Diffusion Co-efficient of the disk. Figure 19 shows the plot of the change in the Relative Error between experimental and computational CDR) wrt. Diffusion Co-Efficient for one of the disk replicates. As shown in figure 19, for a specific Diffusion Co-Efficient value of the disk, the Relative Error between the experimental and computationally computed CDR reached a minimum value, $ER_{min}$. The process as outlined in figure 18 was iteratively repeated until the value of Diffu-

sion Co-Efficient of disk was such that the Relative Error (ER) matched the $ER_{min}$ upto atleast the first decimal place. Also, corresponding to the obtained values of Diffusion Co-Efficient, the Relative Error was also recorded and is reported in the final chapter of the thesis.

## 3.5 Calculation of Cumulative Drug Release

The concentration values at the nodes of the elements are obtained and the value of the cumulative drug release is calculated and compared with the experimental value. This section describes as how the cumulative drug release is computed using the nodal concentration values for 1D and 2D analysis. The cumulative drug released by the disk is equal to the cumulative drug absorbed by the PBS.

$$M(t) = \int_{\Omega} c(\Omega, t) d\Omega \tag{10}$$

In equation 10, $M$ is the cumulative drug released into the PBS solution at any time $t$. The domain of the PBS solution is defined by the region $\Omega$. Here, $c(\Omega, t)$ is the concentration at time $t$ of the solution at a spatial location within the domain $\Omega$.

$$M^e(t) = \int_{\Omega^e} c^e(\Omega^e, t) d\Omega^e \tag{11}$$

$$M(t) = \sum_{e=1}^{nel} M^e(t) \tag{12}$$

After discretizing the domain $\Omega$ using the FEM approach, the cumulative drug released into the PBS solution can be written as the sum of the cumulative drug released over the elements, $M^e$. This is mathematically represented by equation 11 and 12.

Here, $c^e(\Omega^e, t)$ is the value of concentration over element $e$ and $nel$ is the total number of elements. The value of $c^e(\Omega^e, t)$ can be approximated using shape functions and concentration at the nodes of the element $e$.

### 3.5.1 Cumulative Drug Release from 1D Analysis

The instantaneous drug concentration over element $e$ for a 1D axisymmetric problem domain is given by equation 13.

$$c^e(\Omega^e, t) = \sum_{a=1}^{n} N_a(r) c_a^e(t) \tag{13}$$

In equation 13, $n$ is the number of nodes in the element $e$; as this is a 1D case, n=2. $N_a$ and $c_a^e(t)$ is the shape function and nodal concentration over the element $e$. Here $r$ is the radial co-ordinate of the axisymmetric problem. The value of $c^e(\Omega^e, t)$ in equation 13 is put in equation 11 to get the cumulative drug released over 1D axisymmetric element. This is shown in equation 14 and further simplified in 15

$$M^e(t) = \int_{\Omega^e} \left[ \sum_{a=1}^{n} N_a(r) c_a^e(t) \right] d\Omega^e \tag{14}$$

$$M^e(t) = \sum_{a=1}^{n} c_a^e(t) \int_{\Omega^e} N_a(r) d\Omega^e \tag{15}$$

In case of 1D axisymmetric problem, the differential element, $d\Omega^e$ can be written in terms of $dr^e$ as shown by equation 16. In equation 16, h is chosen to be the sum of *h1* and *h2* which are the radius and height of the disks respectively. This is done to take into account the drug release from the periphery of the disks along with the top

surface of disk.

$$d\Omega^e = 2\pi h r dr \tag{16}$$

$$d\Omega^e = 2\pi(h1 + h2) r dr \tag{17}$$

From equation 15 and 16, the cumulative drug released over an element can be written as shown in equation 18. Here, the integration limits $r_1$ and $r_2$ are the radial co-ordinates of the nodes of the 1D element $e$.

$$M^e(t) = 2\pi h \sum_{a=1}^{n} c_a^e(t) \int_{r_1}^{r_2} r N_a(r) dr \tag{18}$$

In equation 18, the integral term is mapped from the physical domain $r \in [r_1, r_2]$ to the parent domain $\xi \in [-1, 1]$. This is represented by equation 19 and further simplified to equation 23 using the relations as given in equations 20,21 and 22. Here, $l_e$ is the length of the element. Also, $\mathrm{r}_1$ and $\mathrm{r}_2$ are the nodal values of the radial co-ordinate in the parent domain.

$$M^e(t) = \pi h l_e \sum_{a=1}^{2} c_a^e(t) \int_{-1}^{1} r(\xi) N_a(\xi) d\xi \tag{19}$$

$$r(\xi) = r_1 N_1(\xi) + r_2 N_2(\xi) \tag{20}$$

$$N_1(\xi) = \frac{1}{2}(1 - \xi) \tag{21}$$

$$N_2(\xi) = \frac{1}{2}(1 + \xi) \tag{22}$$

$$M^e(t) = \pi h l_e \sum_{a=1}^{2} c_a^e(t) \int_{-1}^{1} [r_1 N_1(\xi) + r_2 N_2(\xi)] N_a(\xi) d\xi \tag{23}$$

The summation term in equation 23 is expanded and the integral terms are solved to obtain equation 24 which represents cumulative drug released over an element at

time $t$. The values of $M^e(t)$ are added for all the elements to obtain the cumulative drug released over the entire PBS domain, as earlier shown.

$$M^e(t) = \pi h l_e \left[ c_1 \left( \frac{2}{3} r_1 + \frac{1}{3} r_2 \right) + c_2 \left( \frac{1}{3} r_1 + \frac{2}{3} r_2 \right) \right] \tag{24}$$

### 3.5.2 Cumulative Drug Release from 2D Analysis

For 2D analysis, the differential element $d\Omega^e$ can be expressed in terms of dr,d$\theta$ and dz as shown in equation 25. Due to cylindrical nature of the disks, the definite integral of d$\theta$ over the domain becomes $2\pi$; thus equation 25 can be expressed as equation 26.

$$d\Omega^e = r d\theta dr dz \tag{25}$$

$$d\Omega^e = 2\pi r dr dz \tag{26}$$

The value of d$\Omega^e$ is put in equation 11 to obtain the expression of cumulative drug released over a 2D axisymmetric element; as shown by equation 27.

$$M^e(t) = 2\pi \int_{\Omega_e} c^e(\Omega^e, t) r dr dz \tag{27}$$

In equation 27, c$^e$($\Omega^e$,t) is the value of drug concentration in element e at time $t$. The value of concentration, c$^e$($\Omega^e$,t) can be approximated using shape functions as shown in equation 28. The value of c$^e$($\Omega^e$,t) is put in equation 27 to obtain the cumulative drug released over the element $e$, as shown in equation 29.

$$c^e(\Omega, t) = \sum_{a=1}^{4} N_a(r, z) c_a^e(t) \tag{28}$$

$$M^e(t) = 2\pi \int_{\Omega_e} \left[ \sum_{a=1}^{4} N_a(r, z) c_a^e(t) \right] r dr dz \tag{29}$$

In equation 29 the integral domain is mapped from the physical domain to the parent domain to obtain equation 24. In equation 24, $r_a$ is the nodal value of radial co-ordinate $r$ which is approximated using shape functions over the parent domain. $A_e$ is the area of the element $e$.

$$M^e(t) = \frac{\pi A_e}{2} \int_{-1}^{1} \left[ \sum_{a=1}^{4} N_a(\xi, \eta) c_a^e(t) \right] \left[ \sum_{a=1}^{4} N_a(\xi, \eta) r_a \right] d\xi d\eta \tag{30}$$

$$r = \frac{r_1}{2} - \frac{r_1 \xi}{2} + \frac{r_2}{2} + \frac{r_2 \xi}{2} \tag{31}$$

In iso-parametric formulation, the radial co-ordinate r can be expressed as shown in equation 31. Here,$r_1$,$r_2$ etc. are the nodal values of the radial co-ordinate in the parent domain. The summation term in equation 30 is expanded and the integral terms are solved to obtain equation 32 which represents cumulative drug released over an element at time $t$. Here,$c_1$,$c_2$ etc. are the nodal concentration values over the element $e$.

$$M^e(t) = \frac{\pi A_e}{2} \left[ \left( \frac{2c_1}{3} + \frac{c_2}{3} + \frac{c_3}{3} + \frac{2c_4}{3} \right) r_1 + \left( \frac{c_1}{3} + \frac{2c_2}{3} + \frac{2c_3}{3} + \frac{c_4}{3} \right) r_2 \right] \tag{32}$$

The values of $M^e(t)$ are added for all the elements to obtain the cumulative drug released over the entire PBS domain, as earlier shown.

## 3.6 One-Dimensional Analysis of Burst Release Phase

### 3.6.1 Governing Equations and Boundary Conditions

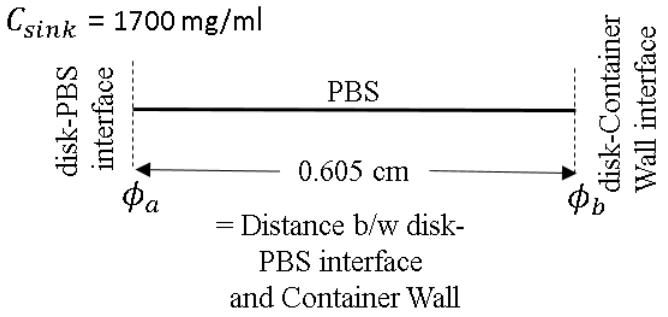


Figure 20: Domain Description of the 1D Burst Release Axisymmetric Model.

$$\frac{\partial C}{\partial t} = D_{PBS}\frac{\partial^2 C}{\partial^2 r} \tag{33}$$

$$D_{PBS}\frac{\partial C}{\partial r}\bigg|_{\phi_a} = K_{1D}(C_{sink} - C|_{\phi_a}) \tag{34}$$

$$D_{PBS}\frac{\partial C}{\partial r}\bigg|_{\phi_b} = 0 \tag{35}$$

As earlier stated, in the analysis of the 1D Burst Release phase, only the PBS region was modeled. The governing differential equation and the boundary conditions of the problem are stated from equations 33 to 35. Here, $r$ is the radial co-ordinate, $D_{PBS}$ is the diffusion co-efficient of PBS, C is the concentration field in the PBS domain, $K_{1D}$ is the mass transfer co-efficient and $C_{sink}$ is the sink concentration at the disk-PBS interface. Equation 33 is the one dimensional form of *Fick's Second Law* of Diffusion. Equation 34 represents the mass convection boundary condition of the disk-PBS interface. Equation 35 represents the *impermeability* boundary condition

on the interface between the disk and the container wall.

### 3.6.2 ABAQUS-FEM Modeling Parameters

Following computational parameters were used for modeling the 1D burst release phase:

1. *Analysis Type and Requested Output*: The governing differential equations of *Mass Transfer* and *Heat Transfer* problems are analogous to each other. The 1D Burst Release process was modeled as an axisymmetric transient heat transfer problem. The physical time duration of the analysis was chosen to be 1 hour as it was the duration of the Burst Release phase. The nodal concentration values of the PBS region were requested as a *Field Output* at the end of the Burst Release phase. The initial, minimum and maximum time increment for the analysis was chosen to 1 seconds, 1 seconds and 100 seconds respectively. The maximum temperature change per increment was set to 0.25 ° C.

2. *Geometry and Material Properties*: The PBS domain was created in ABAQUS *Part Module* as an axisymmetric *wire* of length 0.605 cm, which was the distance between the disk and the container wall, as shown in figure 20. Figure 21 shows the image of the 1D PBS domain as developed in ABAQUS. The value of Density($\rho$) and Specific-Heat($C_p$) were set to unity to make the heat transfer differential equations analogous to the mass transport equations. The value of Diffusion Co-efficient of PBS was assumed to be the same as water and was set to 2.3e-5 $cm^2$/sec.

3. *Boundary and Initial Conditions*: Node $\phi_a$, as shown in figure 21, was given a *Concentrated Film Condition*. This is the same as the convection/dissolution boundary condition represented by the equation 34. The sink value, $C_{sink}$ was set as 1700 mg/ml which is the same as the density of the Vancomycin [3]. The node $\phi_b$ was set as an *insulated* boundary. The initial value of temperature of the PBS region was set to 0 ° C.

4. *Mesh Characteristics and Element Type*: The PBS domain was given a mesh seeding of 5E-04 cm. The element type was chosen to be DCCAX2 which is a 2-noded linear axisymmetric convection/diffusion element [1].

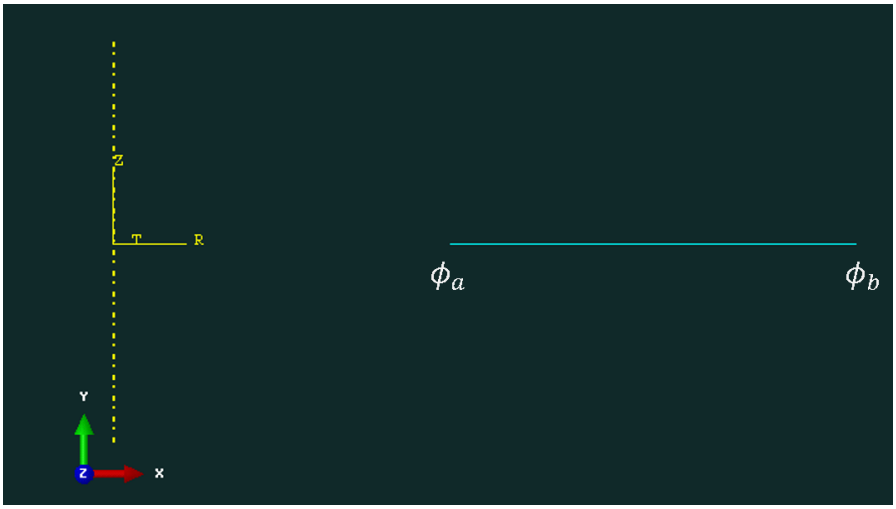


Figure 21: Domain of 1D Burst Release Model developed in ABAQUS.

### 3.6.3 Calculation of Mass Transfer Co-Efficient

The nodal temperature values of the 1D PBS domain were obtained and saved in a data file (.dat), using which, the value of the CDR at the end of the Burst Release phase was calculated using equation 24. The values of Mass Transfer Co-efficient of the disks were obtained as described in section 3.4.1.

## 3.7 Two-Dimensional Analysis of Burst Release Phase

### 3.7.1 Governing Equations and Boundary Conditions

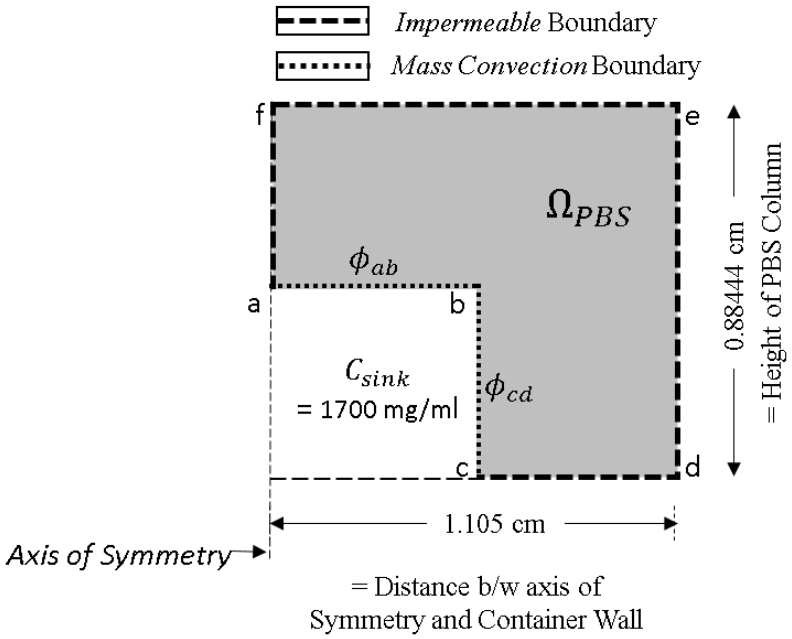


Figure 22: Domain Description of the 2D Burst Release Axisymmetric Model.

In figure 22 is shown the domain for the 2D Burst Release model. The boundary lines $\phi_{ab}$ and $\phi_{cd}$ represent the disk-PBS interface and are shown on figure 22 by dotted lines. The length of $\phi_{ab}$ is 0.5 cm which is equal to the radius of the disk and the length of $\phi_{bc}$ is equal to the height of the disk, i.e 0.5 cm. The height, H of the PBS column is 0.88444 cm and is calculated using equations 36 and 37.

$$H = \frac{4}{\pi D^2}(V_D + V_S) \tag{36}$$

$$V_D = \frac{\pi d^2}{4} h_d \tag{37}$$

In equations 36 and 37, $D$ is the diameter of the container (2.21 cm), $d$ is the

diameter of the disk (1 cm), $h_d$ is the height of the disk (0.5 cm), $V_D$ is the volume of the disk and $V_S$ is the volume of the PBS solution (3 ml).

$$\frac{\partial C}{\partial t} = D_{PBS}\nabla^2 C(r,z) \tag{38}$$

$$D_{PBS}\nabla|_{\phi_{ab}} = K_{2D}(C_{sink} - C|_{\phi_{ab}}) \tag{39}$$

$$D_{PBS}\nabla|_{\phi_{cd}} = K_{2D}(C_{sink} - C|_{\phi_{cd}}) \tag{40}$$

$$D_{PBS}\nabla|_{af,fe,ed,cd} = 0 \tag{41}$$

As in case of 1D burst release, in 2D burst release analysis, only the PBS region is modeled. The governing differential equation and the boundary conditions of the problem are stated from equations 38 to 41. Here $r$ and $z$ are the radial and azimuthal co-ordinates respectively. $D_{PBS}$ is the diffusion co-efficient of PBS, C is the concentration field in the PBS domain, $K_{2D}$ is the Mass Transfer Co-efficient and $C_{sink}$ is the sink concentration of the disk-PBS interface. Equation 38 is the two dimensional form of *Fick's Second Law* of diffusion. Equation 39 and 40 represent the mass convection boundary condition on the disk-PBS interface. Equation 41 represents the *impermeability* boundary condition on the interface between the disk and the container wall as well as the top open surface of the PBS. The cumulative drug release (CDR) is calculated using the nodal concentration values of the PBS region and compared with the experimental results to compute the value of mass-transfer coefficient of the disk-PBS interface, i.e. $K_{2D}$.

### 3.7.2 ABAQUS-FEM Modeling Parameters

Following computational parameters were used for modeling the 2D burst release phase:

1. *Analysis Type and Requested Output*: The 2D burst release process is modeled as an axisymmetric transient heat transfer problem. The physical time duration of the analysis was chosen to be 1 hour. The value of nodal concentration of all the nodes in the PBS region were requested as a *Field Output* at the end of the 1 hour as it was the duration of the Burst Release phase. The initial, minimum and maximum time increment for the analysis was chosen to 1 seconds, 1 seconds and 100 seconds respectively. The value of the maximum temperature change per increment was set to 0.25 ° C.

2. *Geometry and Material Properties*: The PBS domain was created in ABAQUS *Part Module* as axisymmetric *shell* with the dimensions as shown in figure 22. Figure 23 shows the image of the 2D PBS domain as developed in ABAQUS. The values of Density($\rho$), Specific-Heat($C_p$) and Diffusion Co-efficient of the PBS domain were set the same as in case of 1D Burst Release analysis.

3. *Boundary and Initial Conditions*: The edges $\phi_{ab}$ and $\phi_{bc}$, see figure 23, were given a *Surface Film Condition*. This is the same as the convection/dissolution boundary condition given by equation 39 and 40. The sink value, $C_{sink}$ was set as 1700 mg/ml, which is the same as the density of Vancomycin. The remaining edges were set as *insulated* boundaries. The initial value of temperature in the

PBS region was set to 0.

4. Mesh Characteristics and Element Type: The PBS domain was partitioned as shown in figure 23 and then each edge was given a mesh seeding of 0.0125 cm. This was done to obtain square elements of equal dimensions throughout the PBS domain. The element type was chosen to be DCCAX4 which is a 4-noded axisymmetric convection/diffusion element [1].

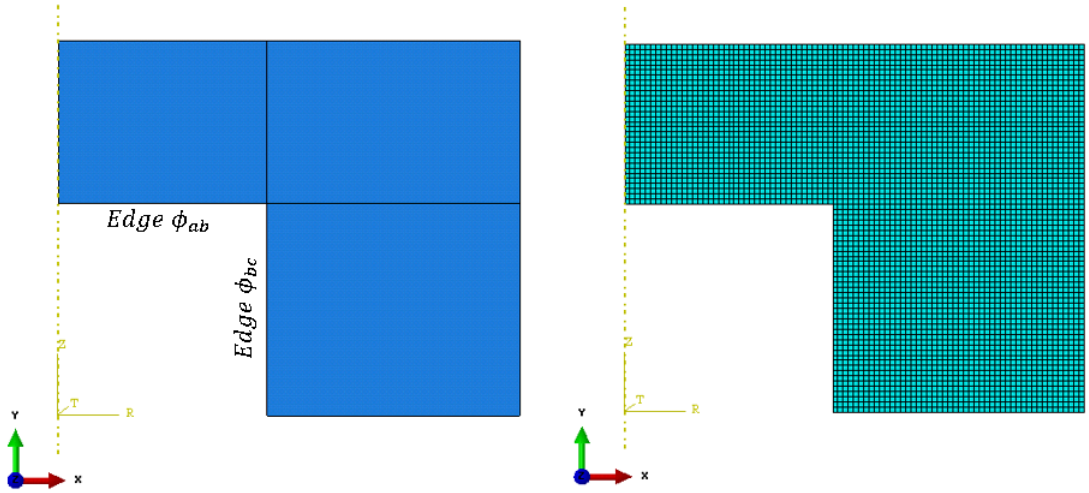


Figure 23: Face Partitioning on PBS region (left) and Mesh generated on the 2D domain (right) of the Burst Release analysis model.

### 3.7.3 Calculation of Mass Transfer Co-Efficient

The nodal temperature values of the 2D PBS domain were obtained and saved in a data file (.dat), using which, the value of the CDR at the end of the Burst Release phase was calculated using equation 32. The values of Mass Transfer Co-efficient of the disks were obtained by comparing the experimental CDR with the computationally evaluated CDR, as described in section 3.4.1.

## 3.8 One-Dimensional Analysis of Sustained Release Phase

### 3.8.1 Governing Equations and Boundary Conditions

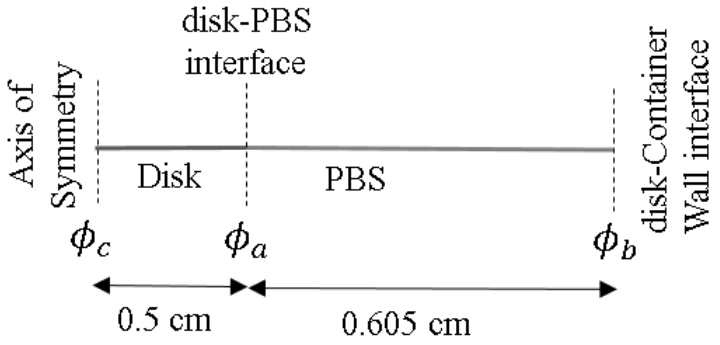


Figure 24: Domain Description of the 1D Sustained Release Axisymmetric Model

$$\frac{\partial C}{\partial t} = D(r)\frac{\partial^2 C}{\partial r^2} \tag{42}$$

$$D(r) = \begin{cases} D_{Disk}, & r \in (\phi_c, \phi_a), \\ D_{PBS}, & r \in (\phi_a, \phi_b) \end{cases} \tag{43}$$

$$D_{Disk}\frac{\partial C}{\partial r}\bigg|_{\phi_c} = 0 \tag{44}$$

$$D_{PBS}\frac{\partial C}{\partial r}\bigg|_{\phi_b} = 0 \tag{45}$$

$$D_{Disk}\frac{\partial C}{\partial r}\bigg|_{\phi_a} = D_{PBS}\frac{\partial C}{\partial r}\bigg|_{\phi_a} \tag{46}$$

In 1D sustained release analysis, both the disk and the PBS regions were modeled. The governing differential equation and the boundary conditions of the problem are stated from equations 42 to 46. Here, $D_{Disk}$ is the Diffusion Co-efficient of the disk.

The notations, $D_{PBS}$, $C$ etc have the same meaning as in case of Burst Release analysis. Equation 42 is the one dimensional form of *Fick's Second Law* of diffusion. Equations 44 and 45 represent the *impermeability* boundary conditions on the axis of symmetry and the disk-Container walls respectively. Equation 46 represent the mass flux continuity at the disk-PBS interface. This implies that there is no resistance to the diffusion of drug molecules at the disk-PBS interface.

### 3.8.2 ABAQUS-FEM Modeling Parameters

Following computational parameters were used for modeling the 2D burst release phase:

1. *Analysis Type and Requested Output*: The 1D sustained release process was modeled as an axisymmetric transient heat transfer problem. From the experimental study it was found that there was a high rate of drug release during the first 1 hour, i.e Burst Release. After the Burst Release, there was 23 hours of significant release at a lower rate, i.e Sustained Release. Thus, the physical time duration of the sustained release analysis was chosen to be 23 hours i.e 82800 seconds. The nodal concentration values of the PBS region were requested as a *History Output* at fixed time points of 10,800 secs, 25200 secs, 54000 secs and 82800 secs. These time points were chosen as corresponding to them , the experimental data of CDR was also available for comparative study.

2. *Geometry and Material Properties*: The PBS domain was created in ABAQUS *Part Module* with the same dimensions as shown in figure 24. The material properties of the PBS were set same as in case of the 1D Burst Release model.

For the Disk, the value of Density($\rho$) and Specific-Heat($C_p$) were set to unity to make the heat transfer differential equations analogous to the mass transport equations.

3. *Boundary and Initial Conditions*: The interaction node between the disk and the PBS domain, i.e $\phi_a$ was modeled as *tie-constrained* region. In *ABAQUS-Heat Transfer* analysis, *Tie-Constraint* equates the temperature at the nodes of the interaction layer of two different regions in contact [1]. This ensures that there is no thermal resistance (or *mass transfer resistance*) between the disk and the PBS region. Also, in setting up of the *Tie-Constraint*, *PBS* region was set as the *Master* Surface and *Disk* region was set as the *Slave* surface. The node on the axis of symmetry and the one corresponding to the disk-PBS interface were modeled as *insulated* boundaries.

$$C_{ini}^{disk} = \frac{M_{Loaded} - M_{BurstRelease}}{V_{disk}} \tag{47}$$

For setting the initial *predefined* field of the PBS region in the Sustained Release model, the output ODB (output database file) of the 1D Burst Release analysis was imported and the last increment of the analysis was set as the initial predefined field of the PBS region in the Sustained Release model. The initial concentration field of the disk region was set according to equation 47. Here, $C_{ini}^{disk}$ is the initial concentration, per unit volume of the disk, $M_{Loaded}$ is the total amount of drug loaded on the disk, $M_{BurstRelease}$ is the amount of drug released during burst release phase and $V_{disk}$ is the volume of the disk.

4. *Mesh Characteristics and Element Type*: The disk and the PBS domain were each given a mesh seeding of 0.0005 cm. The element type was chosen to be DC-CAX2 which is a 2-noded axisymmetric convection/diffusion linear element[1].

### 3.8.3 Calculation of Diffusion Co-Efficient

The values of concentration at the nodes of the PBS region were used to calculate the cumulative drug release (CDR) at 10,800 secs, 25200 secs, 54000 secs and 82800 secs. The value of diffusion co-efficient of the disk was obtained by comparing the experimental values of CDR wrt. computationally obtained values of CDR as explained in section 3.4.2.

## 3.9 Two-Dimensional Analysis of Sustained Release Phase

### 3.9.1 Governing Equations and Boundary Conditions

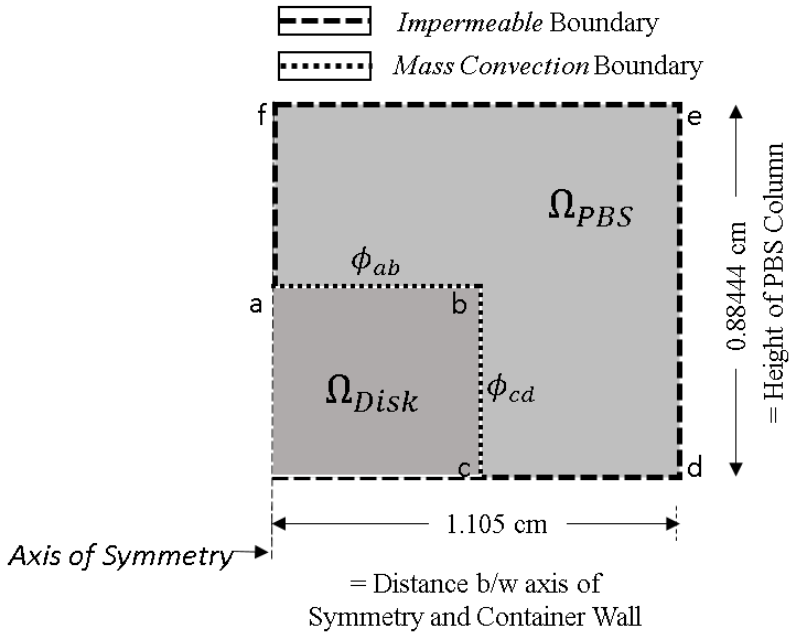


Figure 25: Domain Description of the 2D Sustained Release Axisymmetric Model.

$$\frac{\partial C}{\partial t} = D(\Omega)\nabla^2 C(r,z) \tag{48}$$

$$D(\Omega) = \begin{cases} D_{Disk}, & \Omega \in \Omega_{Disk}, \\ D_{PBS}, & \Omega \in \Omega_{PBS} \end{cases} \tag{49}$$

$$D_{Disk}\nabla C|_{\phi_{ab}} = D_{PBS}\nabla C|_{\phi_{ab}} \tag{50}$$

$$D_{Disk}\nabla C|_{\phi_{cd}} = D_{PBS}\nabla C|_{\phi_{cd}} \tag{51}$$

$$D_{Disk}\nabla C|_{ac} = 0 \tag{52}$$

$$D_{PBS}\nabla C|_{af,fe,ed,cd} = 0 \tag{53}$$

In 2D sustained release analysis, both the disk and the PBS regions are modeled. The governing differential equation and the boundary conditions of the problem are stated from equations 48 to 53. Here, $D_{Disk}$ is the diffusion co-efficient of the disk. The notations, $D_{PBS}$, $C$ etc have the same meaning as in case of the 2D Burst Release analysis. Equation 48 is the two dimensional form of the *Fick's Second Law* of diffusion. Equations 52 and 53 represent the *impermeability* boundary conditions on the axis of symmetry, disk-Container wall as well as the top open surface of the PBS respectively. Equation 50 and 51 represent the mass flux continuity at the disk-PBS interface.

### 3.9.2 ABAQUS-FEM Modeling Parameters

Following computational parameters were used for modeling the 2D Sustaine release phase:

1. *Analysis Type and Requested Output*: The 2D Sustained Release process is modeled as an axisymmetric transient heat transfer problem. As in case of 1D Sustained Release analysis, the physical time duration of the sustained release analysis was chosen to be 23 hours i.e 82800 seconds. The value of nodal concentration of all the nodes in the PBS region were requested as a *History Output* at fixed time points of 10,800 secs, 25200 secs, 54000 secs and 82800 secs.

2. *Geometry and Material Properties*: The PBS domain is created in ABAQUS *Part Module* with the same dimensions as given in figure 25. Figure 26 shows the image of the Disk and the PBS domain as developed in ABAQUS. The

material properties of the PBS was set same as defined in case of the Burst Release model. For the Disk, the value of Density($\rho$) and Specific-Heat($C_p$) was set to unity as in case of 1D Sustained Release analysis. The value of Diffusion Co-efficient of Disk was obtained by comparing the experimental results with the computational results.

3. *Boundary and Initial Conditions*: The interaction region between the disk and the PBS domain, i.e edge $\phi_{ab}$ and $\phi_{bc}$ were modeled as *tie-constrained* region. All the exterior edges of the disk and the PBS region were set as *insulated* boundaries.

   For setting the initial *predefined* field of the PBS region in the Sustained Release model, the output ODB (output database file) of the 2D Burst Release analysis was imported and the last increment of the analysis was set as the initial predefined field of the PBS region in the Sustained Release model. The initial concentration field of the disk region was set according to equation 47. In figure 27 is shown for illustration purpose, the contour plot of the concentration field over the disk and the PBS regions at the initial time increment of the Sustained Release analysis.

4. *Mesh Characteristics and Element Type*: The PBS domain was partitioned as shown in figure 27 and then each edge was given a mesh seeding of 0.0125 cm. This was done to obtain square elements of equal dimensions throughout the PBS domain. The element type was chosen to be DCCAX4 which is a 4-noded axisymmetric convection/diffusion quadrilateral element [1].

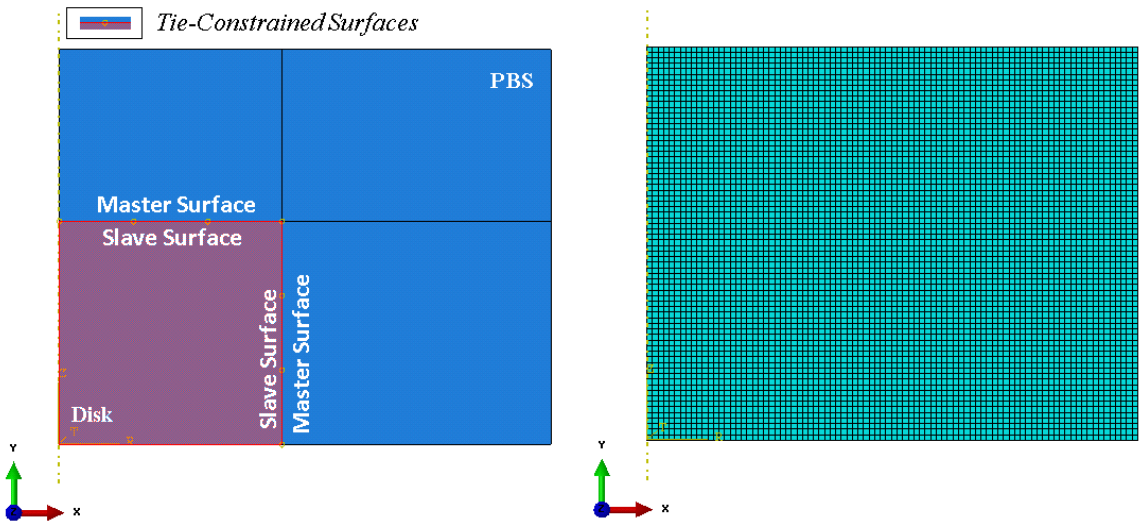


Figure 26: Face Partitioning on PBS and Disk regions (left) and Mesh generated on the 2D domain (right) of the Sustained Release analysis model.

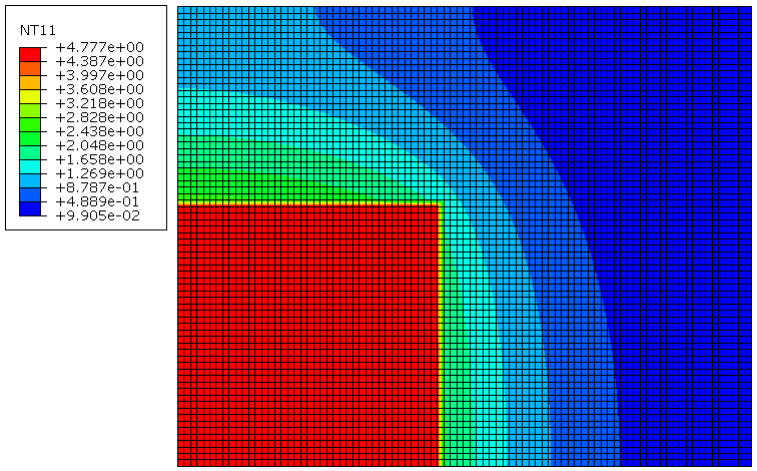


Figure 27: Contour plot of the initial concentration field over the disk and the PBS regions in the Sustained Release analysis for one of the disk replicates.

### 3.9.3 Calculation of Diffusion Co-Efficient

The value of diffusion co-efficient of the disk was obtained by comparing the experimental values of CDR wrt. computationally obtained values of CDR as explained in section 3.4.2.

# CHAPTER 4: RESULTS AND CONCLUSIONS

## 4.1 Analysis of Drug Loading on Disks

### 4.1.1 Hypothesis of Drug Loading Procedure

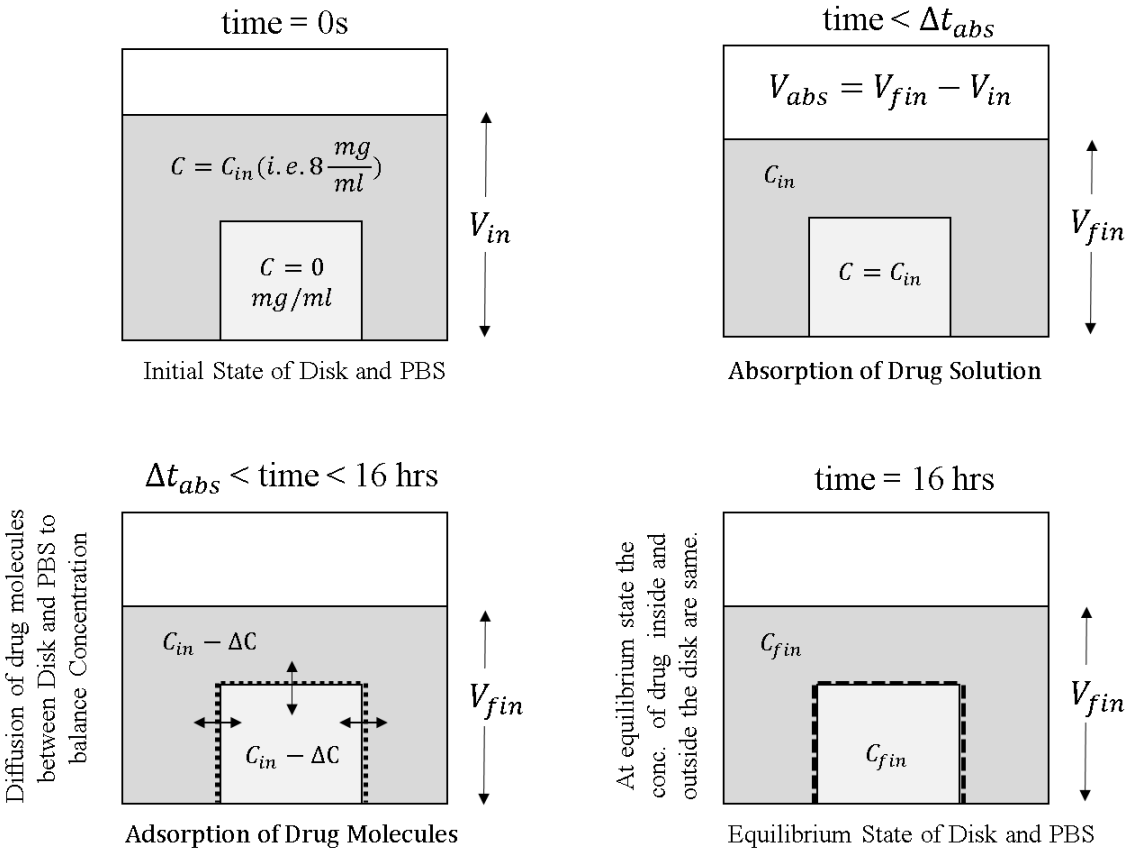


Figure 28: Illustration of the process of Drug Loading.

Drug loading process involves *adsorption* or *adhesion* of drug molecules to the disk surface as well *absorption* of drug molecules into the disk due to the seepage of drug solution into the porous framework of the disk. Drug loading process is

a complicated process involving several phenomenon acting simultaneously. In this section, the process of drug loading is hypothesized and the equations to calculate the total amount of drug loaded on the disk is stated.

In figure 28 is shown the illustration of the process of drug loading on disks by the virtue of *adsorption* and *absorption* which can be summarized as follows:

1. $\alpha$-Cristobalite disks have a highly porous structure with micro and nano scale channels connecting the outer surface with the interior of the scaffold. When these disks are placed in the drug solution, there is a quick influx of the solution into the disks and this mass transport of drug solution reaches its equilibrium state rapidly [21]. It was found from the *Gravimeteric Analysis*, that the *absorption* of drug solution reaches its equilibrium state within the first 1 hour of drug loading. The duration of the onset of the equilibrium state of the transport of drug solution into the disk is designated by $\Delta t_{abs}$. It is assumed that the total drug *adsorbed* on the disk surface is negligible compared to the drug *absorbed* by the disk due to seepage of drug solution into the disk during $\Delta t_{abs}$. The amount of drug *absorbed* by disks by $\Delta t_{abs}$ can be obtained from equation 54.

2. After the *absorption* of drug solution into the disk, *adsorption* of drug molecules from the PBS onto the outer periphery of the disks commence. As the drug is *adsorbed*, the concentration of drug solution in the PBS decrease and a concentration gradient is created between the drug solution within and outside the disk. To diffuse the concentration gradient, *osmosis* of drug molecules in the

solution between the Disk and the PBS commence.

3. During 16 hours of drug loading, drug is *adsorbed* on the disk surface and *osmosis* of drug solution also takes place simultaneously. At equilibrium, total drug loaded on the disk is the summation of the drug loaded on the disk due to *adsorption* of drug molecules on the disk and *absorption* of drug solution into the disk.

Based on the given hypothesis, the equations to calculate the total amount of drug loaded on the disks by *adsorption* and *absorption* were derived. They are as follows

$$Drug_{absorbed}^{t<\Delta t_{abs}} = C_{in} * V_{abs} \tag{54}$$

$$Drug_{absorbed}^{t=16hrs} = C_{fin} * V_{abs} \tag{55}$$

$$Drug_{adsorbed}^{t=16hrs} = (C_{in} - C_{fin}) * V_{in} \tag{56}$$

$$Drug_{TotalLoaded} = Drug_{absorbed}^{t=16hrs} + Drug_{adsorbed}^{t=16hrs} \tag{57}$$

$$Drug_{LeftInPBS} = V_{fin} * C_{fin} \tag{58}$$

The nomenclature associated with the expressions in the equations are as follows:

$C_{in}$: Initial Concentration of Drug Solution in the Container, i.e. 8 mg/ml.

$C_{fin}$: Final Concentration of Drug Solution in the Container, measured using *HPLC*.

$V_{in}$: Inital Volume of Drug Solution in the Container, i.e. 3 ml.

$V_{fin}$: Avg. Final Volume of Drug Solution in the Container.

$V_{abs}$: $V_{fin}$-$V_{in}$, i.e. Avg. Volume of Drug Solution *Absorbed* by the Disks.

Using the equation 55, the amount of drug *adsorbed* on the disks were calculated and using the equation 56 the amount of drug *absorbed* on the disks were calculated.

Also, using equation 57, the cumulative drug loaded on the disks were calculated.

### 4.1.2 Drug Loading on Disks due to Adsorption

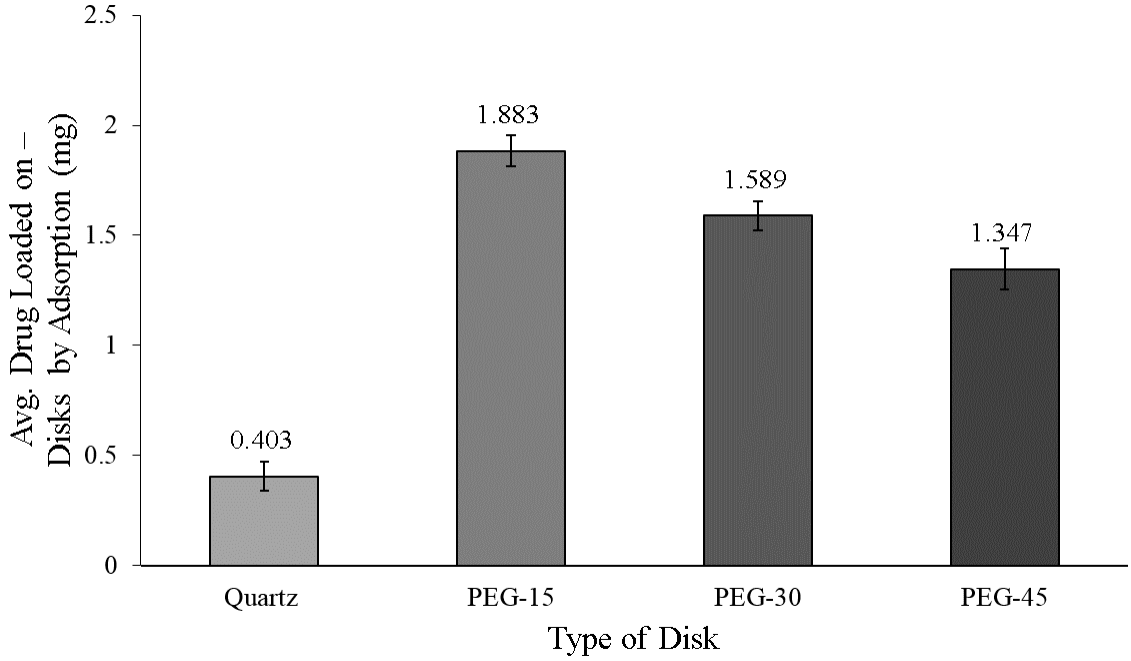


Figure 29: Amount of Drug Adsorbed on the Disks -/+ Standard Deviation.

Table 5: Avg. Drug Loaded on Disks by Adsorption -/+ St. Dev.

| | **Avg. Drug Adsorbed** | **St. Dev** |
|---|---|---|
| Quartz (N=3) | 0.40347 | 0.06651 |
| PEG-15 (N=6) | 1.88288 | 0.07106 |
| PEG-30 (N=6) | 1.58865 | 0.06444 |
| PEG-45 (N=6) | 1.34671 | 0.09491 |

aFigure 29 shows the amount of drug loaded on the disks due to adsorption. The average amount of drug adsorbed was found to be the lowest for Quartz disks. Among Cris-PEG disks, the average amount of drug adsorbed by the disks followed the pattern: PEG-15>PEG-30>PEG-45. To analyze the significance of the difference in the average values of drug adsorbed by the disks, *One Way ANOVA* (OWANOVA) test was performed for $\alpha = 0.05$. From the OWANOVA test it was found that there was statistically significant difference in the average amount of drug adsorbed by the different disk types, *F(3,17)=260, p<0.0001. Tukey's (HSD) Post-hoc* analysis was performed, for $\alpha = 0.05$, to pairwise compare the mean values of drug adsorbed by the disks. The results are reported in table 6. From the *Tukey's HSD* test it was found that the mean value of drug adsorbed by the different disk types were significantly different from each other.

Table 6: Tukey's Post-hoc pairwise Comparison ($\alpha = 0.05$) of the average amount of Drug Adsorbed by the different types of Disks.

| | **Mean Diff.** | **95.00% CI of diff.** | **Difference Significant?** |
|---|---|---|---|
| Quartz vs. PEG-15 | -1.479 | -1.633 to -1.325 | Yes (p<0.0001) |
| Quartz vs. PEG-30 | -1.185 | -1.339 to -1.031 | Yes (p<0.0001) |
| Quartz vs. PEG-45 | -0.9432 | -1.097 to -0.7892 | Yes (p<0.0001) |
| PEG-15 vs. PEG-30 | 0.2942 | 0.1684 to 0.42 | Yes (p<0.0001) |
| PEG-15 vs. PEG-45 | 0.5362 | 0.4103 to 0.662 | Yes (p<0.0001) |
| PEG-30 vs. PEG-45 | 0.2419 | 0.1161 to 0.3677 | Yes (p<0.0001) |

### 4.1.3 Drug Loading on Disks due to Absorption

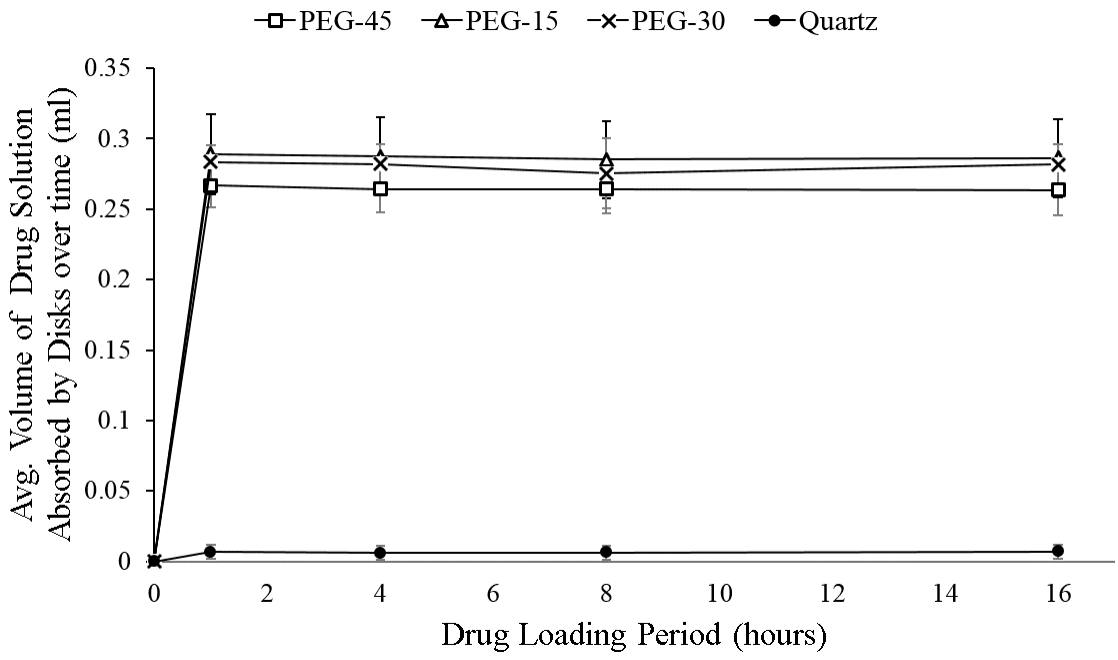


Figure 30: Amount of Drug Loaded on disks due to Absorption over Time.

Figure 30 shows the volume of drug solution absorbed by the disks over time. The volume of drug solution absorbed was the lowest for Quartz disks. This is due to the dense structure of the Quartz disks which does not allow seepage of drug solution into the disks. For all the disk types, there was a *Burst Absorption* of drug solution within the first sampling point of 1 hour. To test the significance of the difference in the volume of drug solution absorbed by the disks after the Burst Absorption phase, a *Repeated Measures (RM) ANOVA* test was performed for $\alpha = 0.05$. The results are reported in table 7.

Table 7: Results of Repeated Measures ANOVA analysis to test the significance of the difference in the volume of drug solution absorbed by the disks over time after the Burst Absorption phase.

| | **N** | **F (DFn, DFd)** | **P value** | **Difference Significant ?** |
|---|---|---|---|---|
| Quartz | 4 | F (1.224, 3.671) = 0.4847 | P=0.5650 | No |
| PEG-15 | 4 | F (1.246, 3.739) = 2.239 | P=0.2200 | No |
| PEG-30 | 4 | F (1.128, 3.383) = 0.751 | P=0.4605 | No |
| PEG-45 | 4 | F (1.035, 3.106) = 1.577 | P=0.2978 | No |

From the *RM ANOVA* test, it was found that there was statistically no significant gain in volume of drug solution after the initial *Burst Absorption* phase in any of the disk types.

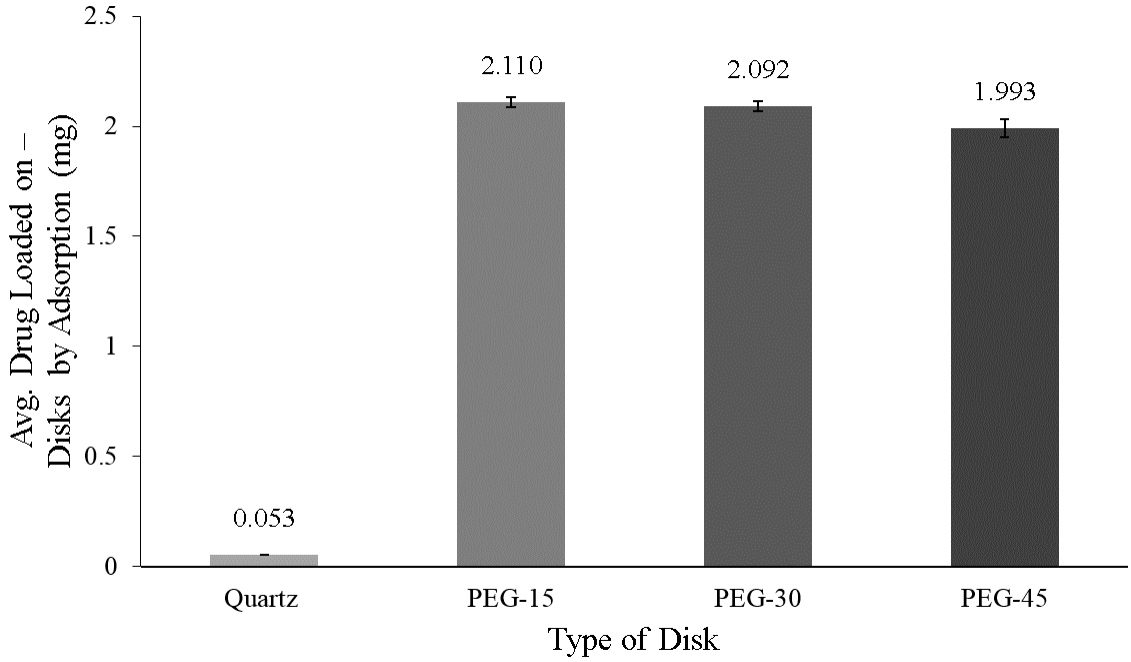


Figure 31: Amount of Drug Adsorbed on the Disks -/+ Standard Deviation

Table 8: Avg. Drug Loaded on Disks by Absorption -/+ St. Dev.

| | **Avg. Drug Absorbed** | **St. Dev** |
|---|---|---|
| Quartz (N=3) | 0.05326 | 0.00069 |
| PEG-15 (N=6) | 2.10997 | 0.02368 |
| PEG-30 (N=6) | 2.09211 | 0.02148 |
| PEG-45 (N=6) | 1.99283 | 0.04051 |

Table 9: Tukey's Post-hoc pairwise Comparison ($\alpha = 0.05$) of the average amount of Drug Absorbed by the different types of Disks.

| | **Mean Diff.** | **95.00% CI of diff.** | **Difference Significant?** |
|---|---|---|---|
| Quartz vs. PEG-15 | -2.057 | -2.098 to -2.015 | Yes (p<0.0001) |
| Quartz vs. PEG-30 | -2.039 | -2.081 to -1.997 | Yes (p<0.0001) |
| Quartz vs. PEG-45 | -1.94 | -1.981 to -1.898 | Yes (p<0.0001) |
| PEG-15 vs. PEG-30 | 0.01786 | -0.02384 to 0.05957 | No (p=0.6347) |
| PEG-15 vs. PEG-45 | 0.1171 | 0.07544 to 0.1588 | Yes (p<0.0001) |
| PEG-30 vs. PEG-45 | 0.09928 | 0.05757 to 0.141 | Yes (p<0.0001) |

Based on the volume of drug solution absorbed by the disks, the average amount of drug *absorbed* by the disks were calculated. Figure 31 shows the mean value of drug absorbed by the disks. The mean value of drug absorbed was the lowest for Quartz disks. To analyze the significance of difference in the average values of drug absorbed by the disks, *One Way ANOVA* test was performed for $\alpha = 0.05$. From the ANOVA test it was found that there was statistically significant difference in the average amount of drug absorbed by the different disk types, *F(3,20)=9138, p<0.0001. Tukey's (HSD) Post-hoc* analysis was performed, for $\alpha = 0.05$, to pairwise compare the mean values of drug absorbed by the disks. The results are reported in table 9. From the *Tukey's HSD* test, it was found that the difference in the average amount of drug absorbed by PEG-15 and PEG-30 were not statistically significant, *p=0.6347*. There was statistically significant difference in the average amount of drug

absorbed between all other disk type pairs.

### 4.1.4 Cumulative Loading by Absorption and Adsorption

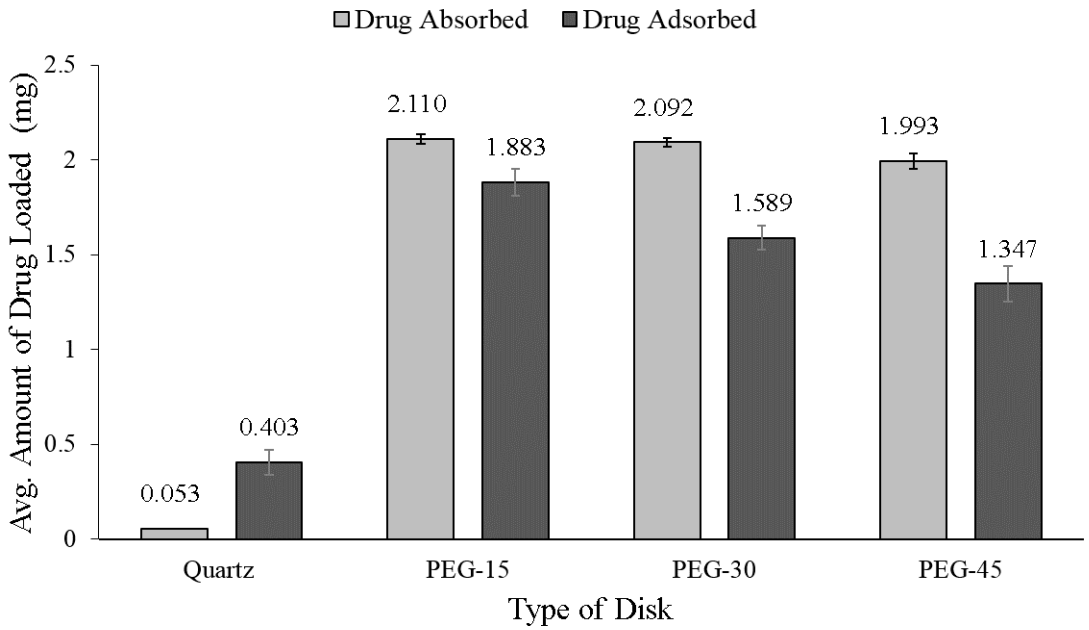


Figure 32: Comparison of the Amount of Drug Loaded due to Absorption and Adsorption.

Figure 32 puts together the mean values of the amount of drug *absorbed* and drug *adsorbed* by the disks. *Student t-test* ($\alpha = 0.05$) was performed to analyze the significance of the difference in the average amount of drug adsorbed and drug absorbed by different types of disks. For Quartz disks, the average drug adsorbed was significantly higher compared to drug absorbed. However, among Cris-PEG disks, the average drug absorbed was significantly higher compared to drug adsorbed.

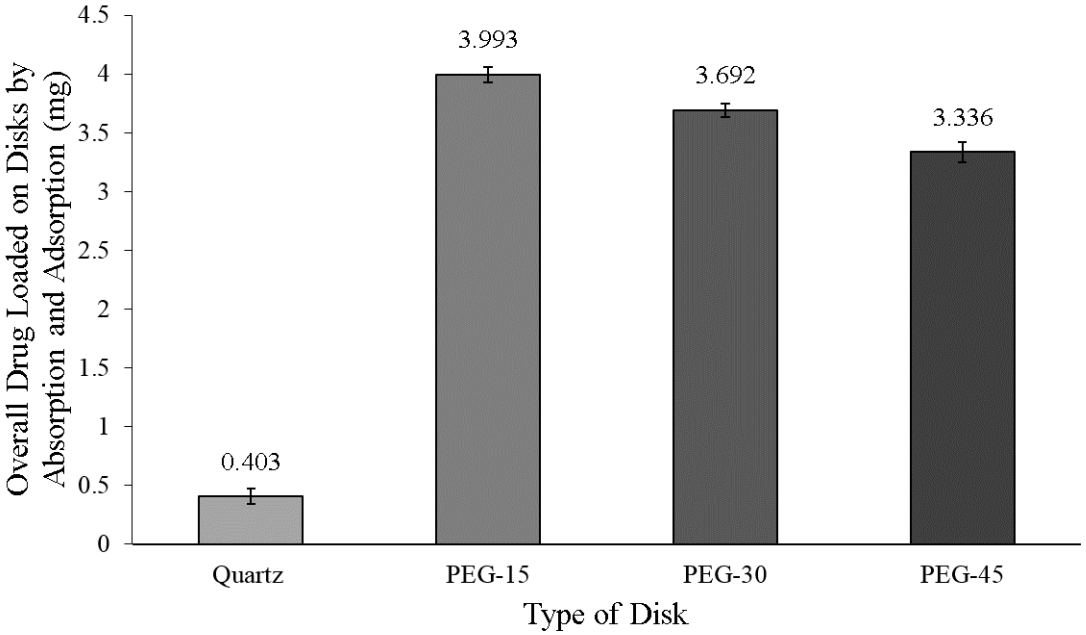


Figure 33: Overall amount of Drug Loaded on Disks due to Absorption and Adsorption.

Figure 33 shows the mean value of the overall amount of drug loaded on the disks by *adsorption* and *absorption*. In the calculation of the total amount of drug loaded, the amount of drug *absorbed* by Quartz disks was not accounted for and is considered as an experimental or procedural error. To analyze the significance of difference in the average values of overall drug loaded by the disks, *One Way ANOVA* test was performed for $\alpha = 0.05$. From the ANOVA test it was found that there was statistically significant difference in the average amount of drug loaded by the different disk types, $F(3,20)=3386,\ p<0.0001$. *Tukey's (HSD) Post-hoc* analysis was performed, for $\alpha = 0.05$, to pairwise compare the mean values of drug loaded on the disks. The results are reported in table 11. From the *Tukey's HSD* test it was found that each of the disk types were significantly different from each other wrt. the mean value of the overall drug loaded.

Table 10: Avg. Overall Drug Loaded on Disks by Absorption and Adsorption -/+ St. Dev.

| | **Avg. Overall Drug Loaded** | **St. Dev** |
|---|---|---|
| Quartz (N=6) | 0.40347 | 0.06651 |
| PEG-15 (N=6) | 3.99285 | 0.06428 |
| PEG-30 (N=6) | 3.69233 | 0.05839 |
| PEG-45 (N=6) | 3.33643 | 0.08658 |

Table 11: Tukey's Post-hoc pairwise Comparison ($\alpha = 0.05$) of the average amount of Overall Drug Loaded by the different types of Disks.

| | **Mean Diff.** | **95.00% CI of diff.** | **Difference Significant?** |
|---|---|---|---|
| Quartz vs. PEG-15 | -3.589 | -3.702 to -3.477 | Yes (<0.0001) |
| Quartz vs. PEG-30 | -3.289 | -3.402 to -3.176 | Yes (<0.0001) |
| Quartz vs. PEG-45 | -2.933 | -3.046 to -2.82 | Yes (<0.0001) |
| PEG-15 vs. PEG-30 | 0.3005 | 0.1878 to 0.4132 | Yes (<0.0001) |
| PEG-15 vs. PEG-45 | 0.6564 | 0.5437 to 0.7691 | Yes (<0.0001) |
| PEG-30 vs. PEG-45 | 0.3559 | 0.2432 to 0.4686 | Yes (<0.0001) |

## 4.2 Analysis of Drug Release from Disks

### 4.2.1 Cumulative Drug Release from Disks

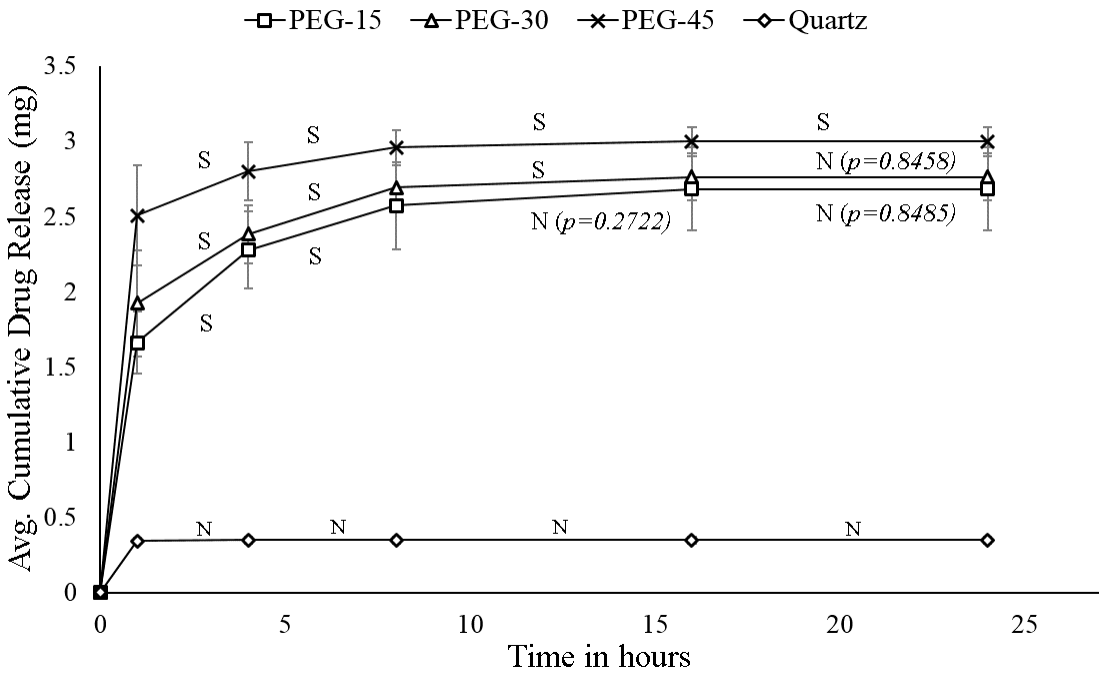


Figure 34: Average Cumulative Drug Release from Disks over time

Table 12: Results of Repeated Measures ANOVA analysis to test the significance of the difference in the Cumulative Drug Release after the Burst Release Phase.

| | **N** | **F (DFn, DFd)** | **P value** | **Difference Significant ?** |
|---|---|---|---|---|
| Quartz | 3 | F (1, 2) = 6.624 | P=0.1236 | No |
| PEG-15 | 6 | F (2.001, 10.010) = 127.6 | P<0.0001 | Yes |
| PEG-30 | 6 | F (1.271, 6.353) = 69.71 | P<0.0001 | Yes |
| PEG-45 | 6 | F (1.008, 5.040) = 23.75 | P=0.0045 | Yes |

Figure 34 shows the cumulative drug release profile from the disks. For all the disk types, there was an initial *Burst Release* phase followed by *Sustained Release* of drug into the PBS. After 24 hours, the analysis was stopped as the CDR lowered below the Minimum Effective Dosage of Vancomycin. To test the significance of the difference in the CDR of drug from the disks after the Burst Release phase, a *Repeated Measures ANOVA* test was performed for $\alpha = 0.05$. The results are reported in table 12. It was found from the ANOVA test that there was statistically in-significant drug release from the Quartz disks after the Burst Release phase; $F(1,2)=6.624,\ p<0.1236$. However, in Cris-PEG disks, there was significant difference in the CDR at different time points after the Burst Release phase.

*Tukey's (HSD) Post-hoc* analysis was performed, for $\alpha = 0.05$, to compare the difference in the CDR for the different Cris-PEG disk types at consecutive time points. The results are shown in figure 34 over the graph of avg. CDR vs time. On the graph, $S$ implies that the difference in the avg. CDR between the given two time points is statistically significant; $N$ implies that the difference in avg. CDR between the given two time points is statistically in-significant. Corresponding to $N$, the value of $p$ obtained from the *Tukey's HSD* test is also reported.

To analyze the significance of the difference in the average amount of drug loaded by the different types of Cris-PEG disks at different sampling points, one way ANOVA test was performed followed by *Tukey's Post hoc* test for statistical comparison among the disk types. The results are reported in table 13.

Table 13: Results of ANOVA and Tukey's Post-hoc pairwise comparison analysis for testing the significane of difference in the CDR among Cris-PEG disk types at different time points.

| **Sampling Point F (DFn, DFd) P Value** | **Tukey's HSD Pairwise Comparison test** | | |
|---|---|---|---|
| | **Disk Pairs** | **95.00% CI of diff.** | **Significant? P Value** |
| 1 hour F (2, 15) = 12.17 P=0.0007 | PEG-15 vs. PEG-30 | -0.7165 to 0.1953 | No P: 0.3258 |
| | PEG-15 vs. PEG-45 | -1.301 to -0.3895 | Yes P: 0.0006 |
| | PEG-30 vs. PEG-45 | -1.041 to -0.1289 | Yes P: 0.0119 |
| 4 hours F (2, 15) = 9.937 P=0.0018 | PEG-15 vs. PEG-30 | -0.4267 to 0.2184 | No P:0.6855 |
| | PEG-15 vs. PEG-45 | -0.8455 to -0.2004 | Yes P: 0.0021 |
| | PEG-30 vs. PEG-45 | -0.7413 to -0.09623 | Yes P: 0.0110 |
| 8 hours F (2, 15) = 5.665 P=0.0147 | PEG-15 vs. PEG-30 | -0.4262 to 0.184 | No P: 0.5696 |
| | PEG-15 vs. PEG-45 | -0.6916 to -0.08138 | Yes P: 0.0129 |
| | PEG-30 vs. PEG-45 | -0.5705 to 0.0397 | No P: 0.0932 |
| 16 hours F (2, 15) = 4.395 P=0.0315 | PEG-15 vs. PEG-30 | -0.3662 to 0.2079 | No P:0.7580 |
| | PEG-15 vs. PEG-45 | -0.6019 to -0.02785 | Yes P: 0.0308 |
| | PEG-30 vs. PEG-45 | -0.5228 to 0.05127 | No P: 0.1165 |
| 24 hours F (2, 15) = 4.339 P=0.0326 | PEG-15 vs. PEG-30 | -0.3667 to 0.2083 | No P: 0.7581 |
| | PEG-15 vs. PEG-45 | -0.601 to -0.02603 | Yes P: 0.0319 |
| | PEG-30 vs. PEG-45 | -0.5218 to 0.05319 | No P: 0.1199 |

The average CDR in the Burst Release phase from PEG-45 disks was significantly higher compared to PEG-15 and PEG-30. The difference in the average CDR of PEG-15 and PEG-30 was statistically in-significant throughout the release period.

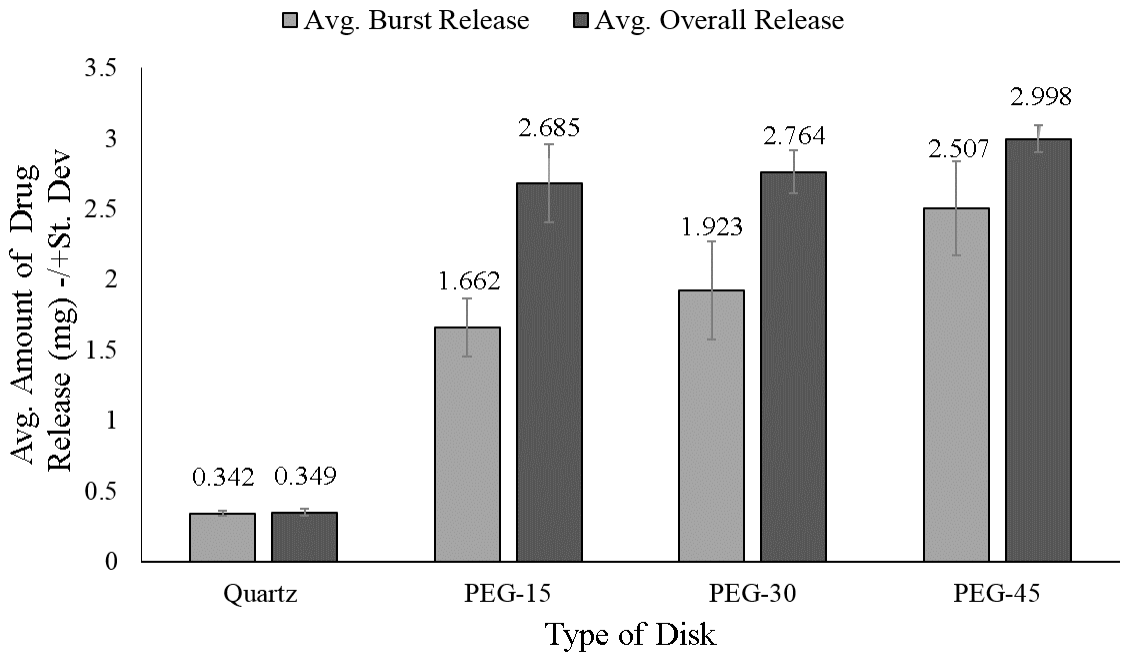


Figure 35: Comparison of Burst and Overall Cumulative Drug Release

Table 14: Burst Release as a % of Overall Cumulative Drug Release by the end of the Drug Release analysis.

| | **Avg. Burst Release ABR** | **Avg. Overall Release CDR** | $\frac{ABR}{CDR}$***100** |
|---|---|---|---|
| Quartz | 0.342 | 0.349 | 97.9 % |
| PEG-15 | 1.662 | 2.685 | 61.8 % |
| PEG-30 | 1.923 | 2.764 | 69.5 % |
| PEG-45 | 2.507 | 2.998 | 83.6 % |

Figure 35 shows the comparison of the average Burst Release with the average

Overall release. Also, table 14 tabulates the values of Burst Release as a % of Overall Cumulative Drug Release by the end of the Drug Release analysis. Quartz disks released almost the entire amount of drug loaded on them in the Burst Release phase. In PEG-15, PEG-30 and PEG-45 disks, 61.8 %, 69.5 % and 83.6 % of the total drug release occurred during Burst Release phase and the remaining during the Sustained Release phase respectively.

### 4.2.2 Cumulative Drug Release as a % of Drug Loaded

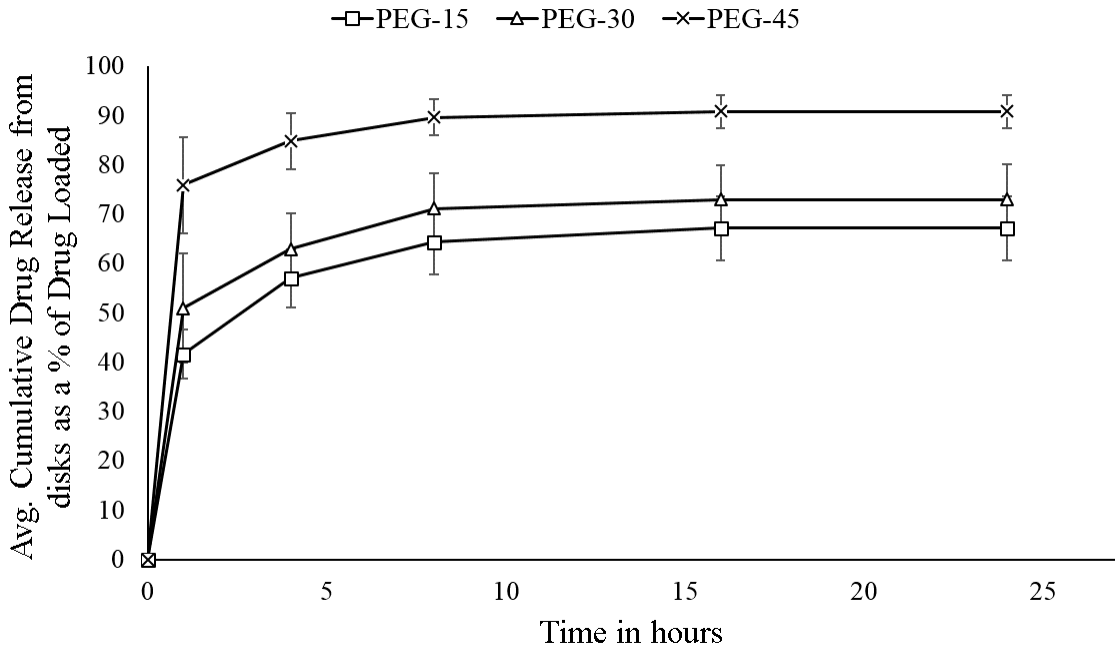


Figure 36: Avg. Cumulative Drug Release from Cris-PEG disks as a % of Drug Loaded.

Figure 36 shows for Cris-PEG disks, the average amount of drug release over time as a percentage of the total amount of drug loaded on the disks. It was found that for all the disk types, majority of the drug loaded released during the initial Burst Release phase.

In Figure 37 is shown a comparison between the average total amount of Drug Loaded (ODL) by disks with the Cumulative Drug Released (CDR) by the disks at the end of the drug release analysis. The relative difference between the ODL and CDR was obtained for the different disk types and is tabulated in table 15. The relative difference can be used to quantify and compare the drug excretion efficacy of the disks. Among Cris-PEG disks, PEG-15 had the lowest drug excretion efficacy followed by

PEG-30. PEG-45 disks on an average released around 90% of the total drug loaded on them and had the highest drug excretion.

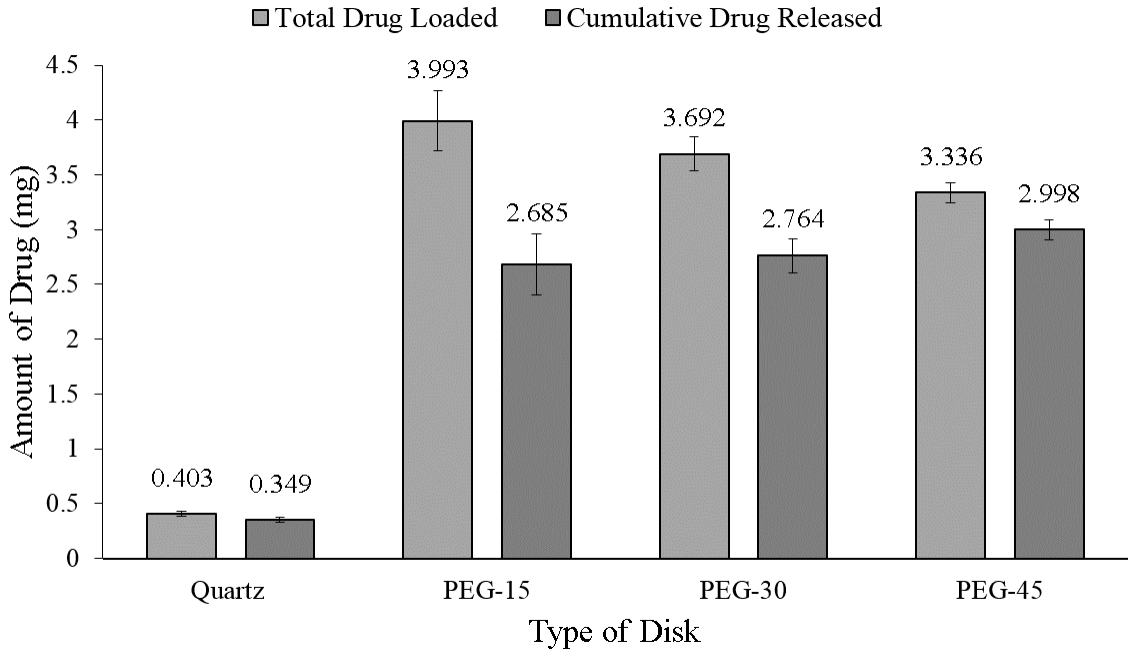


Figure 37: Comparison of the Overall Drug Loaded vs Cumulative Drug Released by the end of Drug Release analysis.

Table 15: Relative Difference between the average Total Drug Loaded on the disks and the average Cumulative Drug Released from the disks by the end of Drug Release analysis.

| | **Avg. Drug Loaded DLO** | **Avg. Drug Released CDR** | **Relative Difference (DLO-CDR)/DLO** |
|---|---|---|---|
| Quartz | 0.403 | 0.349 | 0.133 |
| PEG-15 | 3.993 | 2.685 | 0.327 |
| PEG-30 | 3.692 | 2.764 | 0.251 |
| PEG-45 | 3.336 | 2.998 | 0.101 |

## 4.3 Results of Computational Modeling

### 4.3.1 Mass Transfer Co-Efficients From 1D Analysis

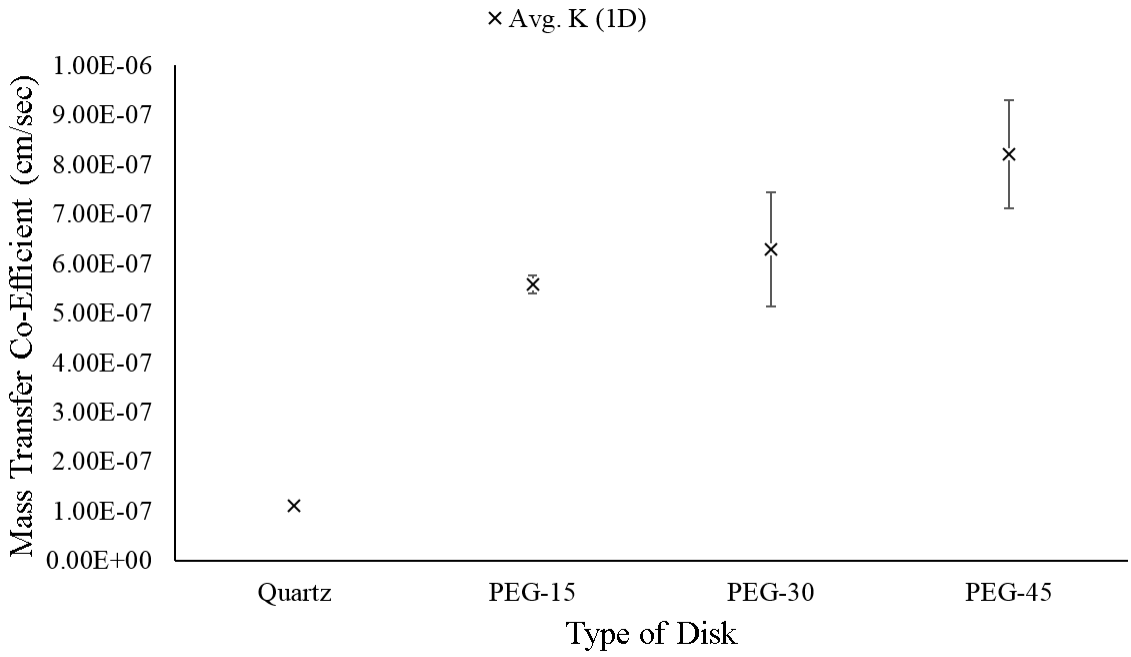


Figure 38: Avg. value of Mass Transfer Co-Efficient, -/+ St.dev, of disk-PBS interface in different types of Disks from 1D Analysis.

Table 16: Avg. value, -/+ St.dev of Mass Transfer Co-Efficient of disk-PBS interface in different types of Disks from 1D Analysis.

| | Avg. K (cm/sec) | St. Dev |
|---|---|---|
| Quartz (N=3) | 1.12E-07 | 6.743E-09 |
| PEG-15 (N=6) | 5.584E-07 | 1.753E-08 |
| PEG-30 (N=6) | 6.293E-07 | 1.149E-07 |
| PEG-45 (N=6) | 8.207E-07 | 1.092E-07 |

Table 16 tabulates the average value of Mass Transfer Co-Efficient ($K$) of disks obtained from 1D analysis along with the corresponding standard deviation. The average value of $K$ was found to be the lowest for Quartz disks. Among Cris-PEG disks, the average value of $K$ followed the pattern: PEG-45>PEG-30>PEG-15. To analyze the significance of difference in the average values of Mass Transfer Co-Efficient, *One Way ANOVA* test was performed for $\alpha = 0.05$. From the ANOVA test it was found that there was statistically significant difference in the average value of $K$ within the different disk types, *F(3,17)=45.39, p<0.0001. Tukey's (HSD) Post-hoc* analysis was performed, for $\alpha = 0.05$, to pairwise compare the mean values of $K$ for the disks. The results are reported in table 17. From the *Tukey's HSD* test it was found that the difference in the average values of the Mass Transfer Co-Efficient of PEG-15 and PEG-30 were not statistically significant. However, there was significant difference in the average value of $K$ among all other disk types.

Table 17: Tukey's Post-hoc pairwise Comparison ($\alpha = 0.05$) of the average value of Mass Transfer Co-Efficient for the different types of Disks obtained from 1D analysis.

| | **95.00% CI of diff.** | **Significant?** | **P Value** |
|---|---|---|---|
| Quartz vs. PEG-15 | -6.203e-007 to -2.724e-007 | Yes | <0.0001 |
| Quartz vs. PEG-30 | -6.912e-007 to -3.432e-007 | Yes | <0.0001 |
| Quartz vs. PEG-45 | -8.826e-007 to -5.347e-007 | Yes | <0.0001 |
| PEG-15 vs. PEG-30 | -2.129e-007 to 7.118e-008 | No | 0.5057 |
| PEG-15 vs. PEG-45 | -4.043e-007 to -1.203e-007 | Yes | 0.0003 |
| PEG-30 vs. PEG-45 | -3.335e-007 to -4.94e-008 | Yes | 0.0066 |

### 4.3.2 Diffusion Co-Efficients From 1D Analysis

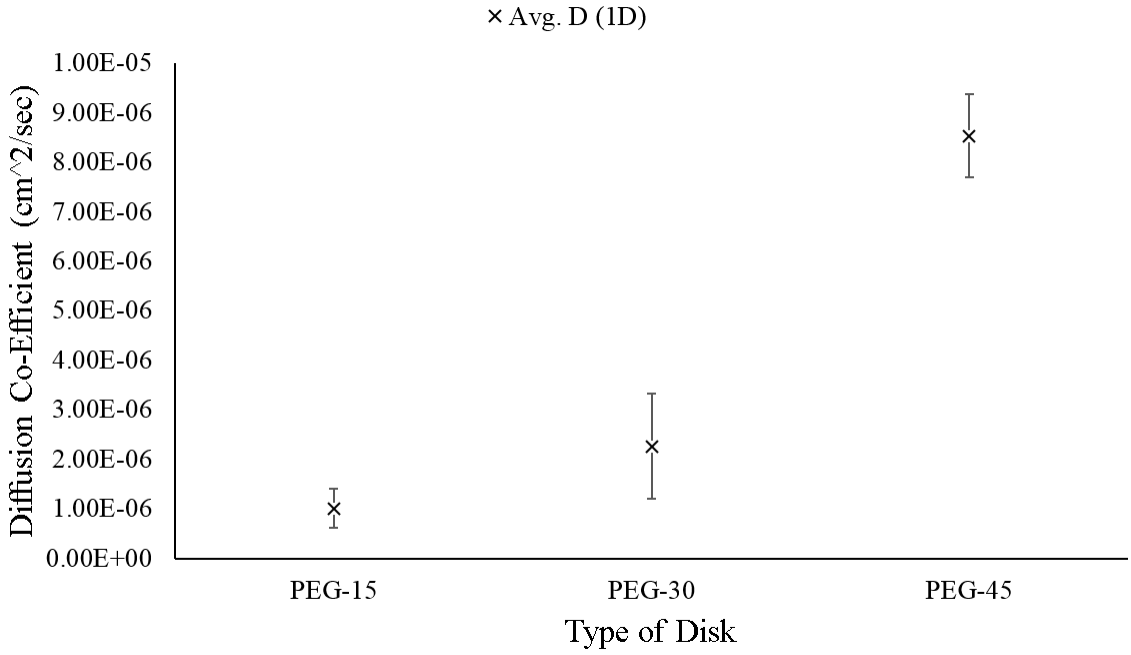


Figure 39: Avg. value, -/+ St.dev of Mass Transfer Co-Efficient of disk-PBS interface in different types of Disks from 1D Analysis.

Table 18: Avg. value, -/+ St.dev of Diffusion Co-Efficients and corresponding Avg. value, -/+ St.dev of Relative Error, of different types of Disks from 1D Analysis.

| | Avg. $D$ ($cm^2$/sec) (-/+ St.Dev) | Relative Error (-/+ St.Dev) |
|---|---|---|
| PEG-15 (N=4) | 1.01E-06 (-/+ 3.86E-07) | 5.35E-02 (-/+ 1.92E-02) |
| PEG-30 (N=4) | 2.26E-06 (-/+ 1.06E-06) | 2.68E-02 (-/+ 1.36E-02) |
| PEG-45 (N=4) | 8.53E-06 (-/+ 8.36E-07) | 5.07E-02 (-/+ 1.81E-02) |

Table 18 tabulates the average value of Diffusion Co-Efficient (D) of disks obtained from 1D analysis along with the corresponding standard deviation. For the given $D$ value, the average Relative Error between the experimental and computationally computed CDR is also reported. Among Cris-PEG disks, the average value of $D$

followed the pattern: PEG-45>PEG-30>PEG-15. To analyze the significance of difference in the average values of Diffusion Co-Efficient, *One Way ANOVA* test was performed for $\alpha = 0.05$. From the OWANOVA test it was found that there was statistically significant difference in the value of $D$ within the different disk types, *F(2,9)=98.83, p<0.0001. Tukey's (HSD) Post-hoc* analysis was performed, for $\alpha = 0.05$, to pairwise compare the mean values of $D$ for the disks. The results are reported in table 19. From the *Tukey's HSD* test it was found that the difference in the average values of the Diffusion Co-Efficient of PEG-15 and PEG-30 were not statistically significant. However, there was significant difference in the average value of $D$ among all other disk types.

Table 19: Tukey's Post-hoc pairwise Comparison ($\alpha = 0.05$) of the average value of Diffusion Co-Efficient for the different types of Disks obtained from 1D analysis.

| | **95.00% CI of diff.** | **Significant?** | **P Value** |
|---|---|---|---|
| PEG-15 vs. PEG-30 | -2.85e-006 to 3.504e-007 | No | 0.1283 |
| PEG-15 vs. PEG-45 | -9.12e-006 to -5.92e-006 | Yes | <0.0001 |
| PEG-30 vs. PEG-45 | -7.87e-006 to -4.67e-006 | Yes | <0.0001 |

Out of the N=6 available replicates of each type of Cris-PEG disks, the average values of Diffusion Co-Efficient from 1D analysis were calculated using the experimental values of CDR of N=4 replicates. The time evolution of CDR for the remaining two replicates of each type of Cris-PEG disks were predicted using the average value of the diffusion co-efficient obtained from the 1D analysis. The Relative Error between

the experimental and computationally predicted CDR over time in the Sustained Release phase were also obtained. The graph of the experimental vs predicted CDR over time along with the corresponding Relative error for PEG-15, PEG-30 and PEG-45 are shown from Figure 40 to 42.

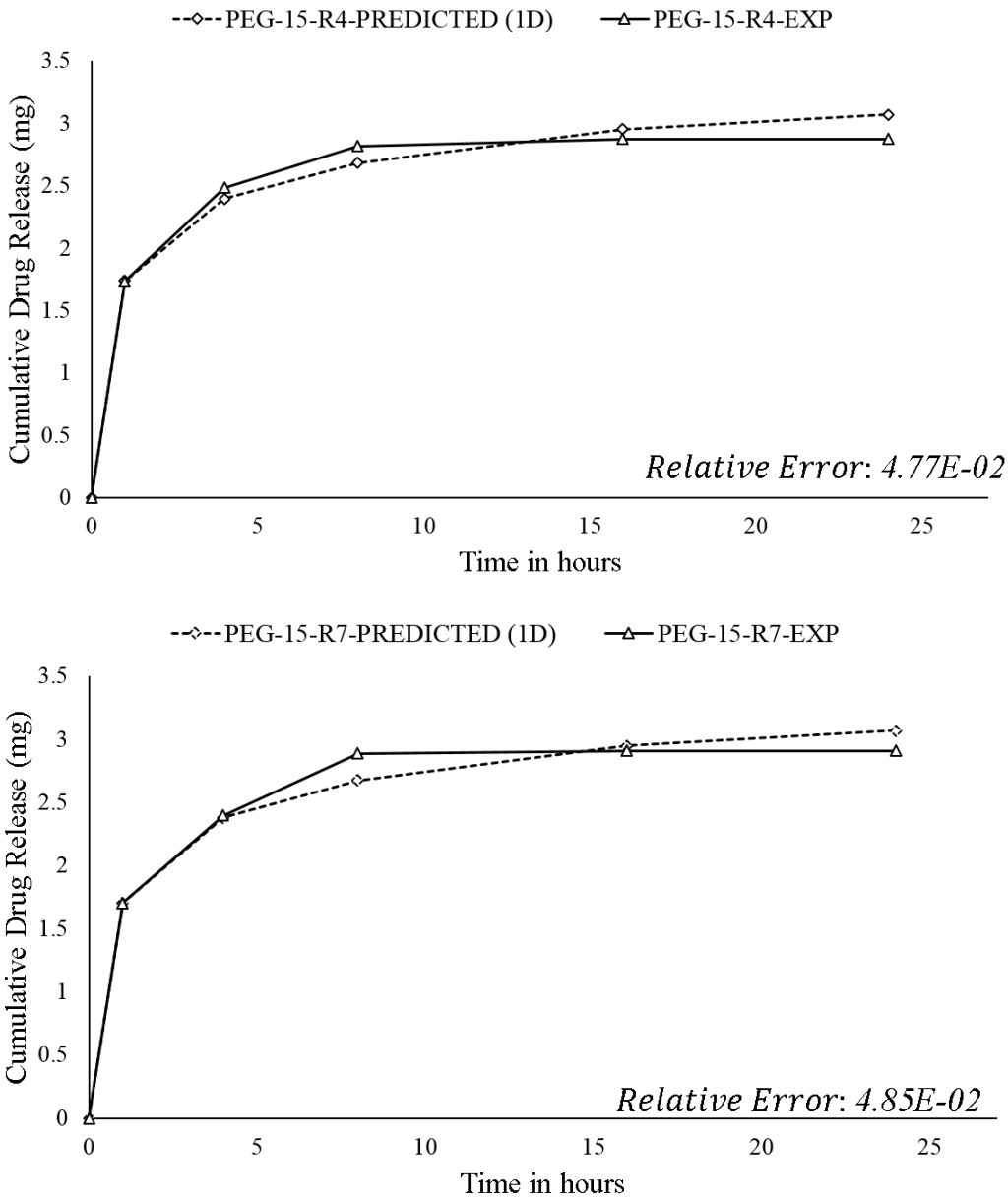


Figure 40: Comparison of Predicted Cumulative Drug Release from 1D Analysis with Experimentally obtained Cumulative Drug Release for two different PEG-15 Replicates.

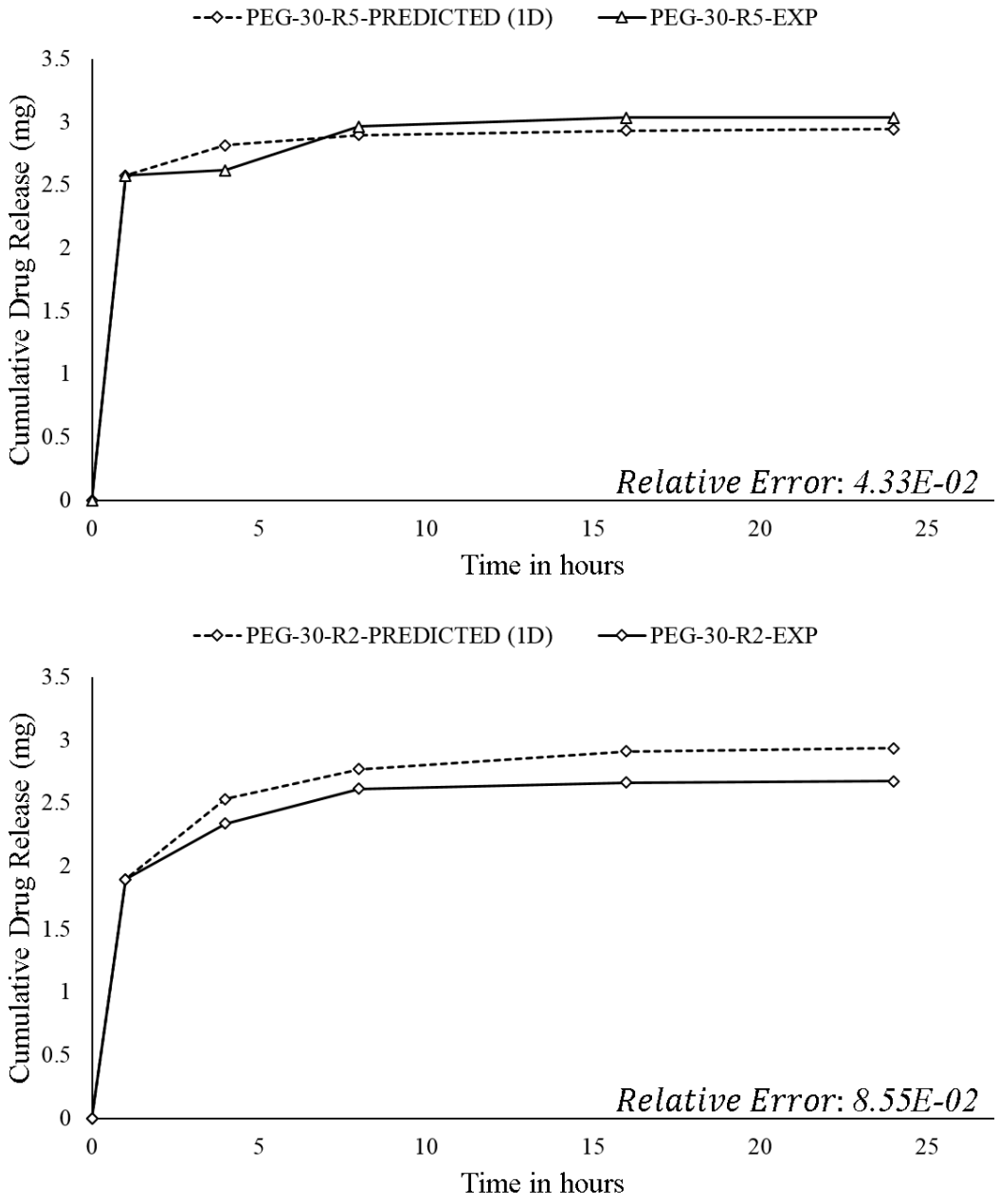


Figure 41: Comparison of Predicted Cumulative Drug Release from 1D Analysis with Experimentally obtained Cumulative Drug Release for two different PEG-30 Replicates.

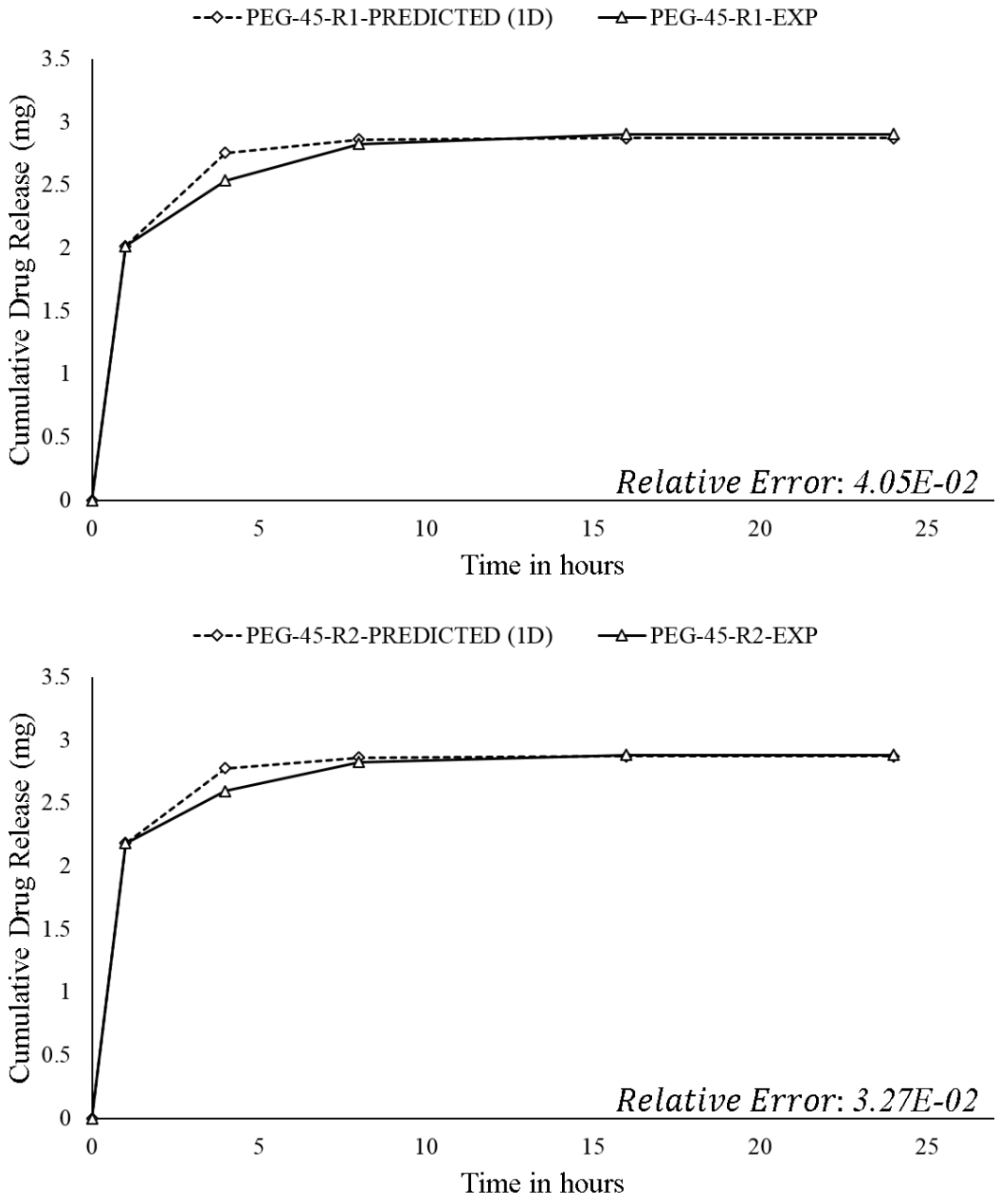


Figure 42: Comparison of Predicted Cumulative Drug Release from 1D Analysis with Experimentally obtained Cumulative Drug Release for two different PEG-45 Replicates.

### 4.3.3 Mass Transfer Co-Efficients From 2D Analysis

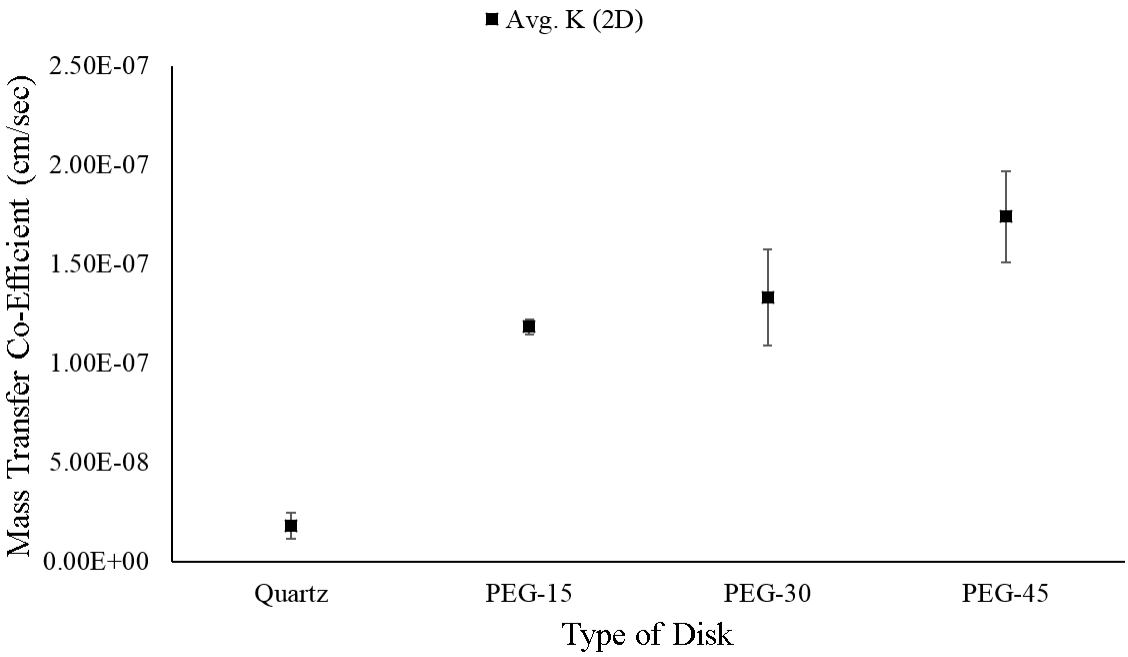


Figure 43: Avg. value, -/+ St.dev of Mass Transfer Co-Efficient of disk-PBS interface in different types of Disks from 2D Analysis.

Table 20: Avg. value, -/+ St.dev of Mass Transfer Co-Efficients of disk-PBS interface in different types of Disks from 2D Analysis.

| | Avg. K (cm/sec) | St. Dev |
|---|---|---|
| Quartz (N=3) | 1.81E-08 | 6.466E-09 |
| PEG-15 (N=6) | 1.183E-07 | 3.713E-09 |
| PEG-30 (N=6) | 1.333E-07 | 2.435E-08 |
| PEG-45 (N=6) | 1.738E-07 | 2.314E-08 |

Table 20 tabulates the average value of Mass Transfer Co-Efficient (K) of disks obtained from 2D analysis along with the corresponding standard deviation. The av-

erage value of $K$ was found to be the lowest for Quartz disks. Among Cris-PEG disks, the average value of $K$ followed the pattern: PEG-45>PEG-30>PEG-15. To analyze the significance of difference in the average values of Mass Transfer Co-Efficient, *One Way ANOVA* test was performed for $\alpha = 0.05$. From the OWANOVA test it was found that there was statistically significant difference in the average values of $K$ within the different disk types, *F(3,17)=47.79, p<0.0001. Tukey's (HSD) Post-hoc* analysis was performed, for $\alpha = 0.05$, to pairwise compare the mean values of $K$ for the disks. The results are reported in table 21. From the *Tukey's HSD* test it was found that the difference in the average values of the Mass Transfer Co-Efficient of PEG-15 and PEG-30 were not statistically significant. However, there was significant difference in the average value of $K$ among all other disk types.

Table 21: Tukey's Post-hoc pairwise Comparison ($\alpha = 0.05$) of the average values of Mass Transfer Co-Efficient obtained for the different types of Disks obtained from 2D analysis.

| | **95.00% CI of diff.** | **Significant?** | **Adjusted P Value** |
|---|---|---|---|
| Quartz vs. PEG-15 | -1.374e-007 to -6.295e-008 | Yes | <0.0001 |
| Quartz vs. PEG-30 | -1.524e-007 to -7.795e-008 | Yes | <0.0001 |
| Quartz vs. PEG-45 | -1.929e-007 to -1.185e-007 | Yes | <0.0001 |
| PEG-15 vs. PEG-30 | -4.541e-008 to 1.541e-008 | No | 0.5151 |
| PEG-15 vs. PEG-45 | -8.591e-008 to -2.509e-008 | Yes | 0.0004 |
| PEG-30 vs. PEG-45 | -7.091e-008 to -1.009e-008 | Yes | 0.0073 |

### 4.3.4 Diffusion Co-Efficients From 2D Analysis

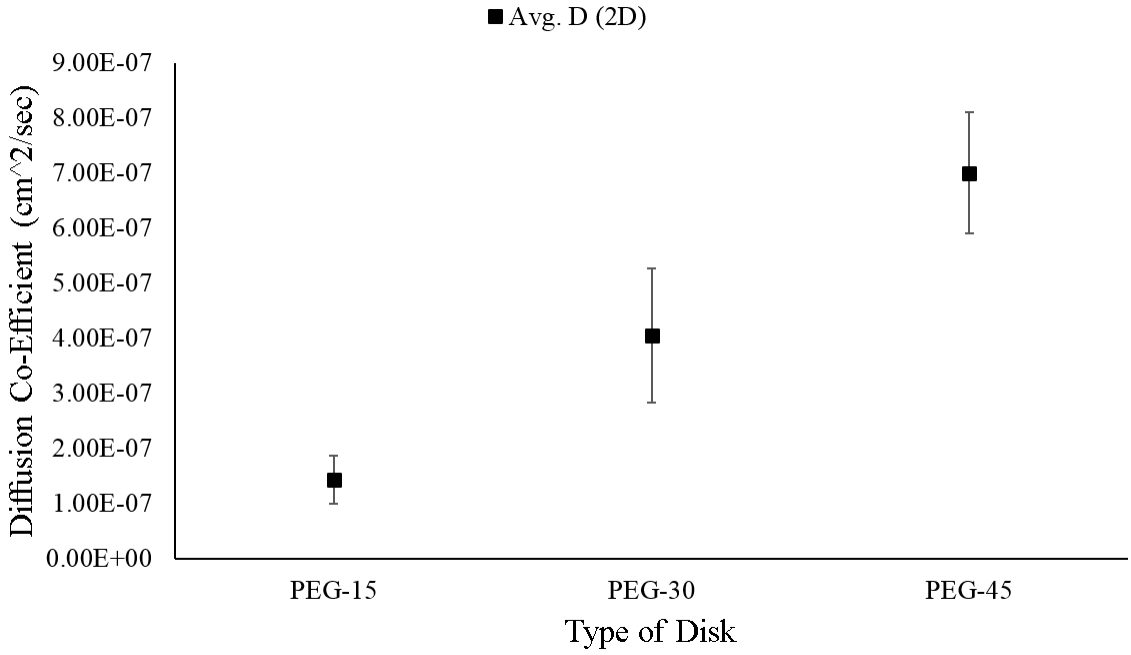


Figure 44: Avg. value, -/+ St.dev of Mass Transfer Co-Efficient of disk-PBS interface in different types of Disks from 2D Analysis.

Table 22: Avg. value, -/+ St.dev of Diffusion Co-Efficients and corresponding Avg. value, -/+ St.dev of Relative Error, for different types of Disks from 1D Analysis.

| | Avg. $D$ ($cm^2$/sec) (-/+ St.Dev) | Relative Error (-/+ St.Dev) |
|---|---|---|
| PEG-15 (N=4) | 1.40E-07 (-/+ 4.40E-08) | 6.13E-02 (-/+ 2.13E-02) |
| PEG-30 (N=4) | 4.05E-07 (-/+ 1.22E-07) | 4.69E-02 (-/+ 2.69E-03) |
| PEG-45 (N=4) | 7.04E-07 (-/+ 1.1E-07) | 2.31E-02 (-/+ 9.32E-03) |

Table 22 tabulates the average value of Diffusion Co-Efficient (D) of disks obtained from 2D analysis along with the corresponding standard deviation. For the given $D$ value, the average Relative Error between the experimental and computationally computed CDR is also reported. Among Cris-PEG disks, the average value of $D$

followed the pattern: PEG-45>PEG-30>PEG-15. To analyze the significance of difference in the average values of Diffusion Co-Efficient, *ANOVA* test was performed for $\alpha = 0.05$. From the ANOVA test it was found that there was statistically significant difference in the value of $D$ within the different disk types, *F(2,9)=33.04, p<0.0001.* *Tukey's (HSD) Post-hoc* analysis was performed, for $\alpha = 0.05$, to pairwise compare the mean values of $D$ for the disks. The results are reported in table 23. From the *Tukey's HSD* test it was found that the difference in the average values of the Diffusion Co-Efficient of PEG-15 and PEG-30 were not statistically significant. However, there was significant difference in the average value of $D$ among all other disk types.

Table 23: Tukey's Post-hoc pairwise Comparison ($\alpha = 0.05$) of the average value of Diffusion Co-Efficient for the different types of Disks obtained from 2D analysis.

| | **95.00% CI of diff.** | **Significant?** | **P Value** |
|---|---|---|---|
| PEG-15 vs. PEG-30 | -4.588e-007 to -7.116e-008 | Yes | 0.0103 |
| PEG-15 vs. PEG-45 | -7.578e-007 to -3.702e-007 | Yes | <0.0001 |
| PEG-30 vs. PEG-45 | -4.928e-007 to -1.052e-007 | Yes | 0.0050 |

Out of the N=6 available replicates of each type of Cris-PEG disks, the average values of Diffusion Co-Efficient from 2D analysis were calculated using the experimental values of CDR of N=4 replicates. The time evolution of CDR for the remaining two replicates of each type of Cris-PEG disks were predicted using the average value of diffusion co-efficient obtained from the 2D analysis. The Relative Error between the experimental and computationally predicted CDR over time in the sustained release

regime were also obtained. The graph of the experimental vs predicted CDR over time along with the corresponding Relative error for PEG-15, PEG-30 and PEG-45 are shown from Figure 45 to 47.

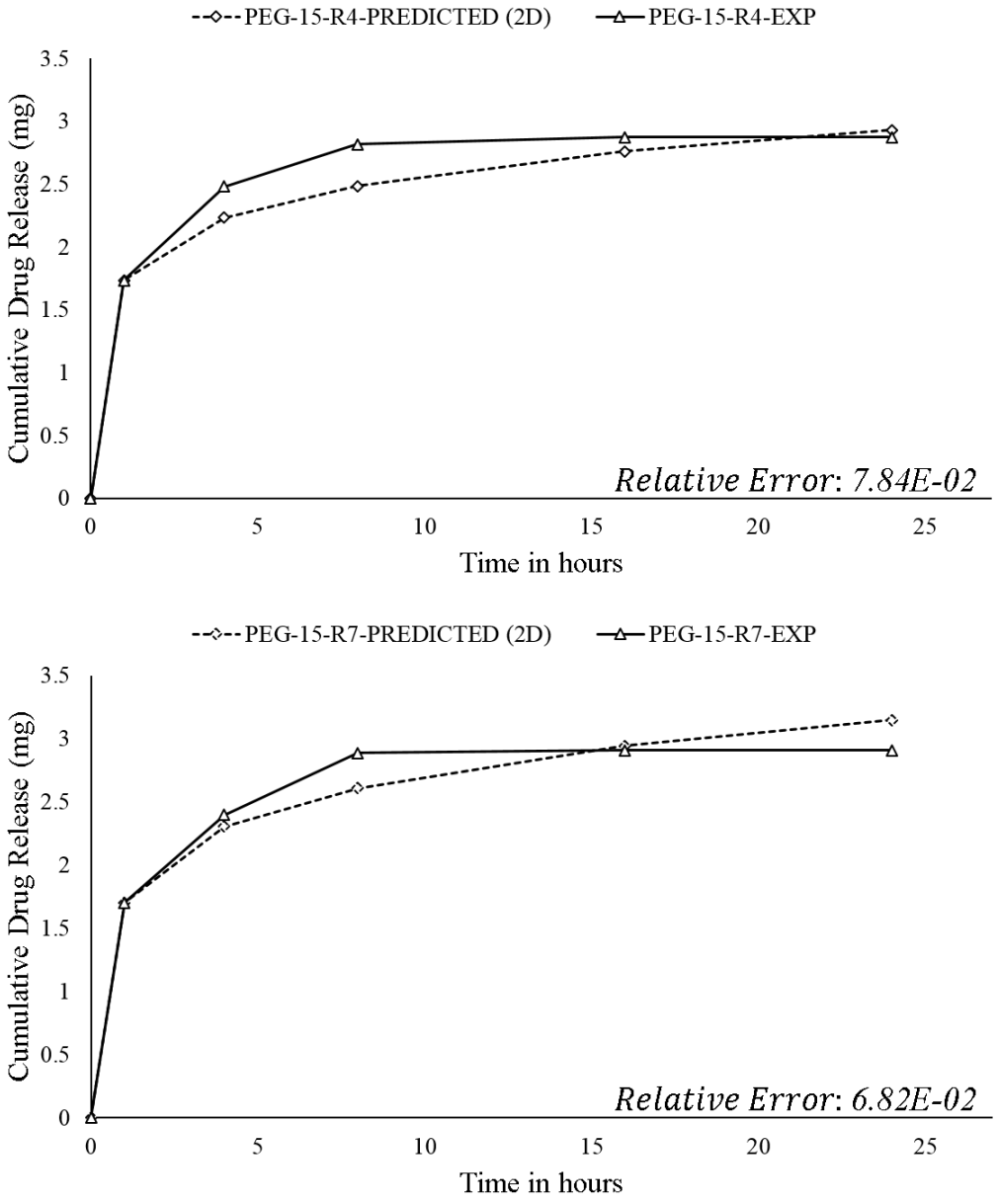


Figure 45: Comparison of Predicted Cumulative Drug Release from 2D Analysis with Experimentally obtained Cumulative Drug Release for two different PEG-15 Replicates.

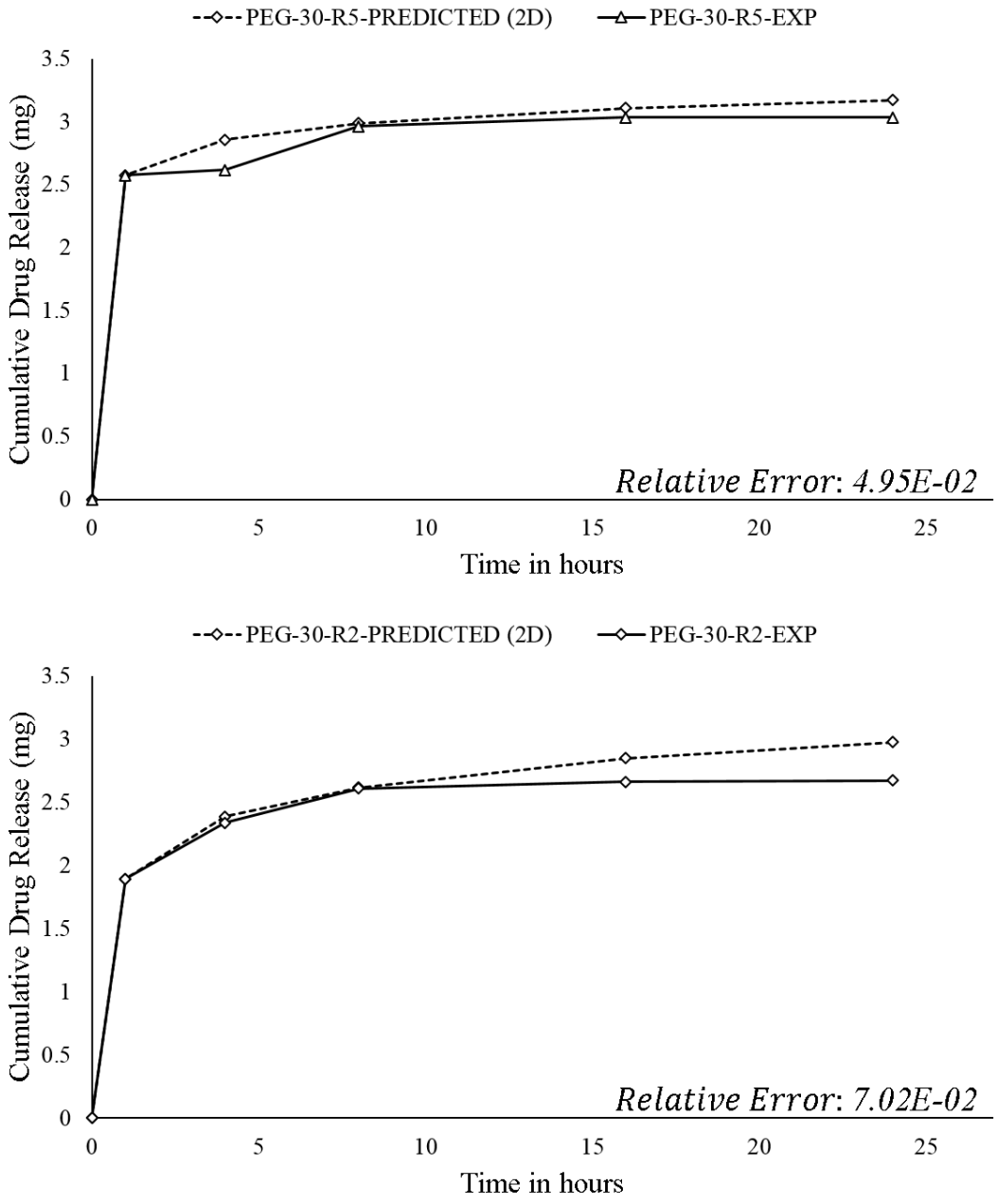


Figure 46: Comparison of Predicted Cumulative Drug Release from 2D Analysis with Experimentally obtained Cumulative Drug Release for two different PEG-30 Replicates.

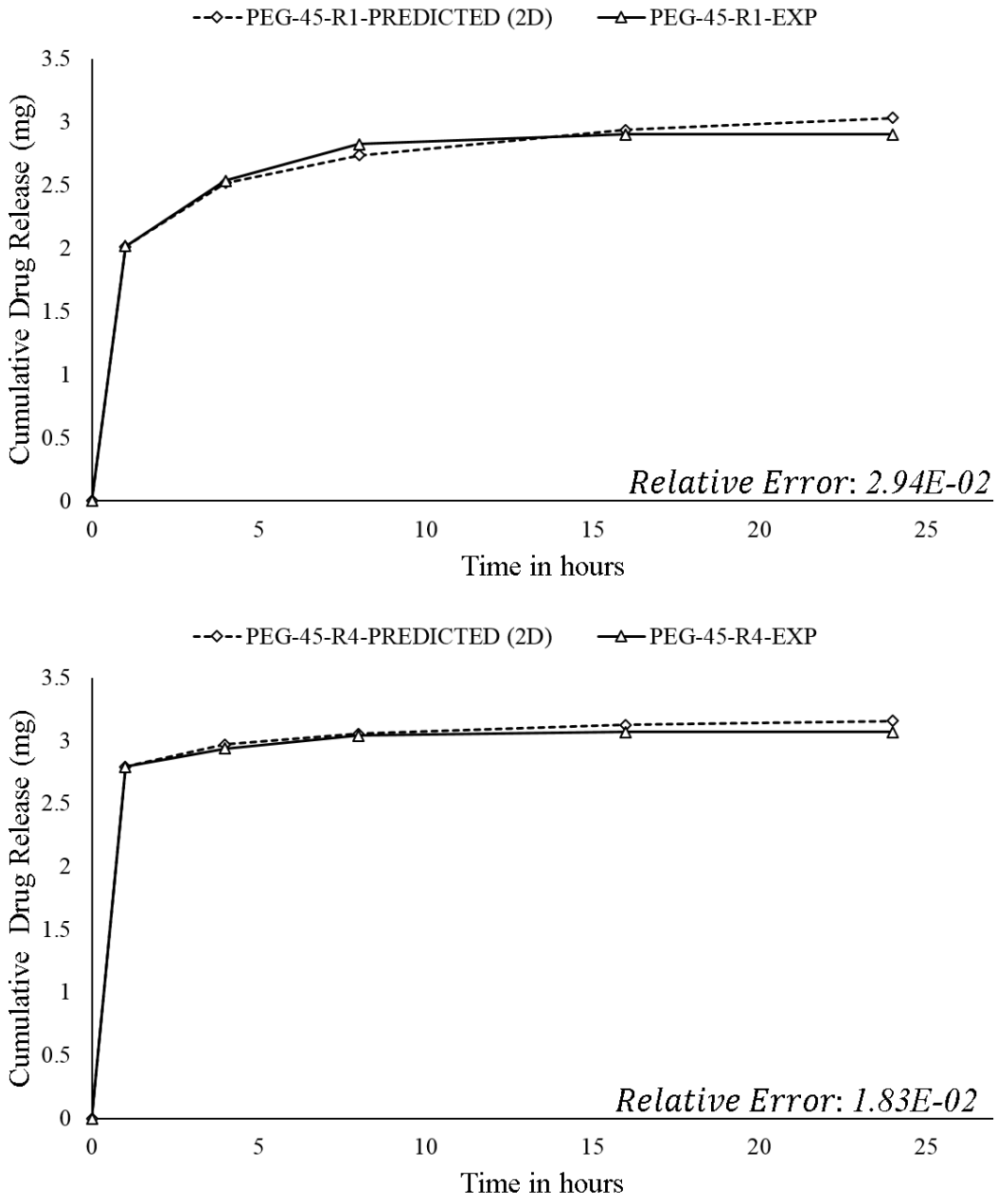


Figure 47: Comparison of Predicted Cumulative Drug Release from 2D Analysis with Experimentally obtained Cumulative Drug Release for two different PEG-45 Replicates.

### 4.3.5 Comparison of Results from 1D and 2D Models

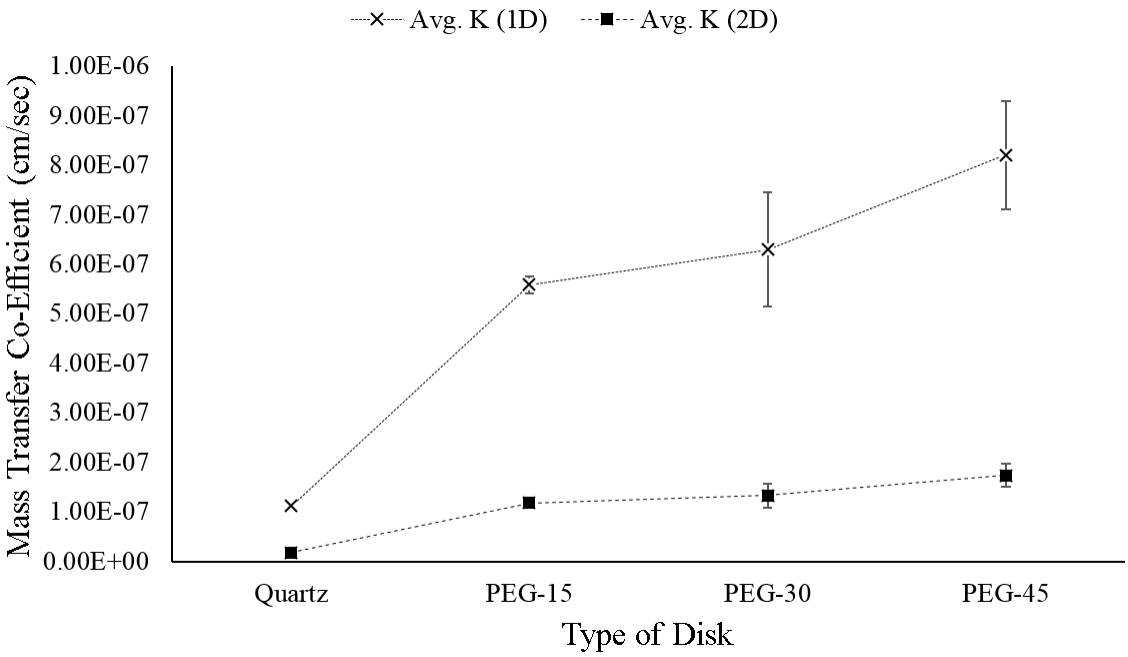


Figure 48: Comparison of Mass Transfer Co-Efficient Values From 1D and 2D Analysis.

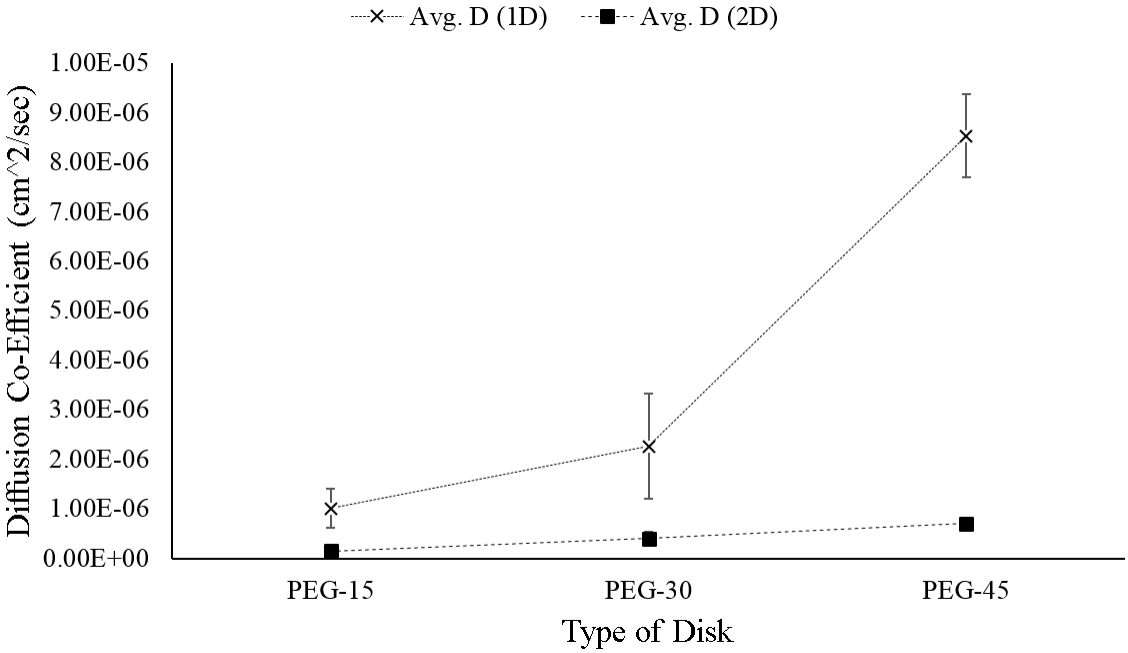


Figure 49: Comparison of Diffusion Co-Efficient Values From 1D and 2D Analysis.

Figure 48 shows the average values of Mass Transfer Co-Efficient from 1D and 2D analysis plotted on the same graph. Figure 49 shows the average values of Diffusion Co-Efficient from 1D and 2D analysis plotted on the same graph.

It was found that the value of $K$ and $D$ as computed from the 1D analysis were significantly higher compared to the 2D analysis. This is due to the reason that in 1D analysis, diffusion from only the periphery of the disk is taken into consideration whereas diffusion from the top surface of the disk is not taken into consideration. In 2D analysis, diffusion from the periphery as well as the top surface of the disk is considered. Thus, the values of $K$ and $D$ as predicted from the 2D analysis are more accurate compared to the 1D analysis.

The obtained values of diffusion co-efficient in this study match well with the nominal values of $D$ for matrix based drug delivery systems as reported in the literature [27].

## 4.4 Pore Distribution and Surface Characteristics of Disks

### 4.4.1 Pore Size Distribution in PEG-15 Disk Sections

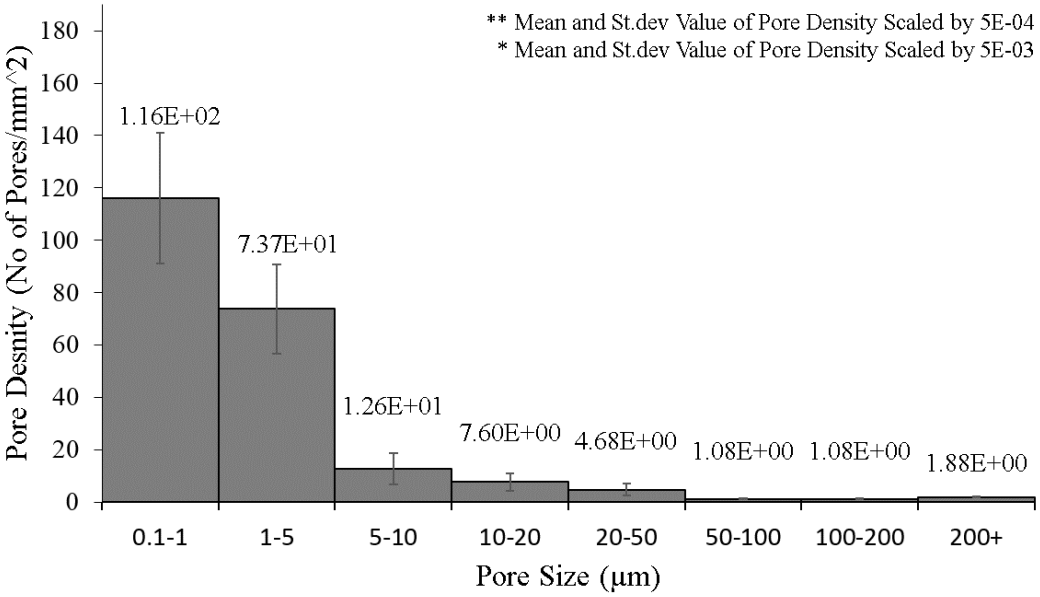


Figure 50: Average value of Pore Density (-/+ St.dev) of pores in different pore size categories in PEG-15 Disk Sections.

Table 24: Average value of Pore Density (-/+ St.dev) of pores in different pore size categories in PEG-15 Disk Sections.

| **Pore Size ($\mu$m) :max($P_w$,$P_h$)** | **N: (ND,NR)** | **Pore Density :No. of Pores/mm$^2$** | **St. dev** |
|---|---|---|---|
| 0.1-1 | 4: (2,2) | 2.32E+05 | 5.00E+04 |
| 1-5 | 4: (2,2) | 1.47E+04 | 3.39E+03 |
| 5-10 | 4: (2,2) | 1.26E+01 | 6.05E+00 |
| 10-20 | 4: (2,2) | 7.60E+00 | 3.30E+00 |
| 20-50 | 4: (2,2) | 4.68E+00 | 2.21E+00 |
| 50-100 | 4: (2,2) | 1.08E+00 | 1.55E-01 |
| 100-200 | 4: (2,2) | 1.08E+00 | 1.55E-01 |
| 200+ | 4: (2,2) | 1.88E+00 | 2.36E-01 |
| ND: Number of disk sections analyzed.<br>NR: Number of regions analyzed on each disk section.<br>N: Total number of regions analyzed.<br>$P_w$: Width of Pore.<br>$P_w$: Height of Pore. | | | |

### 4.4.2 Pore Size Distribution in PEG-30 Disk Sections

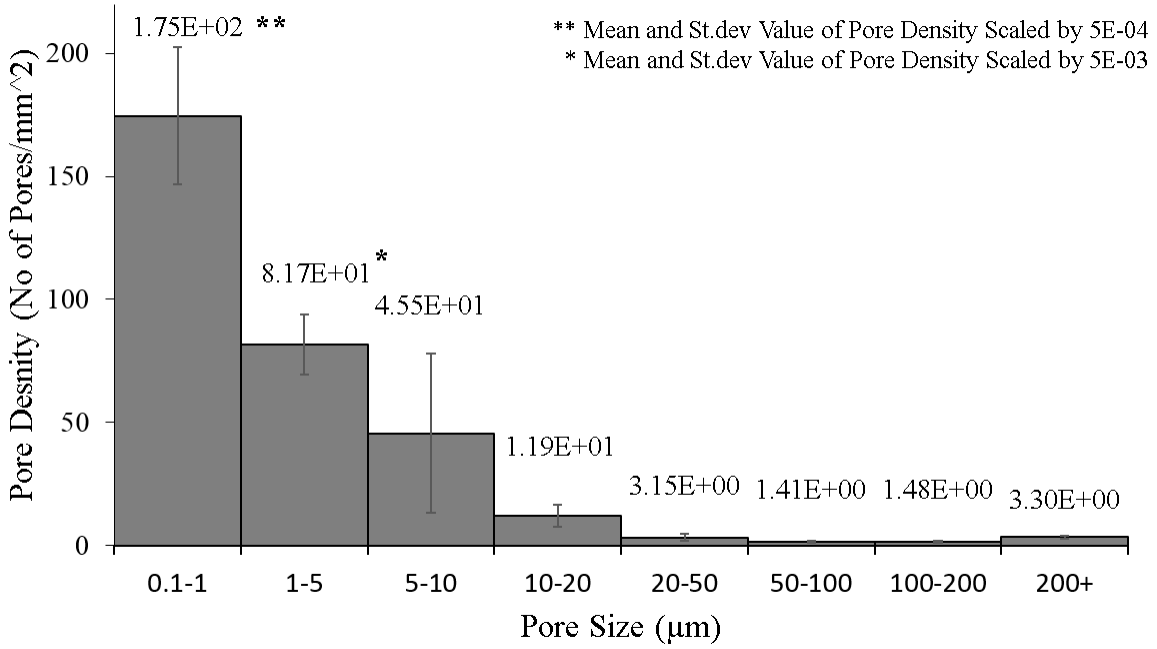


Figure 51: Average value of Pore Density (-/+ St.dev) of pores in different pore size categories in PEG-30 Disk Sections.

Table 25: Average value of Pore Density (-/+ St.dev) of pores in different pore size categories in PEG-30 Disk Sections.

| **Pore Size ($\mu$m) :max($P_w$,$P_h$)** | **N: (ND,NR)** | **Pore Density :No. of Pores/mm$^2$** | **St. dev** |
|---|---|---|---|
| 0.1-1 | 4: (2,2) | 3.49E+05 | 5.57E+04 |
| 1-5 | 4: (2,2) | 1.63E+04 | 2.41E+03 |
| 5-10 | 4: (2,2) | 4.55E+01 | 3.23E+01 |
| 10-20 | 4: (2,2) | 1.19E+01 | 4.45E+00 |
| 20-50 | 4: (2,2) | 3.15E+00 | 1.48E+00 |
| 50-100 | 4: (2,2) | 1.41E+00 | 4.02E-01 |
| 100-200 | 4: (2,2) | 1.48E+00 | 4.01E-01 |
| 200+ | 4: (2,2) | 3.30E+00 | 7.67E-01 |
| ND: Number of disk sections analyzed.<br>NR: Number of regions analyzed on each disk section.<br>N: Total number of regions analyzed.<br>$P_w$: Width of Pore.<br>$P_w$: Height of Pore. | | | |

### 4.4.3 Pore Size Distribution in PEG-45 Disk Sections

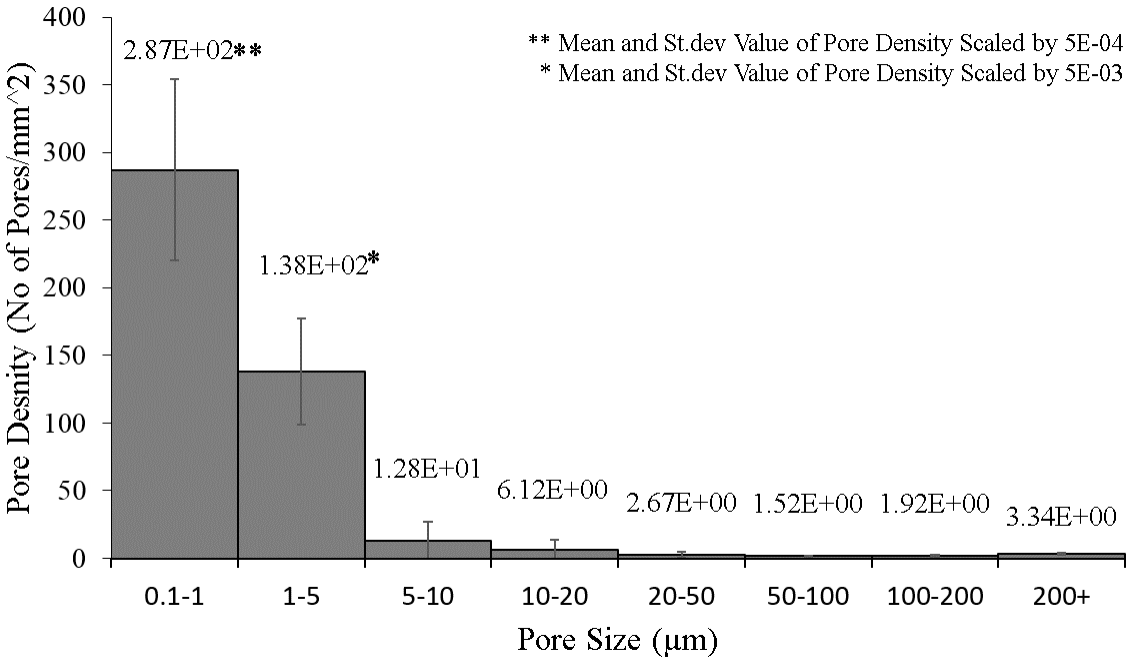


Figure 52: Average value of Pore Density (-/+ St.dev) of pores in different pore size categories in PEG-45 Disk Sections.

Table 26: Average value of Pore Density (-/+ St.dev) of pores in different pore size categories in PEG-45 Disk Sections.

| **Pore Size ($\mu$m) :max($P_w$,$P_h$)** | **N: (ND,NR)** | **Pore Density :No. of Pores/mm$^2$** | **St. dev** |
|---|---|---|---|
| 0.1-1 | 4: (2,2) | 5.74E+05 | 1.34E+05 |
| 1-5 | 4: (2,2) | 2.76E+04 | 7.80E+03 |
| 5-10 | 4: (2,2) | 1.28E+01 | 1.43E+01 |
| 10-20 | 4: (2,2) | 6.12E+00 | 7.54E+00 |
| 20-50 | 4: (2,2) | 2.67E+00 | 1.99E+00 |
| 50-100 | 4: (2,2) | 1.52E+00 | 4.74E-01 |
| 100-200 | 4: (2,2) | 1.92E+00 | 6.70E-01 |
| 200+ | 4: (2,2) | 3.34E+00 | 4.31E-01 |
| ND: Number of disk sections analyzed.<br>NR: Number of regions analyzed on each disk section.<br>N: Total number of regions analyzed.<br>$P_w$: Width of Pore.<br>$P_w$: Height of Pore. | | | |

### 4.4.4 Statistical Analysis of Pore Size Distribution

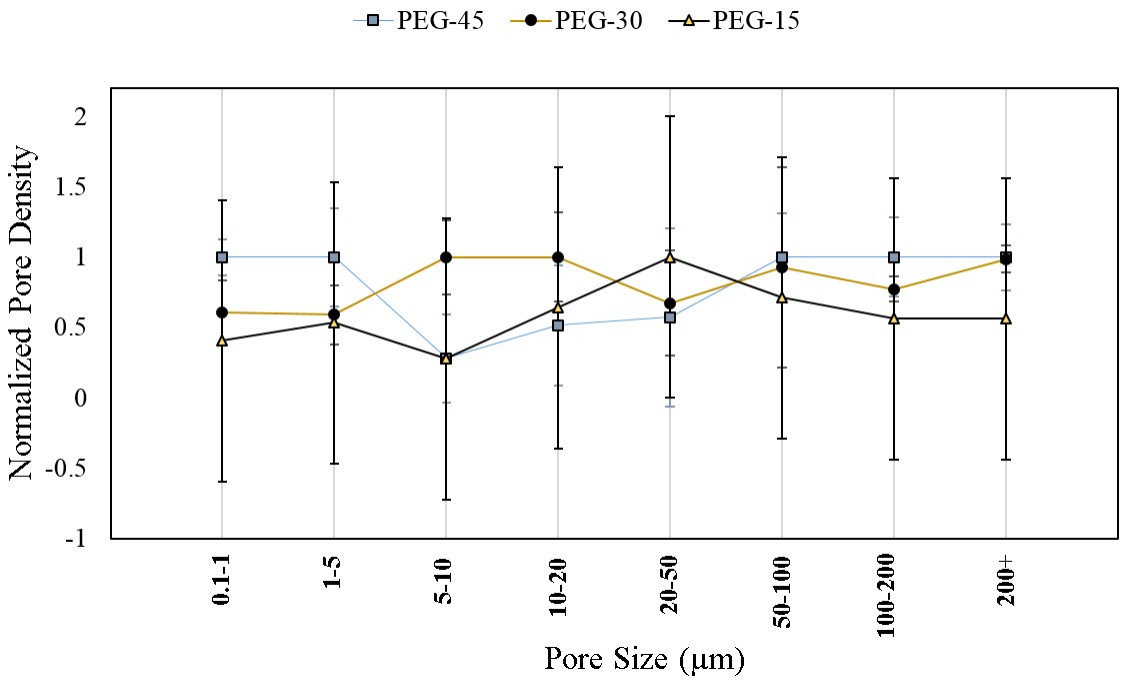


Figure 53: Comparison of Normalized Pore Density (-/+ St.dev) of pores in different pore size categories in different Cris-PEG disks.

The value of Pore Density, i.e No. of pores/mm$^2$, was obtained for PEG-15, PEG-30 and PEG-45 disk sections in N=8 different pore size categories (in $\mu$m): 0.1-1, 1-5, 5-10, 10-20, 20-50, 50-100, 100-200 and 200+. Figures 50, 51 and 52 graphically reports the average values of Pore Density in different pore size categories for PEG-15, PEG-30 and PEG-45 disks respectively. Tables 24, 25 and 26 tabulates for Cris-PEG disk sections, the average values of Pore Density and also reports the number of regions that were analyzed to study the pore distribution. To graphically analyze and compare the Pore Density among PEG-15, PEG-30 and PEG-45 disk sections, the values of Pore Density were Normalized, on a scale of [0,1], along with the corresponding St.dev and plotted on the same graph corresponding to the respective pore

size categories. Figure 53 shows the quantitative comparison of the Normalized Pore Density for different Cris-PEG disks. The Pore Density and St.dev were normalized using equations 59 and 60 respectively.

$$NP_{a-b}^{PEG-XX} = \frac{P_{a-b}^{PEG-XX}}{max(P_{a-b}^{PEG-15}, P_{a-b}^{PEG-30}, P_{a-b}^{PEG-45})} \tag{59}$$

$$NS_{a-b}^{PEG-XX} = \frac{S_{a-b}^{PEG-XX}}{max(P_{a-b}^{PEG-15}, P_{a-b}^{PEG-30}, P_{a-b}^{PEG-45})} \tag{60}$$

The nomenclature associated with equation 59 and 60 are as follows:

1. $\mathrm{NP}_{a-b}^{PEG-XX}$ : Normalized Avg. Pore Density of PEG-XX disk sections in pore size category of a-b $\mu$m.

2. $\mathrm{NS}_{a-b}^{PEG-XX}$ : Normalized St.dev of Pore Density of PEG-XX disk sections in pore size category of a-b $\mu$m.

3. $\mathrm{P}_{a-b}^{PEG-XX}$ : Avg. Pore Density of PEG-XX disk sections in pore size category of a-b $\mu$m.

4. $\mathrm{S}_{a-b}^{PEG-XX}$ : St.dev in Pore Density of PEG-XX disk sections in pore size category of a-b $\mu$m.

From the pore distribution analysis (ref. fig 50, 51 and 52), it was found that for all the Cris-PEG disk types, the pores in the size range of 0.1-1 $\mu$m had the highest pore density followed by pore size range 1-5 $\mu$m. Thus 0.1-5 $\mu$m pore range is the

dominating pore size range wrt. Pore Density. From figure 53, it can be seen that the average Pore Density of PEG-45 is higher compared to both PEG-15 and PEG-30 in the pore size categories of 0.1-1 $\mu$m as well as 1-5 $\mu$m.

To study the significance of the difference in the average Pore Density among Cris-PEG disks for different pore size categories, *One Way ANOVA* test, for $\alpha = 0.05$, was performed. Followed by ANOVA test, Tukey's HSD Post-hoc analysis was performed, for $\alpha = 0.05$, to pairwise compare the Pore Density of the different types of disks and relate it to the release kinetics:

1. *Pore Size Category, 0.1-1 $\mu m$*: From the ANOVA test, it was found that the average Pore Density of Cris-PEG disks were significantly different, F(2,9)=15.4, P=0.0012. The results of Tukey's Post-hoc test for pairwise comparison are reported in table 27.

Table 27: Tukey's Post-hoc pairwise Comparison ($\alpha = 0.05$) of the average Pore Density in Cris-PEG disks for pore size category of 0.1-1 $\mu$m.

| | **95.00% CI of diff.** | **Significant?** | **P Value** |
|---|---|---|---|
| PEG-15 vs. PEG-30 | -291598 to 57987 | No | 0.2039 |
| PEG-15 vs. PEG-45 | -516617 to -167032 | Yes | 0.0010 |
| PEG-30 vs. PEG-45 | -399811 to -50226 | Yes | 0.0144 |

2. *Pore Size Category, 1-5 $\mu m$*: From the ANOVA test, it was found that the average Pore Density of Cris-PEG disks were significantly different, F(2,9)=7.591, P=0.0117. The results of Tukey's Post-hoc test for pairwise comparison are reported in table 28.

Table 28: Tukey's Post-hoc pairwise Comparison ($\alpha = 0.05$) of the average Pore Density in Cris-PEG disks for pore size category of 1-5 $\mu$m.

| | **95.00% CI of diff.** | **Significant?** | **P Value** |
|---|---|---|---|
| PEG-15 vs. PEG-30 | -11665 to 8477 | No | 0.8992 |
| PEG-15 vs. PEG-45 | -22961 to -2819 | Yes | 0.0149 |
| PEG-30 vs. PEG-45 | -21368 to -1226 | Yes | 0.0294 |

3. *Pore Size Category, 5-10 $\mu m$*: From the ANOVA test, it was found that the average Pore Density of Cris-PEG disks were not significantly different for pore size category of 5-10 $\mu$m, F(2,9)=3.353, P=0.0816.

4. *Pore Size Category, 10-20 $\mu m$*: From the ANOVA test, it was found that the average Pore Density of Cris-PEG disks were not significantly different for pore size category of 10-20 $\mu$m, F(2,9)=1.219, P=0.3400.

5. *Pore Size Category, 20-50 $\mu m$*: From the ANOVA test, it was found that the average Pore Density of Cris-PEG disks were not significantly different for pore size category of 20-50 $\mu$m, F(2,9)=1.191, P=0.3478.

6. *Pore Size Category, 50-100 $\mu m$*: From the ANOVA test, it was found that the average Pore Density of Cris-PEG disks were not significantly different for pore size category of 50-100 $\mu$m, F(2,9)=1.502, P=0.2735.

7. *Pore Size Category, 100-200 $\mu m$*: From the ANOVA test, it was found that the average Pore Density of Cris-PEG disks were not significantly different for pore size category of 100-200 $\mu$m, F(2,9)=3.319, P=0.0832.

8. *Pore Size Category, 200+ $\mu m$*: From the ANOVA test, it was found that the average Pore Density of Cris-PEG disks were significantly different for pore size category of 100-200 $\mu$m, F(2,9)=9.946, P=0.0053. The results of Tukey's Post-hoc test for pairwise comparison are reported in table 29.

Table 29: Tukey's Post-hoc pairwise Comparison ($\alpha = 0.05$) of the average Pore Density in Cris-PEG disks for pore size category of 200+ $\mu$m.

| | **95.00% CI of diff.** | **Significant?** | **P Value** |
|---|---|---|---|
| PEG-15 vs. PEG-30 | -2.454 to -0.3773 | Yes | 0.0105 |
| PEG-15 vs. PEG-45 | -2.494 to -0.4179 | Yes | 0.0089 |
| PEG-30 vs. PEG-45 | -1.079 to 0.9975 | No | 0.9935 |

### 4.4.5 Pore Size Distribution and Release Kinetics

From the statistical analysis it was found that the average values of Pore Density of Cris-PEG disk sections were significantly different in only three pore size categories, i.e 0.1-1 $\mu$m, 1-5 $\mu$m and 200+ $\mu$m. ANOVA analysis of Cumulative Drug Release showed that there was significant difference in the amount of drug release from the different types of Cris-PEG disks. It is hypothesized that the pore size categories for which the Pore Density is statistically different are the ones that are responsible for the differential Cumulative Drug Release among Cris-PEG disks. Thus, although the pores in the size category for which the pore density is not significantly different are involved in the diffusion of drug through the ceramic matrix, they do not *control* the drug release kinetics. Thus, pore size categories of 0.1-1 $\mu$m, 1-5 $\mu$m and 200+ $\mu$m are not only involved in drug release, they also actively influence the release kinetics.

1. *Pore Size Category, 0.1-1 $\mu m$ and 1-5 $\mu m$*: In this pore size range, the average value of Pore Density followed the pattern PEG-45>PEG-30>PEG-15. Also, the difference in the Pore Density of PEG-15 and PEG-30 were not statistically significant (*P=0.2039* for 0.1-1 $\mu$m and *P=0.8992* for 1-5 $\mu$m). However, the difference in the average Pore Density of PEG-15 vs PEG-45 and PEG-30 vs PEG-45 were both statistically significant. From the Tukey's pairwise comparison of CDR among Cris-PEG disks, exactly the same statistical relationship was obtained during the first 4 hours of the drug release. It can be hypothesized that this pore size range affects the high rate of drug release during the initial stage of the drug release profile, including the Burst Release phase. The pores in this size range are created by the vapors of PEG particles actively trying to exit the ceramic scaffold.

2. *Pore Size Category, 200+ $\mu m$*: In this pore size range, the average value of Pore Density also follows the pattern PEG-45>PEG-30>PEG-15. Also, the difference in the Pore Density of PEG-15 and PEG-30 were not statistically significant (P=0.0105). This relationship matches the statistical relationship of PEG-15 and PEG-30 disks wrt. CDR for the entire drug release profile. It is found that for this pore size category, the difference in the Pore Density of PEG-30 and PEG-45 are not statistically significant. However, the Pore Density of PEG-15 is statistically different from PEG-30 and PEG-45. The pores in this size range are created when the large (200+ $\mu$m) PEG particles vaporize leaving behind voids at locations where they were initially situated.

### 4.4.6 SEM images of Cris-PEG disk Sections.

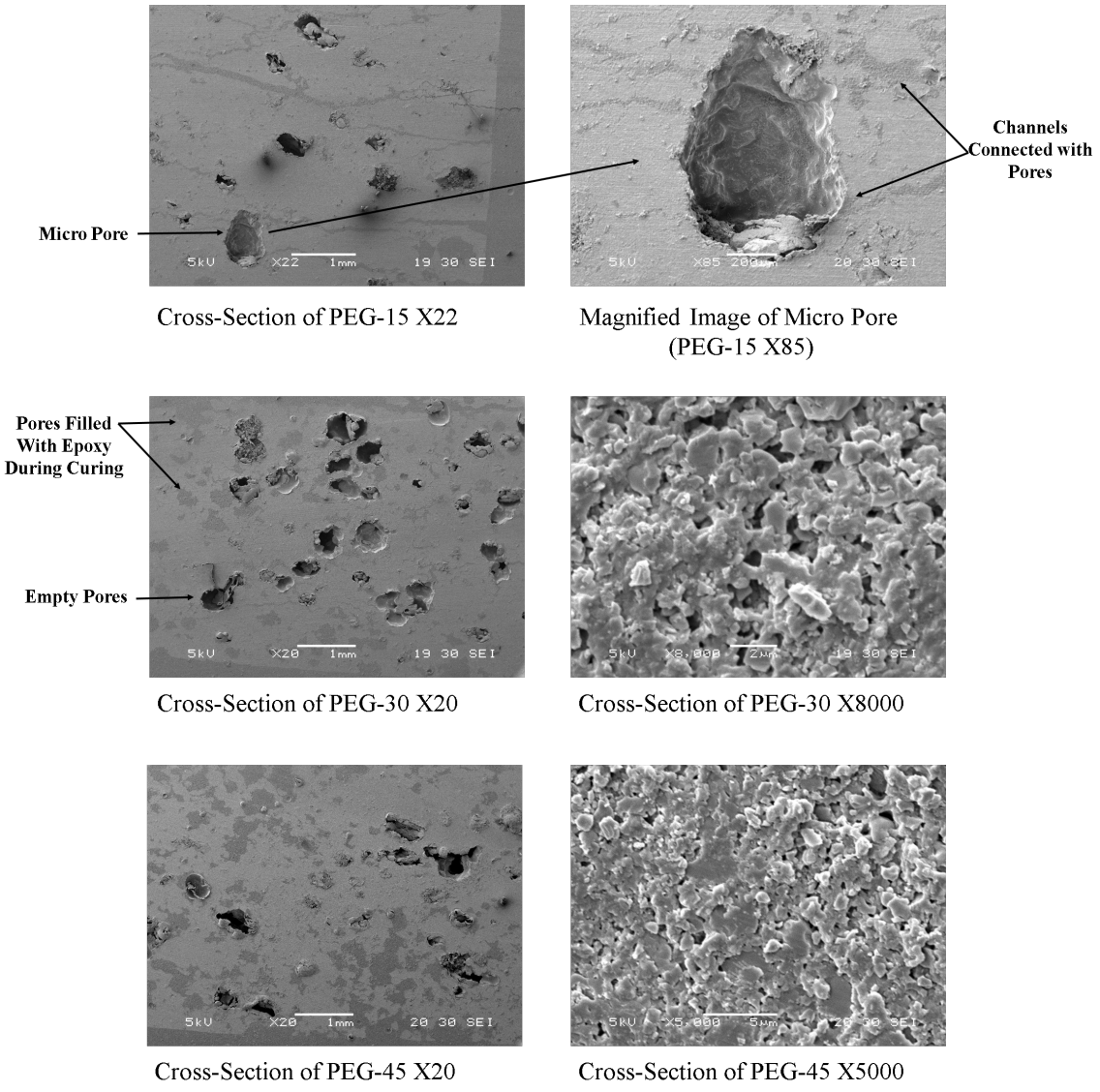


Figure 54: Surface Morphology of Cris-PEG disk sections.

In figure 54 is shown some of the SEM images of the cross sections of the disks at different magnification levels. Interconnection of channels and pores in the disks is clearly visible from the images which gives a qualitative idea about the diffusion of drug molecules from the inner portions of the disks to the outside during *sustained release phase*.

## 4.5 Discussions and Conclusions

The conclusions drawn from this study can be summarized as follows:

1. In the analysis of surface morphology, N=8 pore size categories were analyzed. On the basis of the significance of the difference in the pore density, N=3 pore size categories were identified as the *Dominant Pore Size (DPS) Categories* which actively *control* the release kinetics. Also, the study showed that the Pore Densities of PEG-15, PEG-30 and PEG-45 were significantly different from each other in these Dominant Pore Size Categories: 0.1-1 $\mu$m, 1-5 $\mu$m and 200+ $\mu$m.

2. In the analysis of Drug Loading, the amount of drug *absorbed* and drug *adsorbed* were independently measured. It was found that the overall amount of drug loaded by virtue *absorption* and *adsorption* differed significantly for the different Cris-PEG disk types. As the pore density characteristics of Cris-PEG disks are significantly different from each other in the *DPS* categories, it can be inferred that the Drug Loading efficacy of the disks can be engineered by controlling the pore distribution of the disks in the Dominant Pore Size categories.

3. In the analysis of Drug Release, the amount of CDR wrt. time was studied for the different types of disks. It was found that the CDR of PEG-15 and PEG-30 disks did not significantly defer from each other at any sampling point throughout the drug release period. However, the CDR from PEG-45 disks were significantly different from PEG-15 throughout the drug release period. Also,

the CDR from PEG-45 significantly differed from PEG-30 during the Burst Release phase and also upto over 3 hours in the Sustained Release Phase. From the pore distribution analysis, it was shown the the Pore Densities of PEG-15 and PEG-30 were not significantly different in two of the three Dominant Pore Size Categories (i.e 0.1-1 $\mu$m and 1-5 $\mu$m) but PEG-45 differed from both PEG-15 and PEG-30 in the same DPS categories. Thus, the results of Pore Distribution analysis and Drug Release analysis show the same relation among the Cris-PEG disks. The Cumulative Drug Release of the disks can be engineered by controlling the pore distribution of the disks in these Dominant Pore Size categories: 0.1-1 $\mu$m and 1-5 $\mu$m.

4. It was shown that although Quartz and Cris-PEG disks were loaded with the drug for the same duration of time and in identical conditions, for the dense Quartz disks, there was no significant drug release after the Burst Release phase. However, all the Cris-PEG disks released significant amount of drug after the Burst Phase. The Cris-PEG disks unlike Quartz disks, are porous with tortuous paths of micro and nano scale connecting the outer surface of the disks with the inner most pores of the disks, which facilitate Sustained Drug Release. The average amount of Burst Release from the Quartz disks was also negligible compared to the Cris-PEG disks.

5. In the computational analysis of the Burst Release, Mass Transfer Co-Efficient values ($K$) of the disk-PBS interface for the different disk types were obtained. It was found that the average value of the Mass Transfer Co-Efficient of disks fol-

lowed the pattern PEG-45>PEG-30>PEG-15>Quartz. This relationship also correlates well with the pattern of the average Pore Density in the Dominant Pore Size Categories among Cris-PEG disks. The value of $K$ was obtained by comparing the experimental and computational values of the Cumulative Drug Release during the Burst Phase. The results reported in this thesis can be used to predict the amount of Burst Release for $\alpha$-Cristobalite disks made using different percentages of PEG by mass, by interpolation methods .

6. In the computational analysis of the Sustained Release, Diffusion Co-Efficient values ($D$) for the different disk types were obtained. The values of $D$ for the Cris-PEG disks matched well with the nominal values of $D$ for matrix based drug delivery systems as reported in the literature [27]. The value of $D$ was obtained by comparing the experimental and computational values of the Cumulative Drug Release at different time points during the Sustained Release phase. The results reported in this thesis can be used to predict the amount of overall drug release for $\alpha$-Cristobalite disks made using different percentages of PEG by mass, by interpolation methods .

## 4.6 Future Work

The following recommendations are proposed as a Future Work for this study:

1. Perform *Thermo-Gravimetric* analysis to measure the amount of drug *adsorbed* by the different types of disks and compare with the results provided in this thesis.

2. Perform the same study but with the different types of drug and compare the results.

3. Perform Mercury Porosimetry analysis of the Cris-PEG disks and compare the results with the ones reported in this thesis.

4. Perform computational analysis taking into account the extraction of drug solution and replenishment with fresh PBS at different sampling points.

# REFERENCES


[1] *ABAQUS 6.13 Documentation*. (Accessed on 31/07/2016).

[2] Phosphate-buffered saline, `medicago.se/sites/default/files/pdf/productsheets/PBS_Buffer_v._01.pdf`.

[3] Vancomycin-csid:14253, `chemspider.com/Chemical-Structure.14253.html`. (Accessed on 31/07/2016).

[4] T. M. Allen. Drug delivery systems: Entering the mainstream. *Science*, 303(5665):1818–1822, mar 2004.

[5] B. Arifvianto and J. Zhou. Fabrication of metallic biomedical scaffolds with the space holder method: A review. *Materials*, 7(5):3588–3622, may 2014.

[6] I. Brigger, C. Dubernet, and P. Couvreur. Nanoparticles in cancer therapy and diagnosis. *Advanced Drug Delivery Reviews*, 54(5):631–651, sep 2002.

[7] A. El-Ghannam, K. Ahmed, and M. Omran. Nanoporous delivery system to treat osteomyelitis and regenerate bone: Gentamicin release kinetics and bactericidal effect. *Journal of Biomedical Materials Research Part B: Applied Biomaterials*, 73B(2):277–284, 2005.

[8] A. El-Ghannam, K. Ricci, A. Malkawi, K. Jahed, K. Vedantham, H. Wyan, L. D. Allen, and D. Dréau. A ceramic-based anticancer drug delivery system to treat breast cancer. *J Mater Sci: Mater Med*, 21(9):2701–2710, jul 2010.

[9] K. A. Fisher, K. D. Huddersman, and M. J. Taylor. Comparison of micro- and mesoporous inorganic materials in the uptake and release of the drug model fluorescein and its analogues. *Chemistry - A European Journal*, 9(23):5873–5878, dec 2003.

[10] G. Frenning and M. Strømme. Drug release modeled by dissolution, diffusion, and immobilization. *International Journal of Pharmaceutics*, 250(1):137–145, jan 2003.

[11] Y. Fu and W. J. Kao. Drug release kinetics and transport mechanisms of non-degradable and degradable polymeric delivery systems. *Expert Opinion on Drug Delivery*, 7(4):429–444, mar 2010.

[12] T. Higuchi. Mechanism of sustained-action medication. theoretical analysis of rate of release of solid drugs dispersed in solid matrices. *Journal of Pharmaceutical Sciences*, 52(12):1145–1149, dec 1963.

[13] H.-W. Kim, J. C. Knowles, and H.-E. Kim. Hydroxyapatite polycomposite coatings on hydroxyapatite porous bone scaffold for drug delivery. *Biomaterials*, 25(7-8):1279–1287, mar 2004.

[14] J. H. Lee and Y. Yeo. Controlled drug release from pharmaceutical nanocarriers. *Chemical Engineering Science*, 125:75–84, mar 2015.

[15] Z.-Z. Li, L.-X. Wen, L. Shao, and J.-F. Chen. Fabrication of porous hollow silica nanoparticles and their applications in drug release control. *Journal of Controlled Release*, 98(2):245–254, aug 2004.

[16] R. H. Muller and C. M. Keck. Challenges and solutions for the delivery of biotech drugs – a review of drug nanocrystal technology and lipid nanoparticles. *Journal of Biotechnology*, 113(1-3):151–170, sep 2004.

[17] H. Pacheco, K. Vedantham, Aniket, A. Young, I. Marriott, and A. El-Ghannam. Tissue engineering scaffold for sequential release of vancomycin and rhBMP2 to treat bone infections. *Journal of Biomedical Materials Research Part A*, pages n/a–n/a, feb 2014.

[18] J. Siepmann, H. Kranz, R. Bodmeier, and N. A. Peppas. *Pharmaceutical Research*, 16(11):1748–1756, 1999.

[19] J. Siepmann, F. Lecomte, and R. Bodmeier. Diffusion-controlled drug delivery systems: calculation of the required composition to achieve desired release profiles. *Journal of Controlled Release*, 60(2-3):379–389, aug 1999.

[20] J. Siepmann, K. Podual, M. Sriwongjanya, N. Peppas, and R. Bodmeier. A new model describing the swelling and drug release kinetics from hydroxypropyl methylcellulose tablets. *Journal of Pharmaceutical Sciences*, 88(1):65–72, jan 1999.

[21] J. Siepmann and F. Siepmann. Modeling of diffusion controlled drug delivery. *Journal of Controlled Release*, 161(2):351–362, jul 2012.

[22] J. Siepmann, A. Streubel, and N. A. Peppas. *Pharmaceutical Research*, 19(3):306–314, 2002.

[23] V. P. Torchilin. Recent advances with liposomes as pharmaceutical carriers. *Nature Reviews Drug Discovery*, 4(2):145–160, feb 2005.

[24] L. tseng Fan and S. K. Singh. *Controlled Release*. Springer Science Business Media, 1989.

[25] M. Vallet-Regí, editor. *Bio-Ceramics with Clinical Applications*. Wiley-Blackwell, apr 2014.

[26] C. Wang, C. He, Z. Tong, X. Liu, B. Ren, and F. Zeng. Combination of adsorption by porous CaCO3 microparticles and encapsulation by polyelectrolyte multilayer films for sustained drug delivery. *International Journal of Pharmaceutics*, 308(1-2):160–167, feb 2006.

[27] X. Wu and Y. Zhou. Finite element analysis of diffusional drug release from complex matrix systems. *Journal of Controlled Release*, 51(1):57–71, jan 1998.

[28] W.-W. Yang and E. Pierstorff. Reservoir-based polymer drug delivery systems. *Journal of Laboratory Automation*, 17(1):50–58, jan 2012.

[29] C. Yin and X. Li. Anomalous diffusion of drug release from a slab matrix: Fractional diffusion models. *International Journal of Pharmaceutics*, 418(1):78–87, oct 2011.

# APPENDIX A: MATLAB CODE TO POSTPROCESS ABAQUS DATA AND CALCULATE CUMULATIVE DRUG RELEASE (CDR) OVER TIME FROM 1D AND 2D MODELS

This code calls a batch file, analysis.bat, that executes burst.py/sustained.py which are *Python* codes that edits and solves the ABAQUS model of Burst Release/Sustained Release . Once the codes have executed, the nodal concentration values are fetched and the value of cumulative drug released over the 1D/2D-PBS domain is computed.

```
----------Code Starts----------------------

clc

clear all

close all

%analysis.bat runs and executes burst.py/sustained.py

tic

dos('analysis.bat')

time=toc;

fprintf('Computation Time: %f\n',time)

%-------------------------------------------%

% Load the report with nodal temperature data

% Load the report with the connectivity matrix

[h, node] = hdrload('abaqus.dat'); %Nodal Concentration Values in PBS

load element.rpt                   %Connectivity Matrix

load coordinates.rpt               %Co-ordinates of Nodes
```

```
node=node';

node(1,:)=[];

%-------------------------------------------%

noe= length(element);              %Total Number of Elements

timesteps=4;                       %Time-steps at which dats is requested

Me= zeros(noe,timesteps);

MeTotal= zeros(timesteps,1);

l= 0.0005;                         %Length of the Element

h= 1.0;                            %h=h1+h2= Radius+Height of Disk

for t=1:timesteps

   timestep=t;

   for ele=1:length(element)


    no1=element(ele,2);

    no2=element(ele,3);

    c1=node(no1,timestep);

    c2=node(no2,timestep);

    r1= coordinates(no1,2);

    r2= coordinates(no2,2);


    %% Un-Comment for 2D Analysis

    %no3=element(ele,4);

    %no4=element(ele,5);
```

```
    %c3=node(no3,timestep);

    %c4=node(no4,timestep);

    %r3= coordinates(no3,2);

    %r4= coordinates(no4,2);


    %% CDR for 1D Analysis

    F= (c1*((2*r1/3)+(r2/3)))+(c2*((r1/3)+(2*r2/3)));

    M(ele,timestep)= pi*h*l*F;     %Cumulative Drug Release at 'timestep'


    %% CDR for 2D Analysis

    %F1= r1*((2*c1/3)+(c2/3)+(c3/3)+(2*c4/3));

    %F2= r2*((c1/3)+(2*c2/3)+(2*c3/3)+(c4/3));

    %F=  F1+F2;

    %M(ele,timestep)= pi*0.5*Ae*F;


    MeTotal(t,1)= sum(M(:,timestep));

end

fprintf('Cumulative Drug Release: %f\n',MeTotal(t))

-----------Code Ends---------------------
```

# APPENDIX B: MATLAB CODE TO POSTPROCESS ImageJ DATA AND PERFORM PORE SIZE DISTRIBUTION ANALYSIS

Using the MATLAB function, the results of analysis of SEM images from ImageJ are fetched by MATLAB and the value of *Normalized Area* occupied by pores, minimum, maximum and average pore size along with the pore density of pores within a given range is tabulated. *areaum* is the area of the analyzed sample in $\mu$m.

```
function poreanalysis(lowerlimit,largerlimit,areaum)



areamm= areaum*(1E-6);                      %area of sample in mm^2


load results.dat                            %results from ImageJ
dlmwrite('PEG_15_2300x.dat',results);       %writes the results to seperate file


type= [];


for i=1:length(results)


    width= results(i,5);
    height= results(i,6);
    poresize= max(width,height);
```

```
    if poresize>=lowerlimit && poresize <largerlimit
        newcolumn= [results(i,:) poresize];
        type=[type;newcolumn];

    end
end



narea= sum(type(:,2))/areaum;
minimum= min(type(:,7));
maximum= max(type(:,7));
average= mean(type(:,7));
deviation= std(type(:,7));
nopores= length(type)/areamm;

fprintf('Normalized Area: \t\t%10.6f\n', narea)
fprintf('Minimum Pore Size(um): %10.6f\n', minimum)
fprintf('Maximum Pore Size(um): %10.6f\n', maximum)
fprintf('Average Pore Size(um): %10.6f\n', average)
fprintf('Standard Deviation(um): %10.6f\n', deviation)
fprintf('Number of Pores/mm^2: %10.6f\n', nopores)
end
```